Transport of fluid from the boundary of a lake

by

Michael Stanley Kohn

A thesis submitted to the graduate faculty

in partial fulfillment of the requirements for the degree of

MASTER OF SCIENCE

Major: Civil Engineering (Environmental Engineering)

Program of Study Committee:
Chris Rehmann, Major Professor
Timothy Ellis
Hui Hu

Iowa State University

Ames, Iowa

2010

TABLE OF CONTENTS

ACKNOWLEDGEMENTS

First and foremost, I would like to extend my gratitude to the National Science Foundation Physical Oceanography Program for their financial support, making this project possible. I would also like to extend my deepest gratitude to Dr. Peter van der Linden and the entire staff at Iowa Lakeside Laboratory for providing superb hospitality and facilities during the undertaking of the field work, and always being there when I needed extra help in the field. In addition, I would also like to extend special thanks to Matthew Fairchild, the facilities manager at Iowa Lakeside Laboratory, for always going the extra mile to make sure I had the equipment and tools needed to get the job done. His assistance made the field work a great deal easier. I would also like to acknowledge Gary Owen, Ken Hessenius, Jim Sholly, and their colleagues at the Iowa Department of Natural Resources for allowing me to conduct field experiments at the busiest lake in the state of Iowa and providing bathymetric data. The assistance provided by Tom Clary and Clary Lake Service during the instrument deployment and retrieval was invaluable. I am grateful to the Iowa State University Limnology Laboratory and the Iowa Great Lakes Water Safety Council for allowing me use of their data.

I also would like to recognize Taryn Tigges for the assistance she provided during numerous dye studies and her positive attitude no matter the conditions. Next, I would like to acknowledge Danielle Wain for her instruction and guidance on everything from servicing field instruments to analyzing data. Her support and expertise made this thesis possible. To Josh Scanlon, my research associate, officemate, and roommate, thanks for always being there to lend a helping hand and provide moral support. Simply said, I couldn't have done it without him.

I would like to recognize Dr. Hui Hu and Dr. Timothy Ellis for taking time out of their busy schedules to be members of my thesis committee and providing constructive criticism of my work. I owe a great deal to Dr. David Admiraal of the University of Nebraska-Lincoln whose kind words and recommendation provided me with the opportunity to be a member of Dr. Chris Rehmann's research group. I will be forever indebted to Dr. Chris Rehmann who took a chance and offered a research assistantship to a student he had never met. I would also like to thank Dr. Chris Rehmann for his wisdom and patience, but above all, I really appreciated that he always tried to teach me something new every time I stepped in his office. With his guidance, he has allowed me to make the most of this experience. My family aside, I have no doubt learned more from Dr. Chris Rehmann than any other person in my life. I would like to thank Amanda for the unwavering support and always being just a phone call away no matter how hectic life was. Finally, this brings me to my mom, dad, and sister. Thanks for always pushing me to do my very best and accepting nothing less. I dedicate this thesis to them for all their love and guidance throughout the years.

NOTATION

A = area;
A_d = horizontal area of the dye cloud;
B = basin width;
b = buoyancy flux;
b_0 = the east-west distance from the injection point to the middle of the basin;
C = dye concentration;
$\bar{C}$ = depth-integrated dye concentration;
c = wave slope;
c_p = specific heat of water;
c_2 = constant equal to 0.037;
d = nondimensional vertical diffusivity;
D_T = molecular diffusivity of temperature;
f = Coriolis parameter;
f_t = tank rotation rate;
f_1 = frequency of first vertical mode;
f_2 = frequency of second vertical mode;
f_3 = frequency of third vertical mode;
Fr_t = turbulent Froude number;
g = acceleration of gravity;
g' = modified gravity;
Gr_t = turbulent Grashof number;
H = total depth;
$\overline{H}$ = mean depth;
h_1 = surface layer thickness;
h_i = intrusion thickness;
K = shear velocity constant;
k = horizontal wavenumber;
k_1 = wavenumber;
K_{eff} = effective horizontal diffusivity;
K_ρ = vertical eddy diffusivity;
K_{xd} = dispersion coefficient in the x-direction;
K_x = diffusivity in the x-direction;
K_y = diffusivity in the y-direction;
K_z = vertical eddy diffusivity;
K_{zd} = tracer distribution vertical eddy diffusivity;
K_{zm} = microstructure vertical eddy diffusivity;
K_{zt} = heat budget vertical eddy diffusivity;
L = basin length;
L_c = centered displacement scale;
L_K = Kolmogorov length scale;
L_N = Lake number;

L_o = Ozmidov length scale;
L_R = internal Rossby radius;
L_s = slope length;
L_x = length scale in the x-direction;
l_m = intrusion length;
M = mass of dye;
m_{net} = net mechanical energy;
m = vertical wavenumber;
M_l = mesh length;
MM = mass moment;
N = buoyancy frequency;
n_x = horizontal mode number;
n_z = vertical mode number;
Pe = Peclet number;
Pe_w = Peclet number from wave advection;
R = solar radiation flux;
Re_t = turbulent Reynolds number;
R_f = flux Richardson number;
R_i = bulk Richardson number;
S = tanα, slope of boundary;
S_n = noise spectrum of fluctuating temperature gradient;
S_{obs} = observed spectrum of fluctuating temperature gradient;
T = temperature;
$\bar{T}$ = mean temperature;
t = time;
T_1 = period of the first mode seiche;
U = maximum velocity in the x-direction;
u = velocity in the x-direction;
$\bar{u}$ = mean velocity in the x-direction;
u' = fluctuating velocity in the x-direction;
u_* = water shear velocity;
u_{*a} = wind shear velocity at water surface;
u_w = wind velocity;
W = Wedderburn number;
w = vertical velocity;
WM = wind moment;
x = position in the horizontal direction;
x_0 = longitudinal location of the dye;
y = position in the horizontal direction;
z = position in the vertical direction;
z_0 = vertical location of the dye;
z_G = distance from lake bottom to center of mass;
z_{ih} = instrument height;
z_M = distance from lake bottom to thermocline;

z_{max} = maximum lake depth;
z_T = total depth;
z_V = distance from lake bottom to center of volume;
α = angle of sloping boundary;
Γ = mixing efficiency;
γ = coefficient equal to 1 cm;
δ = boundary layer thickness;
ε = rate of dissipation of turbulent kinetic energy;
ζ = vertical isotherm displacement;
ζ_0 = amplitude of the isotherm displacement;
η = thickness of the turbulent area;
θ = phase angle;
κ = von Kármán constant;
κ_y = dispersion coefficient in the y-direction from the Lagrangian statistics model;
λ = wavelength;
ν = kinematic viscosity of water;
ν_a = kinematic viscosity of air;
ξ = horizontal wave displacement;
ξ_0 = maximum horizontal wave displacement;
ξ_n = Iribarren number;
ρ = density of water;
$\bar{\rho}$ = mean background density;
ρ' = fluctuating density;
ρ_0 = reference density of water;
ρ_a = density of air at water surface;
ρ_{dye} = dye density
ρ_s = density of surface water;
σ = standard deviation;
σ_x = standard deviation in the x-direction;
φ = angle of energy propagation;
χ_T = rate of dissipation of temperature variance;
ω = wave frequency;
ω_0 = oscillation frequency;
ω_c = critical wave frequency;

LIST OF FIGURES

LIST OF TABLES

ABSTRACT

A field study was conducted at West Okoboji Lake near Arnolds Park, Iowa to study transport of fluid resulting from wind forcing on summer stratification. A tracer was injected at the boundary of the lake and surveyed on four separate occasions over a period of three days. The Lake number was less than 10 during the first day of the tracer study. Evidence from three approaches supported the existence of V1H1 and V2H1 modes. Three methods showed that the vertical diffusivity was on the order of 10^{-6} m^2 s^{-1}. From the tracer surveys, the distance traveled offshore and velocity of the tracer was approximately 900 m and 0.8 cm s^{-1}, respectively, with dispersion as the dominant transport mechanism. The horizontal eddy diffusivity was estimated from the horizontal tracer distribution to be between 0.2×10^{-1} m^2 s^{-1} and 4×10^{-1} m^2 s^{-1}. There was no evidence to support boundary mixing or intrusions.

CHAPTER 1. INTRODUCTION

Problem Statement

Stratification in lakes inhibits the transport of nutrients, gases, and other dissolved substances (Saggio and Imberger 2001). As a result, mixing induced from wind disturbances plays a vital role in transporting dissolved and suspended substances because during much of the late spring, summer, and early fall lakes are strongly stratified due to their temperature structure. Internal waves generated by wind have been found to redistribute phytoplankton (MacIntyre et al. 1999; Marcé et al. 2007), nutrients such as phosphorus (e.g., Lemmin and Mortimer 1986, MacIntyre et al. 1999, Eckert et al. 2003), dissolved oxygen (Rao et al. 2008), organic matter (Gloor et al. 1994), sediments (Weyhenmeyer 1996), and methane (Murase et al. 2005). Vertical transport in a lake is dictated by mixing near its boundaries (Eriksen 1985; Lorke et al. 2008). In the littoral zone of lakes, boundary mixing has been found to enhance local nutrient fluxes and bioproductivity (MacIntyre et al. 1999).

When a lake is stratified, mixing can originate from wind induced waves interacting with the boundaries of basins. For the past several decades, the hypothesis in lakes and the ocean is that boundary layer processes dominate mixing (Munk 1966). Sustained wind forcing on a water body can cause internal waves to form. Wind can enhance mixing throughout a stratified basin increasing diapycnal mixing (i.e., mixing across surfaces of constant density) and isopycnal mixing (i.e., mixing between surfaces of equal densities). Internal waves created by the wind reflecting and interacting with the lake boundaries generate regions of elevated mixing along the boundaries (MacIntyre et al. 1999). Along with transport caused by internal waves, intrusive layers have been observed transporting mixed

boundary fluid offshore (Gloor et al. 2000). The reallocation of nutrients, dissolved gasses, and organic matter can potentially alter the trophic status of lakes (Lemmin and Mortimer 1986). Although wind induced waves are well documented, little is known about the actual physical processes that mix and transport fluid, nutrients, sediment, and other particles from the boundary to the interior of a lake.

The findings will help to further explain the complex environment found near the boundaries of lakes. This has significant implications for the temporal and spatial distribution of the temperature structure, dissolved gasses, nutrients, phytoplankton, and zooplankton. Management strategies and the trophic status of lakes may be heavily influenced by the extent to which boundary mixing and the offshore transport of fluid exist.

Hypotheses

The hypotheses of the study included

1. Wind forcing on a stratified basin will generate a first mode internal seiche internal waves that causes vertical and horizontal disturbances in the lake;
2. Internal waves will approach the boundaries of the lake their interaction will cause turbulence which will result in regions of mixed boundary fluid;
3. Where mixed boundary fluid is present, the fluid will gravitationally collapse and form an intrusion along an isopycnal and the mixed fluid will be transported into the interior of the lake.

The following section identifies the manner in which the hypotheses will be examined.

Objectives

Using field experiments, the present work examines the internal behavior of a stratified lake as it undergoes an external force due to the wind, how this mechanical energy applied to the system affects mixing near the boundaries, and the subsequent transport of near-boundary fluid. The objectives to be addressed in this study were

1. Relate the external forcing to the resulting internal wave field and isotherm displacement.
2. Diagnose the presence of mixing from the internal wavefield in terms of location and intensity.
3. Track fluid mixed near the boundaries to determine its fate along with its geometry and spreading rate.

The objectives were attained from the analysis of several measurements during the summer of 2009 at West Okoboji Lake near Arnolds Park, Iowa. Along with a dye tracking experiment, measurements recorded over the course of the summer included wind speed, wind direction, temperature profiles, temperature microstructure, velocity profiles, turbidity, and conductivity.

Organization

This thesis discusses the physical characteristics of wind forcing on a thermally stratified lake and the subsequent reaction of the fluid in the lake. Previous work relevant to the hypotheses is discussed in Chapter 2. Chapter 3 describes the experimental site and methods used to obtain the results described in Chapter 4. The hypotheses are evaluated in

Chapter 5. Chapter 6 reviews the significant discoveries of the experiments and lays the groundwork for future endeavors.

CHAPTER 2. REVIEW OF LITERATURE

Introduction

An extensive review was performed on previous work on physical processes in lakes due to wind forcing, the subsequent waves, the ensuing mixing, and fluid transport produced. The aim of this chapter is to provide background for the work described afterward. The previous work examined provides additional evidence to further the significance, methods, findings, and conclusions which will be discussed later. The literature review and following chapters will be organized by the following topics: stratification and forcing, internal waves, mixing, and transport.

Stratification and Forcing

Temperature Structure and Mixing Regimes

Energy from solar radiation causes thermal stratification at some time of the year for most but not all lakes. Lakes mix completely only when the stratification strength is overcome by the wind forcing to mix the basin entirely. Mixing regimes in lakes are determined by the occurrence of the mixing which is typically caused by the lack of stratification; however, topography and wind patterns may also play a significant role. Lakes that are stratified during all times of the year and never mix are amictic; these lakes typically are found in cold climates at latitudes greater than 75° and are often ice covered year-round. Monomictic lakes mix once per year and can be found in cold climates between latitudes of 70° and 75° or in warm climates of with latitudes less than 40° when the lake is sufficiently deep. Deep lakes in temperate climates at latitudes between 40° and 70° are categorized as

dimictic, meaning they mix completely in the spring and a second time in the fall. Shallow lakes at the same latitudes as dimictic and monomictic lakes usually fail to have strong stratification and mix often; thus, they are polymictic. A diagram of the different mixing regimes may be found in Figure 2.1, which has been modified from Kalff (2002). For this

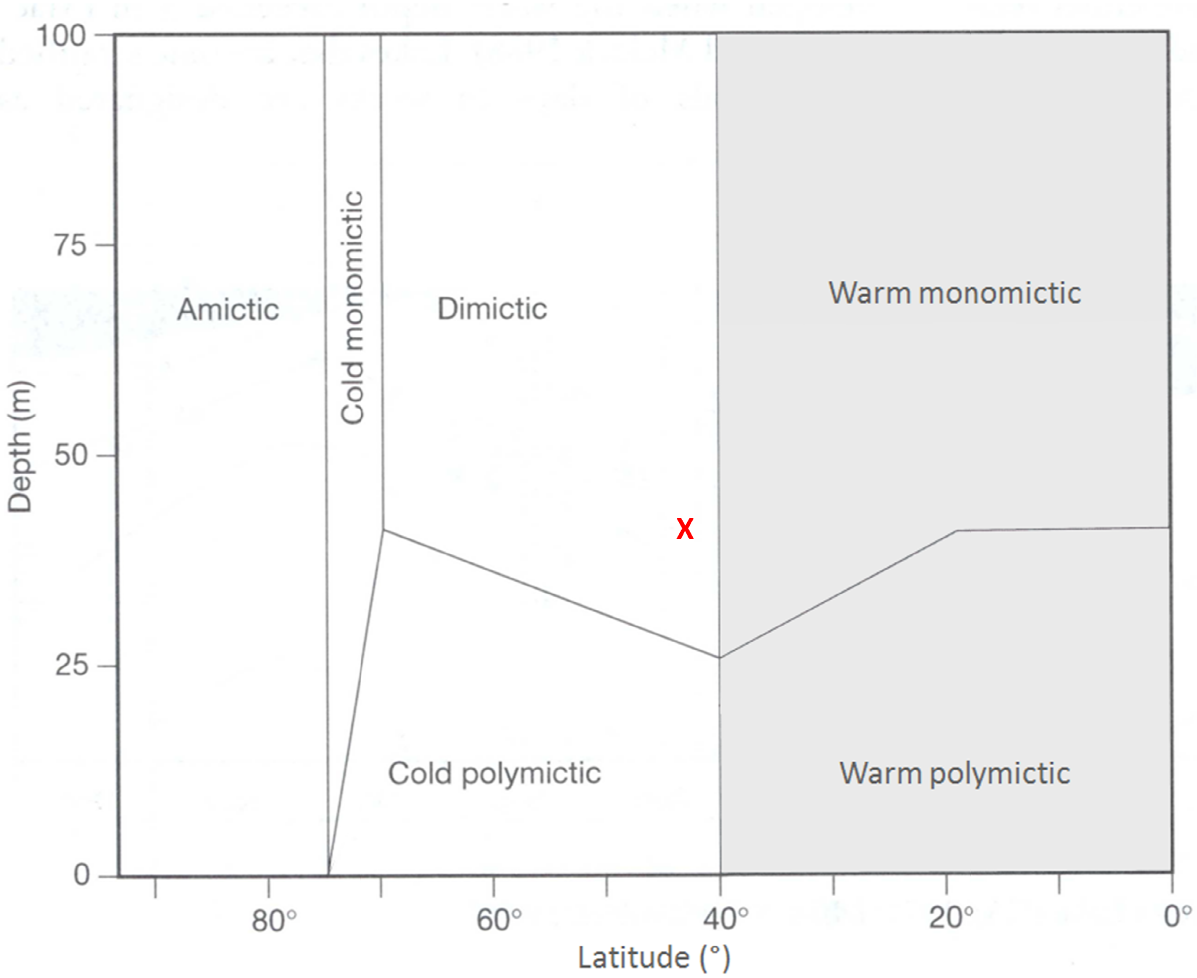

Figure 2.1. The four mixing regimes of lakes modified from Kalff (2002) based off the maximum depth and the latitude. At 43° latitude and a maximum depth of 41 m, West Okoboji falls into the dimictic regime and is represented by the red x.

study we are examining a dimictic lake in the Northern Hemisphere, meaning that during late spring and summer, when the study took place, the lake was thermally stratified.

The basic three layer structure of a dimictic lake such as West Okoboji Lake during summer stratification is as follows (Figure 2.2). A well mixed surface layer with little or no variation in temperature, known as the epilimnion, is stirred by wind forcing resulting in surface waves. Beneath the epilimnion is a region, known as the metalimnion, identified by strong stratification resulting in a sharp density gradient. At times, the metalimnion may be approximated as an interface (thermocline) with a sharp contrast in density separating the

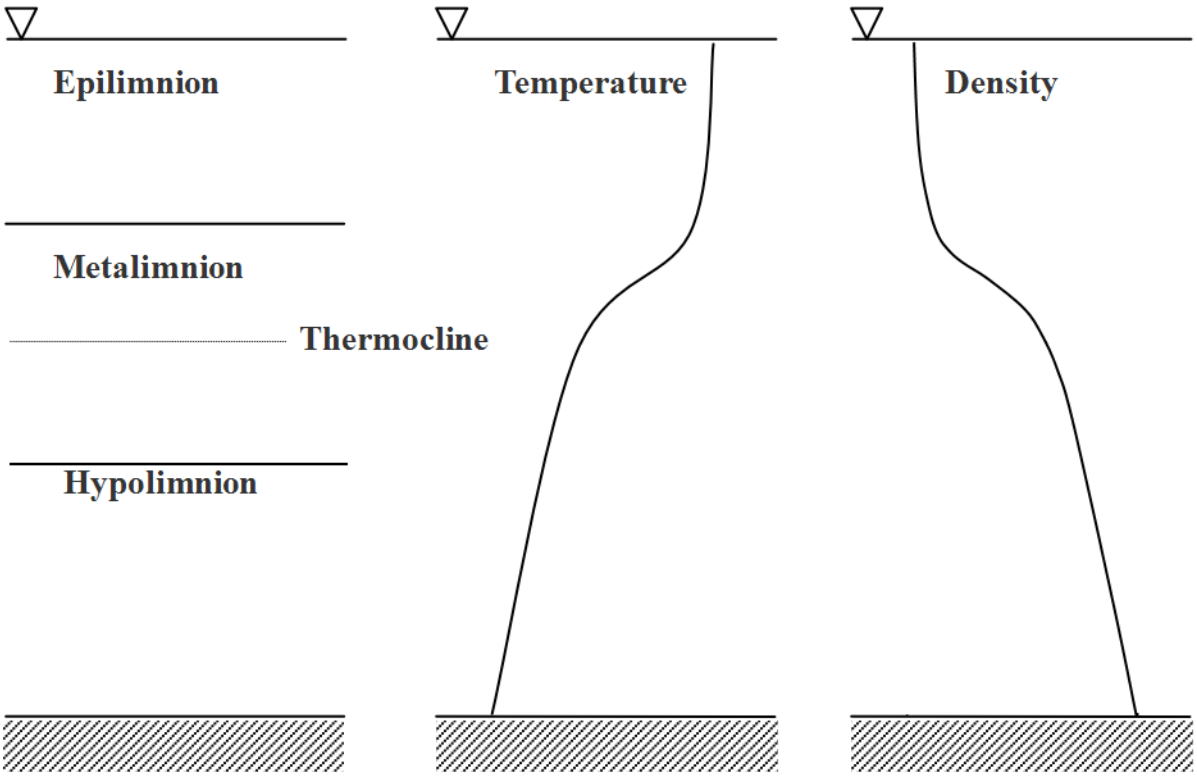

Figure 2.2. Typical thermal structure of a dimictic lake during summer stratification and the resulting density profile.

upper and lower layers. The bottom layer, or hypolimnion, is defined as the region with a slight temperature gradient beneath the metalimnion.

Effects of Stratification on Transport

The strong summer stratification traps oxygen, carbon dioxide, and nutrients—key components to any ecosystem—at certain points in the lake's profile and limits their transport and spatial variability. The limitation of these vital materials has a profound impact on the ecology of aquatic environments. Understanding boundary mixing and resuspension is a prerequisite for understanding biological and chemical processes in lakes. For example, nutrients—such as phosphorus, the primary stimulant to production in aquatic systems—and other substances settle and accumulate at the lake bed, where their only means of further transport is via kinematics of the adjacent fluid. Most of the regions that accumulate settled particles lie in the aphotic zone, where no substantial photosynthetically available radiation is available to generate production. Therefore, the amount of production may be indirectly linked to the amount of mixing near the boundaries of lake as idle nutrients may now be transported where they can be consumed.

The ability of stratification to limit vertical transport can have either positive or negative consequences. For example, Morillo et al. (2008) observed the fate and transport of two rivers flowing into Coeur d'Alene Lake using field data and numerical simulations. The fluid from each river traveled along the lake boundary until each intruded horizontally into the lake's interior at their natural buoyancy. The Coeur d'Alene River is polluted with trace elements such as cadmium, lead, and zinc, while the St. Joe River is polluted with nutrients. The thermal stratification in the lake inhibited transport between the epilimnion and the hypolimnion, thus managing to limit the interaction between the contaminants which would

only compound the effect on the aquatic system. However, limited transport in lakes can also have a negative effect. A large variation of dissolved oxygen concentrations was observed by Rao et al. (2008) between the epilimnion and hypolimnion of Lake Erie due to the thermal stratification via measurements of velocity, temperature, and dissolved oxygen.

Transport during periods of strong stratification can only be provided by external forcing and the resulting internal waves. The wind and the subsequent internal waves have been found to redistribute phytoplankton (MacIntyre et al. 1999; Marcé et al. 2007), nutrients such as phosphorus (e.g., Lemmin and Mortimer 1986, MacIntyre et al. 1999, Eckert et al. 2003), dissolved oxygen (Rao et al. 2008), organic matter (Gloor et al. 1994), and methane (Murase et al. 2005). MacIntyre et al. (1999) noted intense mixing from high winds supported vertical flux of nutrients across the thermocline. The reallocation of nutrients, dissolved gasses, and organic matter can potentially alter the trophic status of lakes (Lemmin and Mortimer 1986).

Boundary mixing was the predominant mechanism supplying nutrients to the lake and primarily responsible for the upward flux of nutrients and phytoplankton in Mono Lake, CA (MacIntyre et al. 1999). In the littoral zone, boundary mixing also drove the enhanced local nutrient fluxes and bioproductivity (MacIntyre et al. 1999). Marcé et al. (2007) found wind generated turbulence along the main axis of the Sau Reservoir and advection caused by seiching motions affected the vertical distribution of phytoplankton. Wind is the dominant factor controlling the distribution of phytoplankton in lentic systems such as lakes and wetlands. Rao et al. (2008) attributed redistribution of dissolved oxygen in the water column during stratification to mixing induced by wind events. Also, Rao et al. (2008) observed a reduction in dissolved oxygen concentration as the particles were resuspended by internal

waves. The resuspended particles consumed oxygen that was not readily available at the bottom of the lake (Rao et al. 2008).

Because internal wave activity was proven to be a key player in the resuspension of boundary sediments (Weyhenmeyer 1996), it can drive the release of nutrients and other contaminants in the sediment. Murase et al. (2005) found that the resuspension of bottom sediment and the subsequent release of methane from the bottom sediments of Lake Biwa were caused by internal waves. The profundal sediments had much less methane content when compared to littoral sediments, which was attributed to offshore transport by internal waves. Confirming this theory was high concentrations of methane in the water near the sediment in the profundal zone and small methane concentration of bottom water in the littoral zone.

Eckert et al. (2003) observed a phosphorus flux along the sediment-water interface and monitored its resuspension, deposition, and accumulation in Lake Kinneret. Previous studies in Lake Kinneret showed that along the boundary in the metalimnion, where the influence of seiches was most prevalent, resuspension was much greater than locations less affected by seiching (Ostrovsky et al. 1996). Eckert et al. (2003) observed the primary location of resuspension change as the region of the metalimnion changed due to fluctuations in the total lake depth. With the reduction of allochthonous phosphorus reaching the basin during the study period, Eckert et al. (2003) determined the changes in phosphorus concentration in the profundal region resulted from internal waves.

Forcing and Dimensionless Parameters

Not only can the wind stir the epilimnion, but it may impart enough energy on the lake to generate internal waves. Similar to surface waves, which occur because of the

difference between the densities of water and air, internal waves occur because of the density difference across isotherms or isopycnals. Additionally, if the wind forcing occurs for a long time, the wind can push the epilimnion towards the downwind side of the lake; this causes the lower layers to tilt in order to maintain equilibrium. When the wind relaxes, the entire basin oscillates, causing basin scale internal motions know as seiches.

To identify the potential response of the lake from wind forcing, the relative strength of the wind forcing compared to the stratification strength must be identified. To compare the relative strength of the wind, which can cause the stable stratification to overturn, to the relative strength of the lake stratification, which resists overturning, the Wedderburn number or Lake number (Imberger and Patterson 1990) can be used. The Wedderburn number W is defined as

$$W = R_i \frac{h_1}{L} = \frac{g' h_1}{u_*^2} \frac{h_1}{L}, \tag{2.1}$$

the product of the bulk Richardson number $R_i = g' h_1 / u_*^2$, and the aspect ratio h_1/L. Modified gravity is defined as $g' = g\Delta\rho/\rho_0$, h_1 is the equilibrium surface layer thickness, u_* is the shear velocity, g is the acceleration of gravity, $\Delta\rho$ is the change in water density, ρ_0 is the reference density, and L is the basin length. When W is large, the baroclinic pressure force (per unit width) $\rho_0 g' h_1^2$ is large compared to the surface force (per unit width) $\rho_0 u_*^2 L$; thus the wind is too weak generate upwelling and little or no isopycnal disturbance occurs (Stevens and Imberger 1996). When W is small, upwelling dominates the stratified fluid; for a two-layer fluid, upwelling occurs when $W \leq 1/2$ (Thompson and Imberger 1980).

The Lake number L_N is the ratio of the mass moment MM to the wind moment WM around the center of volume of the lake (Lindenschmidt and Chorus 1998):

$$L_N = \frac{MM}{WM}. \tag{2.2}$$

The mass moment is the product of the force from the lake's density difference in the stratified water column and the distance between the center of mass and the center of gravity caused by the density profile and the thermocline tilt. The stronger the stratification, the larger this distance becomes. The mass moment MM (Lindenschmidt and Chorus 1998) is found by

$$MM = \frac{z_T - z_M}{\sqrt{A(z_T)}}(z_V - z_G)g \int_0^{z_T} \rho(z)A(z)dz \tag{2.3}$$

where z_T is the distance from the lake bed to the surface, z_M is the distance from the bottom of the lake to the thermocline, A is area at depth z, z_V is the distance to the center of volume, and z_G is the distance to the center of mass. The wind moment WM about the center of volume of the lake is determined using (Imberger and Patterson 1990)

$$WM = \rho_s u_*^2 A(z_T)(z_T - z_V) \tag{2.4}$$

where the density of water at the lake surface is ρ_s. The shear velocity in the water is calculated as

$$u_* = \left(\frac{\rho_a}{\rho_s}\right)^{1/2} u_{*a} \tag{2.5}$$

where the air density at the water surface is ρ_a, and the shear velocity of the wind at the water surface is u_{*a}. For wind velocities of 5 m s^{-1} or greater, the relationship between wind velocity at the water surface u_{*a} and the wind velocity measured $u_w(z_{ih})$ at instrument height z_{ih} is computed with (Wüest and Lorke 2003a)

$$u_w(z_{ih}) = u_{*a}\left[\kappa^{-1}\ln\left(\frac{g z_{ih}}{u_{*a}^2}\right) + K\right], \tag{2.6}$$

where κ is the von Kármán constant equal to 0.41 and the constant K is equal to 11.3. For wind velocities less than 5 m s^{-1}, wind velocity at the water surface is computed with (Wüest and Lorke 2003a)

$$u_w(z_{ih}) = u_{*a}\left[\kappa^{-1}\ln\left(\frac{u_{*a}z_{ih}}{\nu_a}\right) + 5.7\right], \tag{2.7}$$

where the kinematic viscosity of air is ν_a.

The Lake number can indicate whether boundary mixing from seiching and breaking internal waves is present. The smaller the Lake number becomes, the greater the effect the wind has on the entire basin. From dimensionless parameters, Stevens and Imberger (1996) identified four response categories in a laboratory tank. When the Wedderburn and Lake numbers were large ($W, L_N \gg 1$), only small amplitude seiching was present, regardless of the stress duration. With a sufficiently long stress period, the Lake number much greater than one, and the Wedderburn number less than one, second vertical mode seiching was observed. On the other hand, for a large Wedderburn number and a Lake number less than one, seiching was possible in the deeper portion of the water column, but no disturbance at the upper interface was noted. Lastly, when the Wedderburn and Lake numbers were much less than one, large scale interface tilting was observed; additionally upwelling should be prevalent.

When the Lake number reaches or falls below one, upwelling occurs, and when the Lake number is less than 10, the wind stress is sufficient to generate wind set-up throughout the water column (Imberger and Patterson 1990). In the field, seiching motions have been observed in lakes when the Lake number fell below 10 and the wind relaxed (e.g., Stevens and Lawrence 1997, Romero et al. 1998, MacIntyre et al. 1999, 2009). Stevens and Lawrence

(1997) compared the Wedderburn number and Lake number in four lakes in British Columbia and noted that the values of W and L_N always remained similar to each other, never varying by more than a factor of five for any of the lakes studied. MacIntyre et al. (1999) suggested a Lake number of two was the threshold established for the initiation of boundary mixing. At a Lake number of less than two, thermocline compression, steepening of internal waves, and high frequency critical internal waves were found to exist. In a separate study, MacIntyre et al. (2009) observed displacement of the pycnocline during a wind event, leading to seiching motions upon relaxation of the wind in Mono Lake, California. When the Lake number became lower than four, nonlinear internal waves began to occur.

Internal Waves

Waves need a density interface on which to propagate. The most recognizable waves in lakes are those that occur on the lake's surface on the interface between air and water. However, only a slight density difference needs to be present in order to provide a medium for waves. Therefore, internal waves can exist wherever even a small density gradient can be found. Isotherms are an easily identified mechanism for internal waves because a density gradient is present across the isotherms. Waves that occur on an isotherm have the potential for greater amplitude because the density gradient is much less than that at the water surface. The density difference across a media is inversely proportional to the amplitude of the wave. Because the density difference across an isotherm is small relative to the difference at the water surface, a wave with greater amplitude is possible.

Linear wave theory can be applied to waves whose amplitude is small compared to the wavelength. For internal waves in two-dimensional space, the frequency of the wave ω can be related to the buoyancy frequency N and the angle from horizontal to the horizontal wavenumber vector θ, which can be expressed in terms of k and m, the horizontal and vertical components of the wavenumber:

$$\omega = N\left(\frac{k^2}{k^2+m^2}\right)^{1/2} = N\cos\theta. \tag{2.8}$$

The buoyancy frequency is defined as

$$N = \sqrt{-\frac{g}{\rho_0}\frac{\partial\bar{\rho}}{\partial z}} \tag{2.9}$$

where g is the acceleration of gravity, ρ_0 is a reference density and $\bar{\rho}$ is the background density at depth z (Turner 1973). The maximum obtainable wave frequency is the buoyancy frequency. A wave of a given frequency in a fluid at a certain buoyancy frequency must have a phase which propagates at a specific angle. The phase and energy propagate in the same direction for surface waves, but the energy propagates perpendicular to the phase for internal waves ($\varphi = \pi/2 - \theta$).

In order for conservation of energy to hold, the energy from an internal wave must reflect from a lake boundary. Given that the boundary of a lake has a slope of angle α, the angle of energy with respect to the horizontal plane must propagate at the angle φ after reflection. As a result, three scenarios are possible as an internal wave reflects off a sloping boundary in a lake (Figure 2.3). When $\varphi < \alpha$, the energy from the wave is reflected back into the lake's interior as a subcritical reflection. A supercritical reflection occurs when $\varphi > \alpha$, and the wave energy reflects forward up the slope towards the lake surface. Finally,

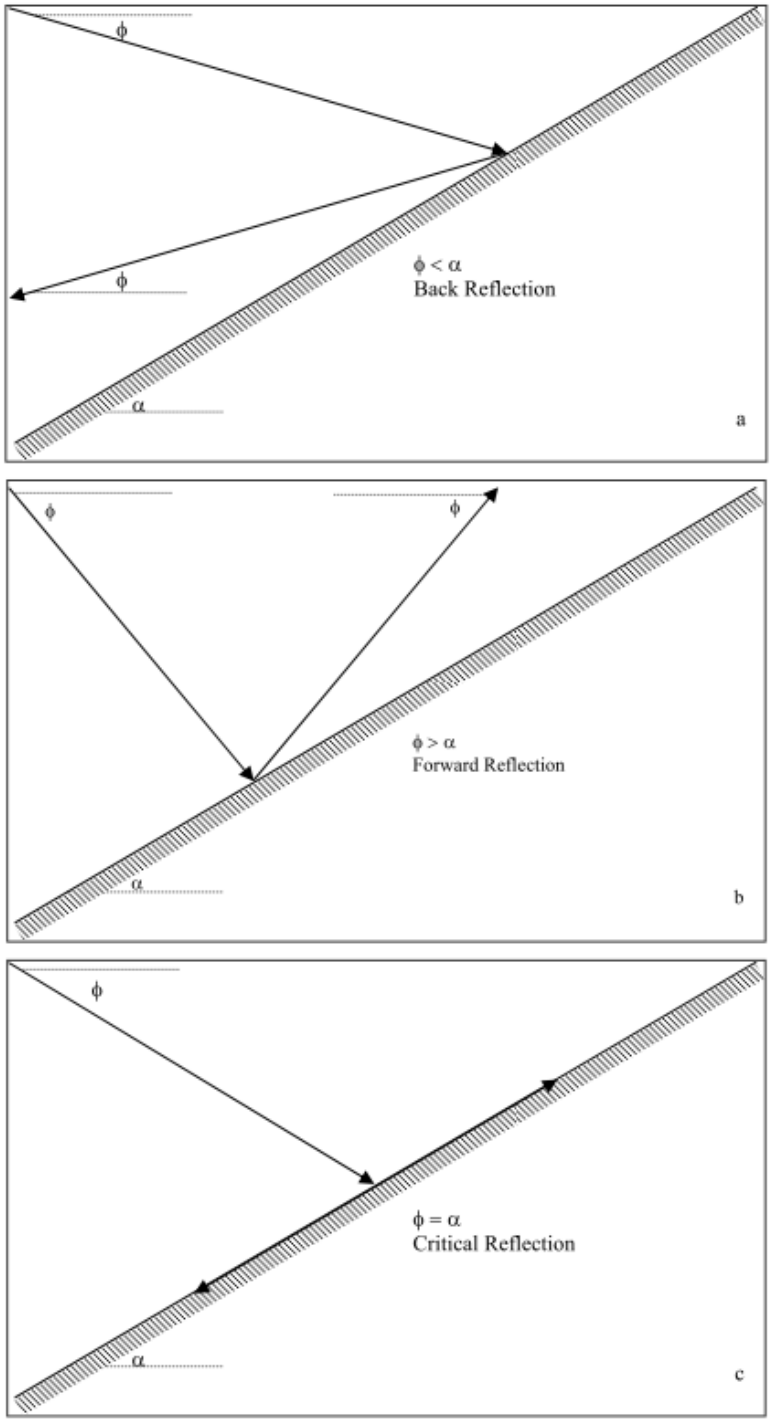

Figure 2.3. Internal waves reflecting off a sloping boundary at angle α, with energy propagating angle φ: (a) subcritical reflection; (b) supercritical reflection; (c) critical reflection.

when $\varphi = \alpha$, a critical reflection occurs, propagating energy along the boundary in both directions.

Cacchione and Wunsch (1974) examined the linear wave theory by generating internal waves in a laboratory tank with stratified fluid to observe their interaction with a sloping boundary. The waves were broken into three classes based on the ratio of boundary slope to wave slope defined $c = [\omega^2/(N^2 - \omega^2)]^{1/2}$, when ω is the wave frequency. When this ratio was less than one (subcritical), they found that the waves followed the linear wave theory before they interacted with the sloping boundary, causing mixing and a great deal of dissipation. When the ratio was approximately one (critical), the waves were damped inducing an unstable bottom boundary layer, which eventually propagated back into the interior. When the ratio was greater than one (supercritical), the internal wave field became inhomogeneous, governed by nonlinear processes and the waves did not break but dissipated via laminar processes.

In many stratified water bodies, waves with a variety of frequencies may be present (Garrett and Munk 1979; Lemckert et al. 2004). Garrett and Munk (1979) described the many different wave fields found in the ocean including waves present at the same time with different frequencies. Spectra of isotherm displacements were identified as the standard method used to examine the content of the internal wave field. Coherence, the statistical measure of likeness, was considered a compelling method to identify vertical and horizontal wavenumbers by comparing two isotherms at the same location and the same isotherm at two locations. Eriksen (1985) evaluated the reflection of the internal wave field near the sloping boundary using a model and discovered that the subsequent energy spectrum was most perturbed when the wave reflection was near-critical. Gilbert and Garrett (1989) studied the

effect of topography on turbulence for a few shapes typical in aquatic systems. They found critical breaking internal waves at a convex boundary were associated with increased energy above the boundary and also greater rates of energy dissipation than if the boundary was concave in a uniformly stratified ocean.

Field measurement of internal waves reflected along the steep sloping bottom in the North Pacific Ocean deviated from predictions using the linear wave theory (Eriksen 1998). Although linear wave theory could be successfully applied to many aspects of the field observations, it was not useful for all the observations. The local critical frequency was accurately identified, but the peak amplitude and vertical offslope decay scale were not. At critical frequencies, the wavenumber vanished instead of extending to infinity, as the linear wave theory predicts. Noncritical waves reflect some of their energy back into the interior, and reflected waves were able to be observed as far as 750 m above the boundary (Eriksen 1998). Dauxois and Young (1999) analyzed critical reflection of nonlinear internal gravity waves along a sloping boundary in a stratified fluid using the method of matched asymptotic expansion. The conditions which reflecting internal waves generated near-shore turbulence and subsequent intrusive offshore transport were also scrutinized.

As mentioned previously, a seiche is a special type of internal waves that occurs when basin scale motions are present in the lake. Sustained wind stress causes the surface layer to tilt, or “set up”, and to compensate for the horizontal pressure gradient created by this tilt, the water below the epilimnion tilts as well. After set-up occurs and the wind relaxes, the tilted layer begins to oscillate. Maiss et al. (1994) observed the wind stress push the surface water towards the downwind end of the lake, causing a horizontal pressure gradient,

leading to the deeper water moving toward the upwind side. As the wind died, an internal seiche was released as the hydrostatic force reversed direction.

The first horizontal mode seiche has one node. In a rectangular basin, the node would be in the center, and the wavelength would be twice the basin length. Second horizontal modes have two nodes, third horizontal modes have three nodes, and so on. Because few natural lakes are rectangular, Lemmin and Mortimer (1986) developed a one-dimensional two-layer model that accounts for the nonuniform bathymetry and hypsography. Field observations showed that reasonable estimates of seiche period and structure could be established with their model for the first three horizontal modes in Lake Zurich and Lake Lugano and the first four horizontal modes in Lake Baldegg. Internal seiche structure is highly dependent on bathymetry and stratification making observations of large horizontal modes infrequent (Fricker and Nepf 2000).

When the basin is large enough, the Earth's rotation becomes significant and affects the direction of the basin scale oscillations. The Rossby radius is the length scale used as the threshold for rotational motion in lakes (Wüest and Lorke 2003a). The internal Rossby radius L_R was defined as (Patterson et al. 1984)

$$L_R = \frac{(g' h_1)^{1/2}}{f} \tag{2.10}$$

where g' is reduced gravity, f is the Coriolis parameter and h_1 is the depth of the thermocline in the lake. Lakes with an internal Rossby radius larger than the width of the lake experience negligible rotational force and typically sustain standing waves. However, when the internal Rossby radius is smaller than the lake dimensions, the rotation of the Earth plays a significant role in the internal wave field. Waves such as Kelvin and Poincaré waves

have been observed on several occasions in Mono Lake (MacIntyre et al. 1999, 2009), Lake Kinneret (Antenucci et al. 2000; Lemckert et al. 2004; Marti and Imberger 2008), and Lake Constance (Appt et al. 2004; Lorke et al. 2008). Kelvin waves propagate along the lake boundary in a counter-clockwise manner such that the boundary is always on the right in the Northern Hemisphere with a maximum velocity along the boundary. Poincaré waves propagate clockwise in the Northern Hemisphere with a maximum velocity at the center of the lake.

Disturbances that do not follow the linear wave theory are also possible. Boegman et al. (2005a) examined the basin scale energy flux of internal waves in a two layer stratified environment in a closed basin. If the inverse Wedderburn number W^{-1} was less than 0.3, then standing basin scale waves should propagate; otherwise, nonlinear surges and solitary waves will be generated. Internal waves and surges can either reflect back into the lake interior upon experiencing the lake boundary or they may break along the boundary of the lake. The breaking of an internal wave on the lake boundary resulted in 10% to 75% of the wave energy lost to dissipation and mixing, while the rest remained with the reflected wave. Boegman et al. (2005b) found that 99% of the available potential energy can be found in the first mode seiche.

In two layer systems such as those considered by Lemmin and Mortimer (1986), Lowe et al. (2002), Horn et al. (2001), and Boegman et al. (2005a,b), only one vertical mode is possible. But in systems with n number of layers, up to the vertical mode n seiche is possible. In lake with a sharp density gradient, vertical mode one can dominate, and when the metalimnion has finite thickness and occupies a significant portion of the water column, mode two is common (e.g., Wiegand and Chamberlain 1987, Münnich et al. 1992). However,

in a lake stratified throughout the water column, a large vertical wavenumber is possible. The vertical mode one seiche is by far the most observed, as high vertical modes are uncommon. However, other vertical modes greater than one have been observed on a few occasions (e.g., Gloor et al. 1994, Stevens and Imberger 1996, Antenucci et al. 2000, Appt et al. 2004, Vidal et al. 2005, Marcé et al. 2007, Marti and Imberger 2008).

Münnich et al. (1992) developed an n-layer model which could be used to identify not only the wave periods and the location of the vertical node but also the resulting velocity profile based on the stratification. The model was based on the vertical mode equation from the momentum and continuity equations. From field data, the vertical mode equation suggested that shear from the second mode was responsible for significantly more mixing at the sediment boundary than in the interior of the hypolimnion. The period of the second vertical mode was found to depend strongly on the metalimnion thickness, while the period of the first mode mainly depended on the mean depth of the metalimnion. Using spectral analysis, Wüest et al. (1996) identified the two dominant seiching modes to be the V1H1 and V2H1 modes also using the model from Münnich et al. (1992).

The vertical and horizontal displacement of fluid is caused by seiches. For first vertical modes the greatest vertical displacement occurs near the lake's side walls with the smallest displacement and thus vertical velocity occurring near the node in the lake's interior. Once a seiche has begun to oscillate, it decays mainly because of friction at the lake boundary but can dissipate quickly when compared to the period of the seiche. Using thermistor chain and wind data from long and narrow Kootenay Lake, Stevens et al. (1996) noted that response times for initiation of internal waves were generally much larger than wind forcing events. They described the seiching amplitudes and periods of the basin using

the horizontal equation of motion and the continuity equation. Also, over 80% of the energy input to the lake from the wind setup is lost within the first internal wave period.

Horn et al. (2001), using a simple two layer laboratory model neglecting the rotation of the Earth, identified mechanisms for the deterioration of interfacial gravity waves. By tilting a tank with a layer of fresh water over a layer of salt water and returning the tank to horizontal, gravity driven disturbances formed. Horn et al. (2001) identified five separate mixing regimes defined by the inverse Wedderburn number W^{-1} and the ratio of the surface layer depth h_1 to total depth H. The five regimes defined by Horn et al. (2001) included damped linear waves, solitary waves or solitons, supercritical flow, Kelvin-Helmholtz billows, and bores and billows. No matter the depth ratio, if the Wedderburn number was greater than 5, damped linear waves were present and outside this region, linear wave theory would not apply. Results from several lakes followed the regimes as well. Horn et al. (2001) determined that most lakes should form solitons, caused by the nonlinear steepening of the initial basin scale wave.

Mixing

Boundary Mixing Theory

Much mixing can originate from wind induced waves interacting with the boundaries of basins. For the past several decades in lakes and the ocean the current hypothesis is that mixing is dominated by boundary processes (Munk 1966). The vertical eddy diffusivity, a parameter used to measure mixing intensity, can be several magnitudes larger onshore in lakes (Wüest et al. 1996; Goudsmit et al. 1997; MacIntyre et al. 1999; Wüest and Lorke 2003b) and the ocean (Ledwell and Hickey 1995; Ledwell and Bratkovich 1995; Polzin et al.

1997; Gregg 1998; Ledwell et al. 2000; Nash et al. 2004). Spatial comparison of microstructure profiles (Polzin et al. 1997; Gregg 1998; MacIntyre et al. 1999; Ledwell et al. 2000; Nash et al. 2004), dye dispersion studies (Ledwell and Hickey 1995; Ledwell and Bratkovich 1995; Wüest et al. 1996; Goudsmit et al. 1997; Wüest and Lorke 2003b), and acoustic velocity profiles (Lorke 2007) were used to come to this conclusion. This evidence leads one to believe that patterns of vertical mixing are linked directly to the local bathymetry.

Munk (1966) used temperature and salinity profiles in the Pacific Ocean to estimate the vertical eddy diffusivity to be roughly 10^{-4} m^2 s^{-1}, balancing heat flux and vertical upwelling in the open ocean. The diffusivity, which was three orders of magnitude larger than the molecular diffusivity of heat, was able to maintain the observed stratification. Wunsch (1970) determined theoretically that isopycnals in lakes or the ocean must satisfy the no flux condition and intersect normal to sloping boundaries, prompting mean up-slope velocity along the boundaries driven by the buoyancy flux. Wunsch (1970) proposed that boundary mixing from the flow along the boundaries may account for a significant portion of the basin circulation and be significant in regards to vertical transport in stratified basins. Phillips (1970) found theoretically and experimentally that isopycnals followed the no flux condition by normal intersection of sloping sidewalls, confirming the findings of Wunsch (1970). Thus, hydrostatic equilibrium could no longer exist, causing the fluid at the boundary to flow up-slope.

A few years later, Armi (1978) proposed that the two processes of boundary mixing and offshore isopycnal transport produced enough mixing that the traditional value in the ocean interior of vertical diffusivity of 10^{-4} m^2 s^{-1} could be obtained. Armi (1978) discovered

turbulent boundaries in the deep ocean approximately 50 m to 150 m thick and the lateral advection from the turbulent boundary layers offshore along isopycnals from profiles of temperature and salinity. The elevated turbulence along the boundary was attributed to shear from mean currents. Armi (1978) also observed suspended particulate matter in the turbulent layer which was transported offshore causing a nepheloid layer. Wind acting on a stratified lake would generate a similar response to that of the deep ocean. Garrett (1979), however, believed that a vertical diffusivity of 10^{-4} m^2 s^{-1} was an overestimation and that the effective vertical eddy diffusivity was no less than an order of magnitude smaller. Garrett (1979) also believed that previously presented mixing efficiencies were too large because boundary mixing simply mixed previously mixed fluid, leading to an inefficient process. Nonetheless, Garrett (1979) did concede that ocean mixing at the boundary and the resulting entrainment into the interior of the ocean could be significant in terms of vertical mixing.

Mixing Efficiency

Garrett (1990) attempted to assess the role of secondary circulation in the boundary layer and how it affects boundary mixing efficiency as well as the ability of secondary circulation to restore stratification after it has been mixed by breaking internal waves. To satisfy the zero flux condition at a boundary, isopycnals must intersect normal to the boundary, causing lighter fluid beneath heavier fluid. This phenomenon creates mixing near-shore due to the buoyancy flux in the vertical referred to as secondary circulation. Garrett (1990) determined that secondary circulation caused an advective buoyancy flux as a result of bidirectional secondary flow parallel to the boundary due to buoyancy flux at the boundary. On the other hand, restratification is also a result of secondary circulation, which in turn may increase the efficiency of boundary mixing, rendering the overall effect of

secondary circulation in terms of boundary mixing to be equivocal. However, several studies have found that water from the interior continually resupplies the mixed water in the boundary (e.g., Ivey and Corcos 1982, Slinn and Riley 1996, Lorke et al. 2008), which would increase the mixing efficiency, contradicting Garrett (1990).

The mixing efficiency, the fraction of mechanical wave energy converted to potential energy via mixing, can be used to determine how effectiveness of mixing processes in the ocean and lakes. Several estimates of mixing efficiencies have been suggested using theoretical considerations (e.g., Garrett 1990, Ivey and Imberger 1991, Garrett et al. 1993), numerical simulations (e.g., Osborn 1980, Slinn and Riley 1996) experiments in stratified fluids in the laboratory (e.g., Ivey and Nokes 1989, Stevens and Imberger 1996, Barry et al. 2001, Rehmann and Koseff 2004, Boegman et al. 2005a), as well as in the ocean (e.g., Ruddick et al. 1997), and lakes (e.g., Gloor et al. 2000, Wüest and Lorke 2003a, Lorke et al. 2008).

Garrett et al. (1993) examined how boundary mixing in the stratified ocean near sloping boundaries affects the interior stratification and how stratification along with bottom slope combines to modify the seafloor's no-slip boundary condition in the interior. Mixing near the slope of lakes and oceans, which was greater than mixing in the interior, can be an important mechanism for the generation of boundary layers. Garrett (1990) argued that previous accepted mixing efficiencies were amplified because reduction in boundary layer stratification was not considered. From the comparison of total flux to vertical diffusive flux, the mixing efficiency along the boundary was defined and determined to be a fraction of the earlier basin-averaged mixing rate.

Ivey and Imberger (1991) derived the mixing efficiency from the turbulent kinetic energy equation to be the ratio of buoyancy flux b to the net mechanical energy available to generate turbulent motions m_{net}. The efficiency of mixing was estimated to be around 0.20 when the turbulent Froude number was approximately equal to one and when the turbulent Reynolds number is greater than 10. However the mixing efficiency also depends on the means which turbulence is generated.

Koop (1976) determined the efficiency of mixing to decrease from 0.25 at low Richardson numbers to 0.01 at a Richardson number of 0.20. The mixing efficiency is typically taken as 0.20 but varied with stratification (Osborn 1980). Slinn and Riley (1996) found the mixing efficiency to be near 35% for critical reflection of internal waves. Another 55% is dissipated as heat and the remaining 10% reflects away from the turbulent boundary layer in the form of a smaller scale gravity wave.

Ivey and Nokes (1989) estimated that the mixing efficiency was typically around 10% and never above 20% in a continuously stratified laboratory tank experiencing critical breaking internal waves. Stevens and Imberger (1996) observed mixing efficiencies between 1% and slightly larger than 31%. The peak efficiency was observed with a Lake number of approximately one and drops when the Lake number is greater than or less than one. The mixing efficiency has also been compared to turbulent parameters such as the turbulence intensity parameter. Barry et al. (2001) found that the mixing efficiency of turbulence from a towed grid decreased from 0.2 with increasing $\varepsilon/\nu N^2$ when ε is the dissipation of turbulent kinetic energy and ν is the kinematic viscosity, contrary to what was observed previously in the open ocean (Ruddick et al. 1997). Ruddick et al. (1997) found the mixing efficiency to increase with the turbulence intensity parameter $\varepsilon/\nu N^2$, ranging from 0.1 to 0.35, in the

upper region of the North Atlantic Ocean from microstructure profiles. Using the Richardson number as a measure of stratification strength as in Osborn (1980), the mixing efficiency increased with strengthening stratification up to 6% due to grid generated turbulence in a laboratory setting (Rehmann and Koseff 2004).

Gloor et al. (2000) found that seiches were regularly excited in Lake Alpnach generating a well mixed layer of fluid near the lake boundary which gravitationally collapsed and moved offshore. The ratio of the rate of change in potential energy caused by turbulence to the loss of energy from bottom friction, or the mixing efficiency, increased from approximately 0.01 for the deepest well-mixed layer to 0.15 in the upper pycnocline. Therefore, mixing in the quasi-stationary layer at the deepest part of the lake exists, but it is inefficient. Periodic generation of well-mixed layers on the sloping boundaries and the resulting intrusions have higher mixing efficiencies due to restratification of mixed fluid. Wüest and Lorke (2003a) performed a review of large data sets from a number different lakes, and estimated the mixing efficiency to be 0.15. Lorke et al. (2008) observed internal seiching motions which resulted in upwelling of cold water along the boundary which lead periods of unstable stratification in Lake Constance. The mixing efficiency varied from 0.1 under stable conditions to 0.2 in unstable stratification.

Mixing Mechanisms

In lakes, two main mechanisms that generate boundary mixing can be identified. The first process is internal waves reflecting critically at the lake boundary. The generation of turbulence by breaking internal waves on slopes leading to boundary mixing processes has been studied in the laboratory (Ivey and Nokes 1989; De Silva et al. 1997; Boegman et al. 2005a), in numerical simulations (Eriksen 1985; Slinn and Riley 1996), in lakes (MacIntyre

et al. 1999; Lorke 2007), as well as in the ocean (Ledwell et al. 2000; Rudnick et al. 2003). The second process occurs when seiching motion is excited in a lake. The bed shear from basin-scale currents interacting with the boundary generates mixing (Fischer et al. 1979; Gloor et al. 1994; 2000; Fricker and Nepf 2000; Wüest and Lorke 2003b; Hondzo and Haider 2004; Lorke and Wüest 2005; Lorke et al. 2005; Marti and Imberger 2008).

A number of observations of internal waves provoking mixing near the boundary of a stratified water body have occurred. Ivey and Nokes (1989) evaluated vertical mixing along a sloping boundary caused by critical breaking internal waves in a continuously stratified fluid in a laboratory tank. A turbulent bottom boundary layer formed on the sloping boundary with its thickness a function of the incident wave amplitude. The fluid in the boundary layer moved offshore not in small-scale intrusions but as a slow cavity-scale circulation over the entire depth of the tank. In a similar study, breaking internal waves formed turbulent mixed fluid along the smooth, sloping boundary; the mixed fluid then collapsed and intruded horizontally into the interior of the linearly stratified fluid along isopycnals (De Silva et al. 1997). As the waves become closer to critical, the turbulence increased. Unlike Ivey and Nokes (1989), who caused waves to break along the entire sloping boundary, De Silva et al. (1997) generated waves only at a localized region similar to the metalimnion of a lake. Therefore, a horizontal pressure gradient between the locally mixed region and the ambient stratification was generated, causing the mixed fluid to move offshore locally along isopycnals in the form of an intrusion. Energy transfer was monitored in another laboratory setting as the wind forced basin generated turbulent motions and energy was lost due to breaking of internal waves along the sloping topography (Boegman et al. 2005a). The ratio of the boundary slope to wave slope (amplitude/wavelength), or the Iribarren number, was used

to estimate the energy loss along the slope, mixing efficiency, and the breaker type. As much as 20% percent of the wind generated potential energy was sustained in the boundary layer at the pycnocline.

A numerical model indicated internal wave reflection near rough topography was the most substantial mechanism leading to mixing near ocean boundaries, which could lead to potential estimates of basin scale vertical diffusivity (Eriksen 1985). Slinn and Riley (1996) used numerical simulations to identify a turbulent boundary layer in the benthic region due the breaking of internal waves over sloping topography. The turbulent boundary layer exhibited quasi-periodic behavior and had a thickness of approximately one-third the wavelength of the oncoming wave.

MacIntyre et al. (1999) found the dissipation rate of turbulent kinetic energy was two to three orders of magnitude higher onshore where the pycnocline intersected the lake boundary compared to a similar depth offshore in Mono Lake, CA. This observation indicated that a large amount of kinetic energy was lost by critical internal waves breaking in the pycnocline at the lake boundary. Lorke (2007) observed diapycnal diffusivities that exceed background values by up to four magnitudes during the presence of high-frequency internal waves. Acoustic velocity profiles revealed the effect high-frequency internal waves had on boundary mixing.

In the coastal ocean, diapycnal diffusivity is rarely greater than 10^{-6} m^2 s^{-1}, as confirmed by dye tracer release experiments (Ledwell et al. 2004) and microstructure measurements (Rehmann and Duda 2000), which is only an order of magnitude larger than the diffusivity of heat. However, microstructure profiles (Ledwell et al. 2000) and temperature profiles (Rudnick et al. 2003) provided clear evidence that with decreasing depth

above the rough sea floor, an increase in diffusivity can occur. Greater turbulence was generated along the ocean boundary primarily due to the breaking of internal waves and is responsible for the majority of the ocean mixing. The energy required to provoke and retain a mixed boundary layer is provided by the interaction of internal waves with rough topography (Rudnick et al. 2003). Also, tide flows caused internal wave reflection or generation near rough bathymetry inducing shear, which is one of the main sources of elevated boundary turbulence. The larger mixing rates previously suggested may play a vital role in closing the heat budget of the ocean basins (Ledwell et al. 2000; Rudnick et al. 2003; Wunsch and Ferrari 2004).

The enhanced turbulence and thus dissipation along the continental slope (Dickson and McCave 1986; Thorpe and White 1988; Rudnick et al. 2003; Nash et al. 2004) and a fjord (Inall 2009) are primarily attributed to the semidiurnal tide reflecting critically on the ridge. The subsequent turbulent layers have also been sources of intrusions, caused by gravitational collapse of the mixed fluid (Thorpe and White 1988; Inall 2009). Additionally, nepheloid layers have been traced back to a boundary nepheloid layer generated by mixing from the reflected tide at the boundary (Dickson and McCave 1986; Thorpe and White 1988). The nepheloid layers were up to 200 m thick (Dickson and McCave 1986) and extended along the ridge for up 100 km and propagated up to 16 km into the interior (Thorpe and White 1988) and the material from the nepheloid layers remained suspended long after the event that generated it ceased.

Observations of mixing provoked by the interaction of seiches with lake boundaries are not quite as common. In Lake Alpnach, the boundary layer, temporally varying between 2 and 7 m in thickness, was caused by shear due to the seiching motion along the lake

boundary (Gloor et al. 1994). Seiching was deemed the cause of the boundary layer because a period of more than a month is required to generate a boundary layer of that magnitude and the varying thickness of the boundary layer was solely caused by it. Fricker and Nepf (2000), from thermistor chain data in Upper Mystic Lake, used a two-dimensional numerical model to identify the consequences of seiching for different basin shapes. Results from the model show that by altering the basins shape, the boundary shear is greatly influenced. Gloor et al. (2000) observed that when regular seiching motion fails to exist, so did a 4 to 5 m thick turbulent bottom boundary layer. Shear-induced convection caused by pockets of colder water above warmer water resulting from internal seiching was introduced as a mechanism that generates buoyancy driven mixing near the slope (Wüest and Lorke 2003b).

Temperature microstructure (Marti and Imberger 2008) and acoustic Doppler velocimeter (Hondzo and Haider 2004) measurements revealed friction caused by a seiche interacting with the sloping boundary created local turbulence generating a turbulent layer near the boundary of a lake. From scaling, Hondzo and Haider (2004) proposed that boundary layer thickness δ depended on the kinematic viscosity ν, dissipation of turbulent kinetic energy ε, the buoyancy frequency, the slope length L_s and angle α of the sloping boundary so that

$$\delta = \left[\varepsilon^{3/2} L_s / \left(N^4 \nu^{1/2} \cos\alpha\right)\right]^{1/3}. \tag{2.11}$$

Like Lemckert et al. (2004), the thickness of the bottom boundary layer depended on the location in the lake and phase of the internal wave field. Marti and Imberger (2008) also used the Estuary and Lake Computer Model (ELCOM) to examine the velocity structure caused by the internal waves and the boundary layer thickness. The model successfully predicted the

spatial and temporal evolution of the benthic boundary thickness. Temperature fluctuations, velocity, and drogue tracks from the model compared well with field observations.

Turbulence in bottom boundary layers induced transport and vertical mixing in stratified lakes or oceans. The vertical diffusivity was 3×10^{-6} m^2 s^{-1} at the injection depth in the hypolimnion of Lake Alpnach, estimated using the vertical spreading of a tracer dye sulfur-hexafluoride (Wüest et al. 1996). Modeling the vertical diffusion with Fick's Law gives the vertical diffusivity as 10^{-6} m^2 s^{-1} to 8×10^{-5} m^2 s^{-1} from uranin, a dye tracer, that was injected into the interior of the hypolimnion, where vertical mixing was insignificant until the tracer contacted the lake boundary where the vertical diffusivity increased by an order of magnitude (Goudsmit et al. 1997). For a second injection near the lake boundary, the vertical diffusivity was high initially and decreased substantially as the tracer was transported off-shore.

Measuring Vertical Mixing

Three different methods have been used to estimate vertical eddy diffusivity: microstructure profile, heat budget method, and tracer distribution. To estimate vertical diffusivity, some of the previous studies have used only microstructure profiles (Gloor et al. 2000; Wain and Rehmann, in press), some have used simultaneous microstructure and heat budget (MacIntyre et al. 1999), some have used the heat budget method simultaneously with a tracer study (Goudsmit et al. 1997; Ledwell et al. 2004; MacIntyre et al. 2009), and some use all three methods simultaneously (Wüest et al. 1996).

Because several studies have used more than one method to estimate the vertical eddy diffusivity the approaches can be compared. Based on the vertical distribution variance of a dye cloud the average vertical eddy diffusivity was 2×10^{-6} m^2 s^{-1} in the pycnocline of the

interior of Mono Lake (MacIntyre et al. 2009). Microstructure was measured at the same level of the dye patches during tracer studies, and they found diffusivities between 10^{-6} m^2 s^{-1} and 10^{-5} m^2 s^{-1}, in agreement to the results from the tracer studies (Ledwell et al. 2004). Using a separate technique, the heat budget method from Jassby and Powell (1975), vertical eddy diffusivities from temperature profiles in the hypolimnion of a Swiss lake were also consistent to what was observed from the tracer study. MacIntyre et al. (2009) also found that the average diffusivity via the heat budget method was less than a factor of four larger than diffusivity via a tracer study, which was attributed to the lack of interaction between the dye tracer and the boundaries. Wüest et al. (1996) measured diapycnal diffusivity from the heat budget method, microstructure profiles and dye profiles in order solve the problem of vertical diffusivity measured via microstructure measurements (10^{-5} m^2 s^{-1}) in the stratified open ocean typically being an order of magnitude smaller than the diffusivity measured with basin-wide tracer studies and heat budget method (10^{-4} m^2 s^{-1}). The apparent variation between the two methods was found to not result from errors in the microstructure method as the techniques yield equivalent results when the effects of boundary mixing are included in the basin wide comparison (Wüest et al. 1996). Therefore, the results lead to the conclusion that even the diffusivity in the stratified region of the ocean is an order of magnitude less than the basin-wide diapycnal diffusivity ocean interior because the basin wide diffusivity in lakes and the ocean is dominated by bottom boundary process (Wüest et al. 1996).

Turbulence Parameters

It is important to quantify boundary turbulence because of its impact on lake mixing. Internal seiching caused recurring periods of stable and unstable temperature structure from oscillating cross-slope currents within the boundary layer (Lorke et al. 2005). Unstable

stratification and convective mixing occur when colder water is transported above warmer water when upwelling velocities are greatest. As the phase of downwelling commences, warmer water travels down-slope causing a thin, strong and stably stratified boundary layer. While the magnitude of velocities in the boundary as a seiche moves up-slope and down slope is the same, that cannot be said for shear induced mixing. Shear-induced mixing lead to a significant increase of vertical diffusivity during unstable stratification (Lorke et al. 2008). Boundary layer current profiles were not consistent with the log law during upwelling and downwelling; additionally the maximum velocity even occurred near the sediment interface during some downwelling spells (Lorke et al. 2005). Using an acoustic Doppler current profiler, estimates of the dissipation of turbulent kinetic energy have been obtained from the inertial dissipation method (Lorke and Wüest 2005) and the structure function method (Lorke 2007; Lorke et al. 2008) over extended time series. A reasonable agreement was discovered to exist between the two methods which provided further confidence in the accuracies of both (Lorke 2007). MacIntyre et al. (1999) quantitatively addressed energy dissipation in the pycnocline of Mono Lake using microstructure profiles.

Regardless of the means, once it is established that turbulence has been induced, the effect it has on overturning the current stratification must be determined. Using scaling, a number of dimensionless parameters have been developed to determine if the turbulence can irreversibly mix stratified fluid. The two most common dimensionless ratios used in stratified shear flows are the turbulent Froude number Fr_t and the turbulent Reynolds number Re_t, defined respectively as (Ivey and Imberger 1991)

$$Fr_t = u/(NL_c), \tag{2.12}$$

and

$$Re_t = uL_c/\nu. \tag{2.13}$$

The length scale of the most energetic overturns from a density profile (the centered displacement scale) is L_c, ν is the kinematic viscosity, and scaling and laboratory testing show the root mean square of the velocity u displays an excellent correlation with the cube root of the product of the turbulent energy dissipation ε, and L_c so that $u \sim (\varepsilon L_c)^{1/3}$. In addition to the centered displacement scale, the turbulent Reynolds and Froude numbers can also be written in terms of the Ozmidov length scale $L_o = (\varepsilon/N^3)^{1/2}$ and the Kolmogorov length scale $L_K = (\nu^3/\varepsilon)^{1/4}$ as $Re_t = (L_c/L_K)^{4/3}$ and $Fr_t = (L_o/L_c)^{2/3}$, respectively. From the Ozmidov scale and the Kolmogorov scale, the dimensionless turbulence intensity parameter is $\varepsilon/\nu N^2 = (L_o/L_K)^{4/3}$ (Ivey et al. 2008).

From the turbulence intensity parameter, the eddy diffusivity can be estimated (Osborn 1980). From the turbulent kinetic energy (TKE) equation (neglecting the unsteady term, transport of turbulence by kinetic energy from the mean flow, and all divergence terms), the turbulent production was found to balance with dissipation and the buoyancy flux.

$$\overline{u_i' u_j'} \frac{\partial \overline{u_i}}{\partial x_i} = \varepsilon + \frac{\overline{u_3' \rho'} g}{\bar{\rho}} \tag{2.14}$$

where the term on the left defines turbulent production, ε is the dissipation, and the term on the right is the buoyancy flux b. To generalize (2.14), Ivey and Imberger (1991) used m_{net} to denote all terms but the dissipation and buoyancy flux and wrote the TKE equation as $m_{net} = \varepsilon + b$. The flux Richardson number can be written as (Ivey and Imberger 1991)

$$R_f = \frac{b}{m_{net}} = \frac{1}{1+\varepsilon/b}. \tag{2.15}$$

Using the equation for vertical diffusivity K_ρ (Ivey et al. 2008),

$$K_\rho = \frac{\overline{u_3' \rho'} g}{\bar{\rho} N^2} = \frac{b}{N^2} = \frac{R_f}{1+R_f} \frac{\varepsilon}{N^2} = \Gamma \frac{\varepsilon}{N^2} \tag{2.16}$$

where N^2 is the buoyancy gradient and Γ is related to the mixing efficiency and typically taken as 0.20 but is variable (Osborn 1980).

Using the Osborn method to determine the vertical eddy diffusivity causes some uncertainties primarily stemming from the value assumed for the mixing efficiency. Barry et al. (2001) used the turbulence intensity parameter $\varepsilon/\nu N^2$ to interpret their turbulence results because it conveniently described the magnitude of turbulent dissipation relative to the damping effects of viscosity and buoyancy. Barry et al. (2001) found that the mixing efficiency Γ decreased from 0.2 with increasing $\varepsilon/\nu N^2$ due to horizontal oscillation of a grid in a linearly stratified laboratory tank. This result is contrary to what was observed previously in the open ocean, where the efficiency increased with $\varepsilon/\nu N^2$ (Ruddick et al. 1997). Using numerical simulations of sheared, stratified turbulence, Shih et al. (2005) outlined regimes in terms of the turbulence intensity parameter. The diffusive regime occurs when $\varepsilon/\nu N^2 < 7$ and is defined by decaying turbulence where the total diffusivity decreases to the molecular level. In the intermediate regime, diffusivity depends linearly on $\varepsilon/\nu N^2$ as predicted by Osborn (1980) and exists when $7 < \varepsilon/\nu N^2 <$100. In the intermediate regime, a value of Γ=0.2 has been proven from lab results to be accurate (Shih et al. 2005). The energetic regime is represented by values of $\varepsilon/\nu N^2 >$ 100, and is defined by growing turbulence where the diffusivity scales with $(\varepsilon/\nu N^2)^{1/2}$. Shih et al. (2005) observed that in the energetic regime the mixing efficiency declines because the turbulence is more than sufficient to break down the stratification, resulting in the mixing of mixed fluid, as observed in the ocean by Garrett (1990).

Transport

A number of studies have been undertaken in order to advance the knowledge of transport in lakes. As previously noted, the transport in lakes has an important chemical, biological, and ecological impact because more than just fluid is being transported; nutrients such as phosphorus, dissolved gasses, sediment, organic material, and pollutants are also influenced. Drifter experiments (Stocker and Imberger 2003) and dye tracer studies (Murthy 1976; Maiss et al. 1994; Lawrence et al. 1995; Wüest et al. 1996; Peeters et al. 1996; Goudsmit et al. 1997; Stevens et al. 2004; MacIntyre et al. 2009) were executed revealing the transport and mixing rates vertically and horizontally in the interior of lakes and the ocean (Okubo 1971; Sundermeyer and Ledwell 2001; Ledwell et al. 2004).

Okubo (1971) performed instantaneous dye tracer experiments in the mixed layer of the ocean on times scales from 2 h to 1 month and length scales of 30 m to 100 km. Okubo (1971) developed a model based on Fickian diffusion to estimate horizontal diffusion from tracer spreading defined as $K = \sigma^2/(4t)$, where σ is the standard deviation of the tracer distribution and t is the time elapsed. Sundermeyer and Ledwell (2001) and Ledwell et al. (2004) performed dye release experiments shelf south of New England near the 70 m isobaths to estimate the diapycnal diffusivity, with temporal and spatial scales of up to 100 h and 50 km^2.

The majority of studies examining the transport in lakes are performed in the surface layer. From the drifter experiments, which typically had durations of 2 to 8 d, the average dispersion coefficient, an estimate of mixing and transport, observed in the surface layer was approximately 1.2-26 m^2 s^{-1} from the standard deviation cluster model, Lagrangian statistics model, and mean shear model (Stocker and Imberger 2003). The standard deviation cluster

model defined dispersion in the x-direction as $K_{xd} = 0.5\ d\sigma_x^2/dt$, where σ_x is the standard deviation of the drifter in the x-direction. The Lagrangian statistics model defined dispersion in the x-direction as $K_{xd} = L_x^2/t$, where L_x is the length scale of the drifters in the x-direction and t is the time scale. Finally, the mean shear model defined dispersion in the x-direction as $K_{xd} = 1.5c_2(\partial u/\partial y)^2\kappa_y t^2$, where c_2 is a constant equal to 0.037, u is the velocity in the x-direction, and κ_y is the dispersion in the y-direction from the Lagrangian statistics model. Stocker and Imberger (2003) concluded that the horizontal shear dispersion values from the mean shear model were on the same order as the observed dispersion rates from the standard deviation cluster model, suggesting that horizontal shear dispersion plays a key role in horizontal mixing in the epilimnion.

Lawrence et al. (1995) used videotapes of dye tracer studies in the epilimnion of a small lake and the diffusion model of Okubo (1971) to estimate the rate of horizontal dispersion, which was found to increase with a decrease in distance from shore. Lawrence et al. (1995) attributed this phenomenon to wind-driven boundary currents, the irregular topography, and differential heating at the lake boundary. Stevens et al. (2004) performed eight tracer experiments in the epilimnion of Kootenay Lake in British Columbia using Rhodamine WT. The horizontal diffusivity was estimated to be between 10^{-2} m^2 s^{-1} and 10^1 m^2 s^{-1} from application of the Fickian diffusion model from Okubo (1971) and a dye tracer (Stevens et al. 2004).

Other experiments have focused on the hypolimnion of lakes. Murthy (1976) performed a total of 12 dye tracer experiments in the epilimnion and hypolimnion of Lake Ontario in order to identify its horizontal diffusion characteristics. The horizontal eddy diffusivity was one to two orders of magnitude larger in the epilimnion when compared to

the hypolimnion. This phenomenon was attributed to the larger amount of turbulent energy available in the epilimnion. The longitudinal eddy diffusivity was a factor of 5-10 larger than the lateral eddy diffusivity initially and 2-3 times greater for large diffusion times. Maiss et al. (1994) injected sulfur hexafluoride into the hypolimnion of Lake Constance and estimated the horizontal dispersion from the 19 surveys in a three-month period to be between 0.7×10^{1} m^2 s^{-1} and 3×10^{1} m^2 s^{-1} from a one-dimensional box diffusion model based on Fickian diffusion. After extensive review of a number of models applied to the eight tracer studies in the interior of the hypolimnion of four lakes, Carter and Okubo (1965) had the model that provided the most accurate description of the temporal development of a dye cloud size and shape (Peeters et al. 1996). The model of Carter and Okubo (1965) is a shear diffusion model that allows for non-radially symmetric distributions that could describe the cloud size and the variance in the direction of the major and minor axes as a function of time. The effective horizontal diffusivity was between 0.02 m^2 s^{-1} and 0.3 m^2 s^{-1}; however when the effect of the shear is removed in the shear diffusion model, the remaining horizontal diffusivity is between 0.02 m^2 s^{-1} and 0.18 m^2 s^{-1}. Tracer experiments performed in the interior of lake focus on mean shear, not the internal wave induced shear.

The previous work does not examine the transport caused by turbulence near the boundary of a water body. When internal waves interact with a sloping boundary, much of their energy is lost while breaking and creating turbulence near the boundary. After turbulence mixes near boundary fluid, the mixed fluid becomes gravitationally unstable, collapses and is transported offshore along isopycnals. These patches of mixed fluid transported offshore are commonly referred to as intrusions and their generation can be followed in Figure 2.4. Intrusions can transport fluid away from the lake boundary to the

lake's interior for a distance on the order of the internal Rossby radius of the lake, when it is less than the lake's lateral dimension (Thorpe 1998).

Evidence suggesting intrusions resulting from boundary layer process exists in lakes (Caldwell et al. 1978; Gloor et al. 2000; Appt et al. 2004) and the ocean (Dickson and McCave 1986; Thorpe and White 1988; Inall 2009). Caldwell et al. (1978) observed a stepped temperature profile from microstructure measurements along the sloping bottom of a Lake Tahoe caused by intrusion layers due to mixing near the lake boundary. Patches of mixed fluid extending approximately 100 m to 200 m horizontally from a turbulent boundary layer horizontally towards the interior of the lake were designated as intrusions (Gloor et al. 2000). Steepening of the isotherms from seiching caused a surge traveling westward; after

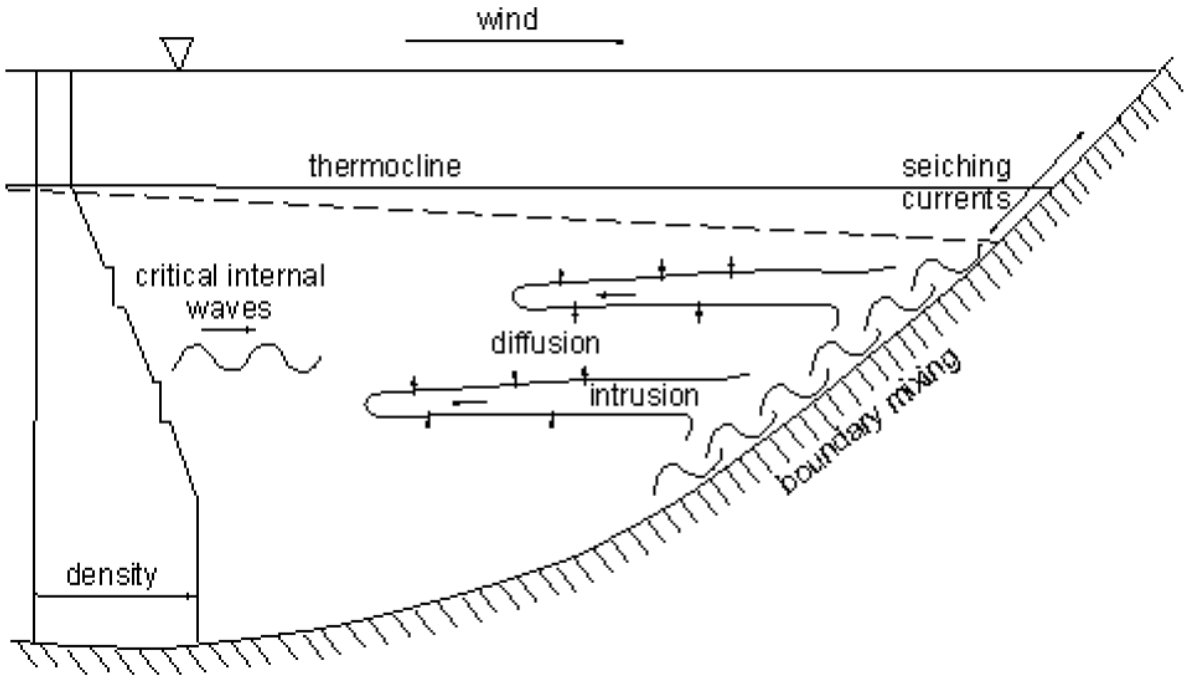

Figure 2.4. Schematic of the physical processes in lakes beginning with wind forcing creating internal waves or seiches which cause mixing and subsequent intrusions.

reflecting off the northwestern boundary, it headed eastward towards the lake's interior. Appt et al. (2004) characterized this as an intrusion. Nepheloid layers, from the breaking of the diurnal M2 tide in the ocean, have also been considered evidence for intrusions (Dickson and McCave 1986; Thorpe and White 1988). With the exception of Inall (2009) and Wain and Rehmann (in press), no field measurements have documented the fate of mixed boundary fluid. Inall (2009) injected a fluorescent dye into the water column near a sloping boundary in a Scottish fjord and intrusions generated from boundary generated turbulence. Wain and Rehmann (in press) used microstructure profiles and the presence of turbid layers as evidence of boundary mixing which was attributed to shearing from seiching currents. Three dimensional dye mapping revealed a distinct intrusion which moved over 200 m offshore with a thickness between 0.5 m and 1m which scaled with the Ozmidov length.

For the most part, the fate and geometry of intrusions have only been identified in a laboratory, not in the field. A number of laboratory experiments have witnessed intrusive gravity currents on the interface separating two fluids (e.g., Lowe et al. 2002, Sutherland et al. 2004). Phillips et al. (1986) provided an expression for the velocity of an intrusion which was based on a viscosity-buoyancy force balance from experiments in a two layer fluid. Lowe et al. (2002) noted that three unique regions could be identified in the intrusion. First, the intrusion front is defined by a nearly uniform velocity front where energy is conserved. Next, the intrusion velocity becomes non-uniform with velocities 50% larger than the front velocities and large billows and mixing occur. Finally, the tail region has little mixing and a nearly uniform velocity slightly larger than the intrusion front. Sutherland et al. (2004) developed an empirical equation to estimate the speed of the gravity intrusive current.

Turbulence along sloping boundary has been generated by an oscillating plate or grid (Thorpe 1982; Ivey and Corcos 1982; Browand et al. 1987; McPhee-Shaw and Kunze 2002; Wells and Helfrich 2004) in the laboratory in linear stratification typical of the hypolimnion of lakes or the thermocline of the ocean to resolve the destination of the mixed boundary fluid. Thorpe (1982) found the thickness of the turbulent area η and the height of the intrusions h_i instigated by the grid were demonstrated to correspond to the buoyancy frequency, amplitude ζ_0, grid oscillation frequency ω_0, and mesh length M_l of the oscillating grid such that η=$0.94{\zeta_0}^{3/4}M_l^{1/4}(\omega_0/N)^{1/2}$ and h_i=$0.34{\zeta_0}^{3/4}M_l^{1/4}(\omega_0/N)^{1/2}$. The once linear density profile becomes step-like in the bottom boundary layer that is generated. Ivey and Corcos (1982) discovered the once linear density profile becomes step-like in the bottom boundary layer and the mixed fluid was transported into the interior of the tank by multiple intrusive layers, proportional to the Ozmidov scale. Hopfinger (1987), from a review, identified a Froude number near one as the threshold for the onset gravitational collapse of turbulent fluid. Hopfinger (1987) stated that intrusions could be described as a buoyancy-inertia force balance unless the intrusions are very weak, where a buoyancy-viscous balance stems from step-like density structure as in Ivey and Corcos (1982). Intrusion thickness was found to be approximately 7 times the Ozmidov scale and the intrusion length is governed by the local Froude number, which decreases as the intrusion length grows (Browand et al. 1987).

After normalizing by the incident energy density flux, the spreading velocity of the intrusions was found to have a linear relationship with the ratio between the incident wave frequency ω, and critical frequency ω_c (McPhee-Shaw and Kunze 2002). Several equally spaced vertical layers developed along the well mixed boundary layer and continued to

spread into the tank's stratified interior with the vertical spacing of the intrusions following ω/ω_c. After a tracer was injected near the oscillating plate, it spread quickly throughout the boundary layer, then collapsed, and moved offshore in the form of an intrusion (Wells and Helfrich 2004). The intrusion transported offshore as a front instead of from diffusion. The effects of rotation of the tank were significant enough to limit the offshore transport of the intrusive layer. Wells and Helfrich (2004) used scaling to estimate the thickness δ of the turbulent boundary layer as $\delta = \gamma(\omega_0/N)^{1/2}$, where γ is a coefficient equal to 1 cm and ω_0 is the frequency of the oscillating bar. The intrusion length l_m is described by $l_m = 0.2N\delta(f_t t)^{0.65}/f_t$, when f_t is twice the tank rotation rate and t is the time.

In additional laboratory experiments, induced internal waves lead to intrusions using a paddle wave maker (Cacchione and Wunsch 1974; Ivey and Nokes 1989; De Silva et al. 1997). Cacchione and Wunsch (1974) observed the propagation of intrusions only for critical reflection of the activated waves. Turbulence attributed to interaction of incident and reflected supercritical internal waves caused intrusions which follow a two dimensional viscous-buoyancy balance, traveling as a front not simply with respect to diffusion or dispersion (De Silva et al. 1997).

Lemckert and Imberger (1993) developed a series of equations to model viscous-buoyancy driven intrusions in a linearly stratified reservoir with a bubble plume. In order to identify the dominant mechanisms controlling the intrusion dynamics from a bubble plume, scaling was used to determine three unitless numbers relating buoyancy, inertia and viscosity (Lemckert and Imberger 1995). The turbulent Froude number, relates the magnitude of inertia and buoyancy forces; the turbulent Reynolds number, relates the magnitude of the inertia and viscous forces; and the turbulent Grashof number Gr_t is the ratio of the buoyancy

to viscous forces, $Gr_t = NL_c^2\nu^{-1}$. When the turbulent Froude number is much greater than one; the buoyancy has no effect on turbulence; thus inertia dominates buoyancy; otherwise buoyancy may affect turbulence (Ivey and Imberger 1991). When the turbulent Reynolds number is much greater than 15; the viscosity has no effect on turbulence; thus inertia dominates viscosity; otherwise viscosity can affect turbulence (Ivey and Imberger 1991). When the turbulent Grashof number exceeds 15; the effects of buoyancy dominates the effects of viscosity; otherwise the opposite is true (Lemckert and Imberger 1995).

A separate mechanism for offshore transport of fluid in the metalimnion was observed by Marti and Imberger (2008). A distinct feature of the second vertical mode seiche is contraction and expansion of the metalimnion as the standing wave oscillates. Marti and Imberger (2008) suggested that increased mixing in the boundary layer enabled resuspension of organic matter and sediment which was transported offshore by metalimnetic jets caused by the presence of a mode two internal wave. In a vertical mode two basin scale internal wave, advection in the metalimnion controls horizontal transport between the lake boundary and the lake interior. Net advection of particles into the lake's interior is the work of residual currents from internal waves and was found to be significant as residual bottom currents were between 15-20% of the currents during seiching (Marti and Imberger 2008).

The total horizontal spreading of the dye cloud is the sum of reversible and irreversible dispersion (Sundermeyer and Ledwell 2001). Reversible transport is purely an advective process, which the spreading can be reversed if the advection reverses direction. The velocities associated with basin scale waves are sinusoidal in form for both the vertical and horizontal direction in a rectangular basin with linear stratification. Irreversible

dispersion includes molecular diffusion, which mixes the cloud in a way that cannot be undone.

Since the velocity in the metalimnion of a vertical mode two switches direction every period, variation in the horizontal velocity causes strain of the middle of water column. Young et al. (1982) inquired about the role of horizontal currents associated with internal waves and their relationship with shear dispersion, which lead to the definition of the horizontal component of velocity u, in an infinite fluid undergoing oscillation as

$$u = U\,cos(mz)\,cos(\omega_0 t), \tag{2.17}$$

where U is the maximum velocity, m is the vertical wavenumber, and ω_0 is the oscillation frequency at depth z, and time t. The effective horizontal diffusivity K_{eff} was given by

$$K_{eff} = K_x + \frac{U^2}{4\omega_0}\frac{d}{1+d^2}, \tag{2.18}$$

where K_x is the horizontal diffusivity without the effect from shear and the nondimensional vertical diffusivity is $d = K_z m^2/\omega_0$, where K_z is the vertical diffusivity. Sundermeyer and Ledwell (2001) used the Fickian diffusion model from the results in Young et al. (1982) and Smith (1982) to investigate effective diffusivity of shearing from four dye tracer studies over the continental shelf. They determined from analysis of on board acoustic Doppler current profiler data that shear dispersion and diffusion cannot account for the observed diffusive spreading observed from the dye. Although internal wave strain has been used to estimate vertical mixing (MacIntyre et al. 2009), internal wave strain has not been studied as a mechanism for transport of near boundary fluid.

Summary

Mixing caused by turbulence generated by internal waves initiated by wind forcing has been proven to be the primary mechanism for vertical and horizontal fluxes in stratified water bodies. That being said, few have studied the entire process that leads to offshore transport of boundary fluid. Wind can generate internal waves that break along the sloping boundary of the metalimnion of a lake, causing turbulence and inducing a layer of mixed fluid near the boundary. Seiching, caused by sustained wind forcing, also causes mixed boundary fluid via shearing along the lake boundary which is intensified by rough topography. Mixed fluid near the boundary then gravitationally collapses and is transferred offshore as intrusions along isopycnals. Offshore transport, however, is not limited to fluid; nutrients, dissolved gas, organic matter, and sediment also can be transported offshore with the mixed fluid. Wave shear and strain can also be a potential mechanism for transport of fluid especially if large vertical mode waves are present. While some work has addressed transport in lakes and the ocean, the fate of mixed, near boundary fluid has not received its due attention.

CHAPTER 3. METHODS

Introduction

The following section outlines the field site, methods used to record the measurements in the field, and procedures used for data processing. The first section provides background and a description of the field site used to obtain all the measurements. The second section describes the sampling strategies, deployment location, and deployment duration of all the instruments that were used to gather meteorological conditions, water temperature, temperature microstructure, and dye profiles. The third and final section describes the data processing techniques for each of the instruments and the criteria that were used to obtain the results in the following chapter.

Field Site

An experiment was performed at West Okoboji Lake near Arnolds Park, Iowa, USA (Figure 3.1) that combined weather conditions, velocity and thermal profiles, microstructure measurements, and a dye release. West Okoboji Lake is a natural lake located in Dickinson County in northwest Iowa on the northwest side of the town of Arnolds Park. It is the primary source of drinking water for several communities near the lake. The thalweg of the lake extends from south to north with two shallow bays on the west side of the lake (Miller's and Emerson Bay) and one on the east (Smith's Bay), all of which are towards the south end of the lake. West Okoboji Lake has a surface area of 15.6 km^2, a mean depth of 12 m, and a

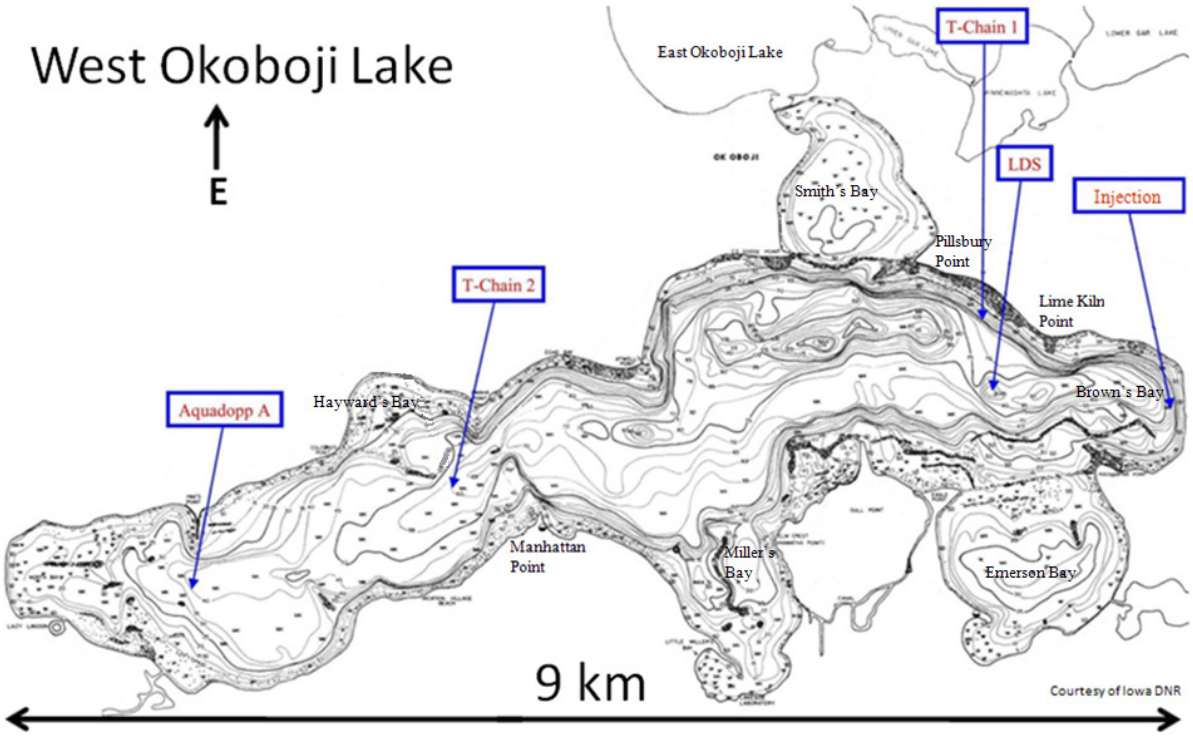

Figure 3.1. Map of West Okoboji Lake courtesy of the Iowa Department of Natural Resources. Depth contours are marked every five feet. The location of all the instruments is displayed along with the location of the dye tracer injection.

maximum depth of 41 m. The fetch of the lake is along the primary wind direction and is approximately 9 km in length, extending north to south.

The lake's density structure evolved as the summer proceeded with a well-mixed epilimnion above a strongly stratified metalimnion and a weakly stratified hypolimnion. The inflow from the lake comes from groundwater and surface runoff from a catchment basin of 61 km^2. The lake's outflow is through Smith's Bay and into East Okoboji Lake through a channel that is approximately 3 m deep. Because the channel is much shallower than the

summer thermocline, the outflow from West Okoboji Lake consists only of epilimnetic waters. Although boat traffic on the lake can be heavy at times, it should only affect the top of the epilimnion.

Most of the south end of the lake has moderately steep sides with the exception of the three bays, and the steepness of the sides of the lake decreases towards the north end of the lake. Along the lake's main axis, the slope of the lake bed at the north end is approximately 0.5% and the slope at the south end, where the dye was injected, is approximately 10%. The injection location was chosen because it lies along the major wind axis in the area and because the side slopes were large enough for critical wave reflection and intrusion formation. Great care was used in determining the injection location because a local water treatment facility draws water from the south end of the lake. However, the injection was 9 m deeper than the intake and 400 m away horizontally.

Measurements

Meteorological Conditions and Stratification

A Lake Diagnostic System (LDS), which is manufactured by Precision Measurements Engineering, Inc. and the Centre for Water Research, was installed on West Okoboji Lake from May 21 to July 23, 2009 to monitor local winds along with other meteorological and lake conditions. The LDS was located in the thalweg near the south end of the lake, just west of Lime Kiln Point (Figure 3.1). The location was chosen because it was one of the deepest points in the lake and because boat traffic in the area was not as heavy.

Considerable planning and precaution in conjunction with the Iowa Department of Natural Resources were used not only to keep the instruments undamaged from boats but

more importantly to keep boaters safe near the instruments. The LDS was marked with four white and orange regulatory buoys. Each was mounted with a one-mile amber solar light at the lake's surface flashing at 1 Hz. The buoys were placed in the shape of a diamond around the LDS. The four regulatory buoys were each moored to the bottom of the lake with a 45 kg weight connected via 6.35 mm chain. The buoys with lights successfully protected the boaters and the LDS for the entire length of deployment.

The LDS mooring system comprised a number of floats anchored in approximately 25 m of water by two 230 kg concrete anchors. Since the station adjusts to fluctuations in the lake depth, the mooring, which spanned 80 m, needed to be deployed where the bottom of the lake was nearly flat. The LDS measured wind speed, wind direction, solar radiation, net radiation, relative humidity, air temperature, and the water temperature profile. To determine the wind forcing on the lake, the wind speed and wind direction were measured approximately 2 m above the water surface by a propeller anemometer and a wind vane, respectively, both manufactured by Met One Instruments, Inc. To help estimate the heat fluxes into or out of the water surface of the lake, a pyranometer made by LI-COR was used to measure the solar radiation, and net radiation was measured using a pyrradiometer made by Middleton Solar. The relative humidity and air temperature, used in the heat budget, were also measured roughly 2 m above the water surface by a combined sensor designed by Vaisala.

A thermistor chain, which measured the temperature profile, was suspended from the LDS. The thermistor chain had a single electrical cable connecting 29 temperature sensing nodes, each consisting of a thermistor in a protective tube. The thermistor chain was approximately 30 m long with nodes every meter, and consequently the LDS was able to

record the water temperature every meter to the bottom of the lake. Since the LDS was deployed in only 25 m of water, the bottom four thermistor nodes were not used in any data analysis. All the sensors on the LDS were set to sample every 15 s. The LDS has an internal data logger that can store data for up to 96 h and allow data to be downloaded manually as well. The LDS can also transmit data via cell phone network every two hours so that recent meteorological and lake conditions can be easily and quickly observed. However, the signal from the cell phone network was so poor that the data had to be downloaded directly from the LDS at least every 96 h.

Two additional stand-alone thermistor chains (thermistor chain #1 and #2) produced by Precision Measurements Engineering, Inc. were deployed at roughly 18 m depth. Thermistor chains #1 and #2 each had 29 nodes starting approximately one meter below the surface and spaced every meter thereafter. As a result of the thermistor chain being longer than the deployment depth, the last 10 m of both chains were folded back up the chain. This allowed the bottom half of the chain to have nodes every 0.5 m and still avoid tension on the chain if lake stage was to rise. The temperature chains were moored to the bottom of the lake with a 45 kg weight connected via 6.35 mm diameter chain to a white and orange regulatory buoy with a one mile amber solar light at the lake's surface flashing at 1 Hz. The data were sampled continuously and recorded on data cards in a submersible data logger. The data cards were removed from the data loggers every 3 to 4 weeks to access the data. The temperature-time series that were obtained from these measurements were used to determine the temperature profile, compute the buoyancy frequency, and examine the internal wave field in the lake.

Thermistor chain #2 was placed north of the LDS along the thalweg and primary wind axis between Manhattan Point and Hayward's Bay (Figure 3.1). The north thermistor chain, or thermistor chain #2, was deployed from May 18 to July 23, 2009. Because the basin scale seiches are standing waves, it was important that the thermistor chains not be placed at the node of the dominant seiche, so great care was taken when determining the location of each thermistor chain. The second of the two thermistor chains was placed directly east of the LDS roughly 300 feet off shore, between Pillsbury and Lime Kiln Points, to form a right triangle at the LDS. The south thermistor chain, or thermistor chain #1, was deployed from May 15 to July 23, 2009. The thermistor chains were placed in a triangular shape because three or more noncollinear thermistor chains are required to determine the properties of internal waves.

Like the thermistor chain on the LDS, thermistor chains #1 and #2 were sampled at 15 s intervals. Because the sampling frequency of 240 cph was eight times the buoyancy frequency, the maximum frequency of internal waves, the high-frequency waves were resolved. The thermistor chains didn't "sleep" between measurements if they sampled faster than every 15 s; consequently, the sampling rate maximized functionality and minimized power consumption. While this sampling rate only provided coarse resolution of the highest frequency waves, typically most of the energy in the internal wave field in a stratified basin is contained in lower frequency motions (Boegman et al. 2005b).

Temperature microstructure

Profiles of temperature fluctuations generated by turbulence were measured with a Self-Contained Autonomous MicroProfiler (SCAMP) manufactured by Precision Measurements Engineering, Inc. The SCAMP uses two Thermometrics FP07 thermistors,

whose response time, nominally 7 ms, depends on probe speed and sensor construction (Gregg 1999). The SCAMP falls under its own weight through the water column at a fall velocity tuned using floats or additional weights to maintain a target of 10 cm s^{-1}. Temperatures were recorded at 100 Hz, and profiles of temperature gradient were computed from the time derivative of the voltage signals from the thermistors using Taylor's hypothesis. The SCAMP also has an optical backscatter sensor to measure turbidity and a conductivity-temperature sensor. The conductivity-temperature sensor does not respond as rapidly as the fast response thermistors, but it provides more accurate density profiles.

The SCAMP profiles were collected in the downward mode, in which the SCAMP measured from the top of the water column to the lake bed with the sensor end leading. Using this profiling mode excluded the upper 0.6 m of the water column, which is the distance between the pressure transducer and the sensors, because initially the pressure transducer was placed at the water surface to begin its descent. The SCAMP was set to begin recording after a 15 s delay to allow enough time to lower the SCAMP over the edge of the boat so that the pressure transducer (which was zeroed at atmospheric pressure) could be placed at the water surface. The SCAMP was set to stop recording after a certain number of scans based on the SCAMP's sampling rate of 100 scans s^{-1} and a fall velocity of approximately 10 cm s^{-1}. The expected number of scans was increased by 50% to ensure that the entire water column was sampled for each profile.

During the three days in which the dye surveys were performed, microstructure measurements at the injection site were recorded a total of four times with each measurement comprising three profiles to improve the turbulence statistics. Also, throughout June and July of 2009 many sets of SCAMP measurements, each typically containing ten profiles, were

collected at both offshore and onshore positions to observe differences in the turbulence over the flat bottom and sloping boundary, respectively. These additional SCAMP measurements, taken over rough and smooth bottoms, were used to compare the effects of the topography on turbulence. The GPS coordinates of each measurement site were recorded and used to guide the sampling so that each profile occurred in approximately the same location. A small buoy was also used to help the boat driver find the correct sampling location.

Transport of Dye

Rhodamine WT was used to track mixed fluid from the slope into the interior. Dye tracking surveys were used to measure properties of the intrusions, including length, thickness, velocity, and mass. Rhodamine WT, a non-toxic tracer designed to track water, was used for the dye tracer study. The United States Geological Survey recommends it because of its high detectability, low tendency to be absorbed by vegetation, and low diffusivity (Wilson et al. 1986). Rhodamine WT dilutes naturally in lakes and photodecays; however, because it was injected into the metalimnion of the lake (where sunlight does not reach), decay should not have affected the results on the time scales of the tracking experiments. The dye was injected in the south end of the lake, where the steeper side slopes may allow intrusions to form.

The depth at which the first vertical modal amplitude was greatest was determined to be the location of the middle of the metalimnion or thermocline and was used as the target injection depth of 13.25 m on the 19° C isotherm. 2 L of Rhodamine WT were mixed with 1.35 L of ethyl alcohol and 88 L of surface water to match the density on the target isotherm using a mass balance. The ethyl alcohol was used with the permission of the Iowa Department of Natural Resources to lower the density of the dye and limit the volume of the

dye mixture. The ethyl alcohol was used to increase the density of the mixture near the predicted density and then it was fine tuned with surface water.

Before the injection, rinse water was pumped from the injection depth and stored on the research vessel. A conductivity-temperature-depth (CTD) instrument was used to ensure the rinse water was pumped from the correct depth so the water would be of the same density as the dye mixture. The mixing of the dye occurred directly on the research vessel, which is also where the injection took place. At 9:15 am on July 20, 2009, the 91 L dye mixture was pumped from a 121 L container on the boat to hoses that dropped straight down to the isobath where the chosen isotherm intersected the lake boundary. The injection device included a depth sensor so that the diffuser could be set to the target depth. At the end of the hose, a diffuser pipe decreased the turbulence generated by the injection. The dye was injected at a point by anchoring the research vessel at the injection location. Once the dye mixture was emptied from the container in which it was mixed, the residual dye was rinsed from the 121 L container and flushed out the hoses with rinse water from the injection depth. The dye injection itself lasted 4 min, with an additional 4 min for rinsing.

After the dye was injected, it was tracked using the Self-Contained Underwater Fluorescence Apparatus and Conductivity, Temperature, and Depth profiler (SCUFA/CTD). Using optical filters, the SCUFA, manufactured by Turner Designs, Inc., measures Rhodamine WT by emitting light at a wavelength of 530 nm from an excitation light source (two green LEDs) that causes the Rhodamine WT in the measurement volume to fluoresce. The emitted light from Rhodamine WT has a wavelength of 600 nm. The fluorescence is measured by two detectors (silicon photodiodes) that detect the light emitted just at this wavelength. The SCUFA and CTD were mounted together in the same protective cage and

integrated with GPS using Seasave V7 from Sea-Bird Electronics, Inc to sample simultaneously at 4 Hz. The SCUFA compensates for the effect of temperature on fluorescence, and it responds linearly to concentrations up to 200 ppb (Turner Designs, pers. comm.). The majority of concentrations measured when mapping the cloud were less than 100 ppb. Therefore, the SCUFA was calibrated using a 50 ppb Rhodamine WT standard and the calibration was checked using 5 and 100 ppb standards. The calibration was confirmed after the completion of the tracer study by a solid standard.

The CTD, manufactured by Sea-Bird Electronics, Inc., which is mounted in a protective cage with the SCUFA, was lowered using an electric winch at approximately 0.25 m s^{-1}. As the CTD is raised and lowered, water is pumped past temperature and conductivity sensing elements while the depth is measured by a strain gauge pressure sensor. The temperature is measured by a glass coated thermistor bead in a stainless steel tube. The conductivity is measured in a flow through glass cell with internal electrodes.

A tow-yo method was used to capture the vertical and horizontal extents of the dye cloud. The Self-Contained Underwater Fluorescence Apparatus and Conductivity, Temperature, and Depth profiler (SCUFA/CTD), which measured the dye concentrations, were raised and lowered through the dye cloud to identify its upper and lower bounds, while the research vessel traveled through the cloud from one edge to the other. Additional measurements were taken along new transects until background fluorescence levels were reached to ensure the entire dye cloud was captured. The background fluorescence varied from 0.27 to 0.30 ppb as determined from several surveys before the injection. Therefore, background fluorescence of 0.30 ppb was subtracted from the raw data to ensure that all fluorescence readings were due solely to the injected dye.

The boat was maneuvered to ensure that the dye was completely encompassed for each dye survey. The dye cloud was bounded on the north and south by an east-west transect in which no dye was detected and to the east and west by the lake's bathymetry. The unique topography of the location of the dye injection provided greater ease when determining the boundaries of the cloud as the steep walls of the bay in which the study took place allowed for fewer avenues of escape.

Processing

Buoyancy Frequency

A temporal average of temperature and buoyancy frequency as a function of depth was computed from both the thermistor chain at the LDS in the south end of the lake and from the thermistor chain #2 on the north side of the lake. The temperatures from each of the thermistor nodes were averaged over the three day period and interpolated onto a 1 m grid. Density at any given depth was computed with the equation of state from Chen and Millero (1977), and the buoyancy frequency was computed with Equation (2.9), with mean density from the density profile as the reference density.

Lake Number

To compare the relative strength of the wind, which can cause the stable stratification to overturn, to the relative strength of the lake stratification, which resists overturning, the Lake number is used, as defined in Equations (2.2)-(2.5). For wind velocities of 5 m s^{-1} or greater, the relationship between wind velocity at the water surface u_{*a} and the wind velocity measured by the LDS $u(z_{ih})$ at instrument height z_{ih} was computed with (Wüest and Lorke 2003a)

$$u(z_{ih}) = u_{*a}\left[\kappa^{-1}\ln\left(\frac{gz_{ih}}{u_{*a}^2}\right) + K\right], \tag{3.1}$$

where κ is the von Kármán constant equal to 0.41 and the constant K, is equal to 11.3. For wind velocities less than 5 m s^{-1}, wind velocity at the water surface is computed with (Wüest and Lorke 2003a)

$$u(z_{ih}) = u_{*a}\left[\kappa^{-1}\ln\left(\frac{u_{*a}z_{ih}}{\nu_a}\right) + 5.7\right], \tag{3.2}$$

where the kinematic viscosity of air is ν_a. All the meteorological data and the temperature profiles needed to determine the Lake number were obtained from the LDS, and the surface area at every meter of depth was obtained from a hypsograph provided by the Iowa Department of Natural Resources. Before the Lake number was calculated, a moving average over a 15 min period was determined for all of the data obtained from the LDS. Also, the temperature profile, obtained from the thermistor nodes, was interpolated onto a 1 m grid to match the hypsograph data. Identifying the location of the thermocline is hindered by the ever changing temperature profile and the non-constant buoyancy frequency in the metalimnion. Therefore, the maximum modal displacement was determined and depth of the thermocline was the location of the maximum vertical isotherm displacement of the first vertical mode seiche. The Lake number series was then computed for the entire duration of the LDS deployment, which is a period of more than two months, from late May to late July.

Vertical Mode Structure

The displacement of isotherms time series was determined via interpolation from the temperature sensing nodes at known depths from the LDS thermistor chain and thermistor chain #2 over the entire time series of interest. The n-layer model from Münnich et al. (1992) was used to calculate the frequency of the natural seiches in the lake. Temperature data from

the thermistor chain at the LDS was used because, located in 25 m deep water, it provided temperature data of a larger portion of the water column than did the temperature chain #1 or #2. Data from 20-22 July 2009 was used in the model as that was the time period in which the dye study was performed. A temporal mean for the 72 h period was computed for each of the 25 temperature sensors, the deepest of which is located at 25.2 m below the water surface. Since the model simplifies that lake as a rectangular prism, it is essential to estimate the temperature profile of the lake from the surface all the way to the maximum depth of 41 m.

In order to estimate the temperature profile below 25.2 m, temperature data from the Iowa State University Limnology Laboratory (ISULL) was employed. The ISULL collected the temperature profile on 8 July 2009. Although the temperature data were not collected at the same time, the temperature profile below 25.2 m was constant over time. Also, when profile from the LDS thermistor chain was overlaid with the ISULL temperature profile, the two had excellent agreement throughout the metalimnion and into the hypolimnion. Therefore the ISULL temperature profile below 25.2 m depth was added to the LDS temperature profile to form a composite profile. From the composite profile, the temperature profile was linearly interpolated to a grid of 0.25 m steps which encompassed the entire water column. The buoyancy frequency profile was determined from the resulting density structure.

To determine the phase speeds of the first three vertical modes, the eigenvalue problem was solved. At the depth of the thermocline, the fetch was approximately 7600 m along the primary axis of the lake. The fetch length had an uncertainty of 10% causing a wave period uncertainty of 10% which is small when the periods are used with power spectra ranging over several orders of magnitude. The wind acted along this axis during the period of

the dye study. The theoretical frequencies of the modes were computed from fetch length and the corresponding phase speeds.

Internal Wave Spectra

Since estimations of the structure and frequency for the first three theoretical vertical modes have been established, phase spectra and coherency were used to determine possibility of the existence of these higher modes. Temperature data from both the thermistor chain at the LDS and thermistor chain #2 were used. By linearly interpolating from each temperature node in the thermistor chain, the depth of each isotherm was determined every 15 s for the entirety of the dye study. The isotherms present during the 72 h period encompassing the dye study ranged from 14°C to 20.5°C in 0.5°C increments. The temporal mean depth for each isotherm was determined and then removed from every individual depth at each respective isotherm to reduce the affect of basin-scale heating or cooling. The coherency and phase spectra were computed from the isotherm displacement using Welch's averaged, modified periodogram method using a 72 h window and a sampling frequency 0.067 Hz. The window length of 72 h was chosen because the period of the third vertical mode was 62.3 h and the dye study was three days long.

The coherency spectrum indicates how well two signals correspond to each other at a given frequency. Values for coherency range from zero, for no correlation, to one, one for signals that correspond perfectly. If signals are coherent, the phase spectrum can be used to determine the lag between signals. At equal frequencies, two sine waves will be both coherent and in phase; however, at that same frequency, a cosine wave will be coherent but 90 degrees out of phase with the sine waves. The depths of the peaks in theoretical modal amplitude for each mode were computed as in Münnich et al. (1992). Using coherency and

phase spectra between two isotherms at the same location, the potential for existence of higher vertical mode can be determined (e.g., Münnich et al. 1992). Also, coherency and phase spectra from the same isotherm at two different locations can determine if internal waves are coherent basin-wide, shedding light on the horizontal mode present (e.g., Lemckert et al. 2004).

Vertical Eddy Diffusivity: *Microstructure*

The temperature gradients were then used to compute the dissipation of temperature variance χ_T and vertical eddy diffusivity K_{zm}. As in Soga and Rehmann (2004), χ_T was computed by assuming isotropy and integrating the difference of the observed spectrum S_{obs}, computed in segments of 256 points, or about 0.25 m, and the noise spectrum S_n over the wavenumber k_1,

$$\chi_T = 6D_T \int_0^\infty [S_{obs}(k_1) - S_n(k_1)]dk_1, \tag{3.3}$$

where D_T is the molecular diffusivity of temperature. The eddy diffusivity was computed with the relation from Osborn and Cox (1972),

$$K_{zm} = \frac{\chi_T}{2(\partial\bar{T}/\partial z)^2}. \tag{3.4}$$

The mean temperature gradient $(\partial\bar{T}/\partial z)$ was determined by fitting a line to the temperature in each segment. Values of $(\partial\bar{T}/\partial z)$ and χ_T were assigned to 0.25 m intervals in the vertical, and profiles of the ensemble averages and their 95% confidence limits were computed for each sampling site from 200 bootstrap resampled populations. The statistics for χ_T and the temperature gradient were used to compute profiles of K_{zm} and their 95% confidence limits using Equation (3.4). Wain and Rehmann (2005) addressed the uncertainty in the eddy diffusivity K_{zm} computed with the Osborn-Cox method, which comes from the assumption

of isotropy, the fit of the mean temperature gradient for each segment, the resolution of χ_T, and the validity of the Osborn-Cox balance. This method provides a profile of vertical eddy diffusivity as a function of depth at the measurement location. The combined dye tracer/microstructure study began on a moderately windy day on July 20, 2009. The winds were blowing steadily out of the south at approximately 5 m s^{-1}. We measured the temperature microstructure 0.5 h before the dye injection and 5.0 h, 25.5 h, and 52.5 h after injection.

Vertical Eddy Diffusivity: *Heat Budget Method*

Temperature profiles from thermistor chain #2 (Figure 3.1) and the thermistor chain at the LDS were also used to calculate the vertical eddy diffusivities during the three-day tracer study. The heat budget method (Jassby and Powell 1975) assumes that the vertical turbulent transport of heat is equal to the rate of change of the heat content below z:

$$K_{zt}(z) = \frac{1}{\partial \bar{T}/\partial z}\left(\frac{1}{A(z)}\frac{d}{dt}\int_z^H A(z)T(z)dz - \frac{1}{c_p\,\rho}R(z)\right) \tag{3.5}$$

where T is temperature, $A(z)$ is the area at vertical position z, t is time, H is the maximum lake depth, $R(z)$ is the solar radiation flux computed from Equation 6 in Jassby and Powell (1975), ρ is the density of water, and c_p is the specific heat of water. The albedo term was ignored when computing the solar radiation flux because the mixing term ($[d/(dt\,A(z))]\int_z^{z_m} A(z)T(z)dz$) was much larger (~$10^2$) than the radiation term ($R(z)/c_p\,\rho$) in the metalimnion. In addition, the method assumes no heat flux through the boundaries of the lake and no internal heat sources. The only external heat source considered is the net solar radiation measured by the LDS at the lake surface. The daily temporal average of vertical diffusivity as a function of depth was determined from each sample every

15 s while the LDS and thermistor chains #1 and #2 were deployed. By computing a temporal average over the three days of the dye study from the daily averages, a profile of vertical eddy diffusivity as a function of depth during the dye experiment was determined.

Vertical Eddy Diffusivity: *Dye Tracking*

The vertical eddy diffusivity K_{zd}, can be estimated from the moment of the concentration distribution using $K_{zd} = (\sigma_{t+\Delta t}^2 - \sigma_t^2)/(2\Delta t)$, where Δt is the time between two vertical dye concentration profiles, $\sigma^2 = M_2/M_0 - (M_1/M_0)^2$, and $M_0 = \int C dz$, $M_1 = \int zC dz$, and $M_2 = \int z^2 C dz$ where C is the dye concentration detected at depth z (Fischer et al. 1979). Mean dye concentration profiles were collected from dye surveys at 10.5 h and 29.2 h following the dye injection. First, only data points where the concentrations were greater than background were used in analysis. These points were placed on a three dimensional grid consisting of latitude, longitude, and temperature. After integrating the dye concentration with respect to latitude and longitude, dividing by the horizontal area of the dye cloud produced the mean dye concentration as a function of temperature. From interpolation of the three day mean temperature profile at the LDS, the mean dye concentrations as a function of temperature can be converted to a function of depth. This approach enables the mean dye profile to be independent of seiches or internal waves that may temporarily skew the depth of the dye cloud. Also, the mass of dye $M = A_d \rho_{dye} \int_0^{z_{max}} C dz$, was calculated where A_d is the horizontal area of the dye cloud, ρ_{dye} is the density of the dye, z_{max} is the maximum depth of the lake, and C is the concentration of the dye.

Horizontal Eddy Diffusivity

The tracer maps were generated by separating the tow-yo transects into individual vertical profiles. The individual vertical profiles were determined by finding the point where the instrument changed direction in the vertical. This approach created two independent vertical profiles for every descent and adjacent ascent. To determine the approximate location of each profile, the average location from corresponding GPS data was computed giving all the data points in each profile equal weight. The column integral of each vertical profile was then computed by integrating the concentration profile over its length and placed onto a regular grid as in Ledwell et al. (2004). The column integral allows neglect of the effect of internal waves and seiches on the depth of the dye cloud because the quantity of dye at a certain point is determined over the entire depth. The column integral determined for each profile yielded a two-dimensional plan view map of the dye cloud. The mass of dye was computed as $M = dx\ dy\ \rho_{dye} \sum \bar{C}$, when M is the mass of dye, dx and dy the horizontal the horizontal grid spacing, ρ_{dye} the density of the dye, and $\bar{C}$ the depth integrated dye concentration over column integral.

At times during the sampling, the cage protecting the sampling instruments would inadvertently hit the lake bed. When the instrument cage struck the bottom, the turbidity—and occasionally the fluorescence—rose drastically. When the turbidity rose above 10 NTU, the data points also had high fluorescence (Figure 3.2). Because these points were due to the high turbidity, they were considered to be spurious and removed from the data analysis. All but 20 of the several thousand data points that had fluorescence greater than background were found at depths greater than 8 m. These 20 points all had depths less than 6 m as well.

Since these points were so dissimilar to the vast majority, they were also disregarded in the data analysis.

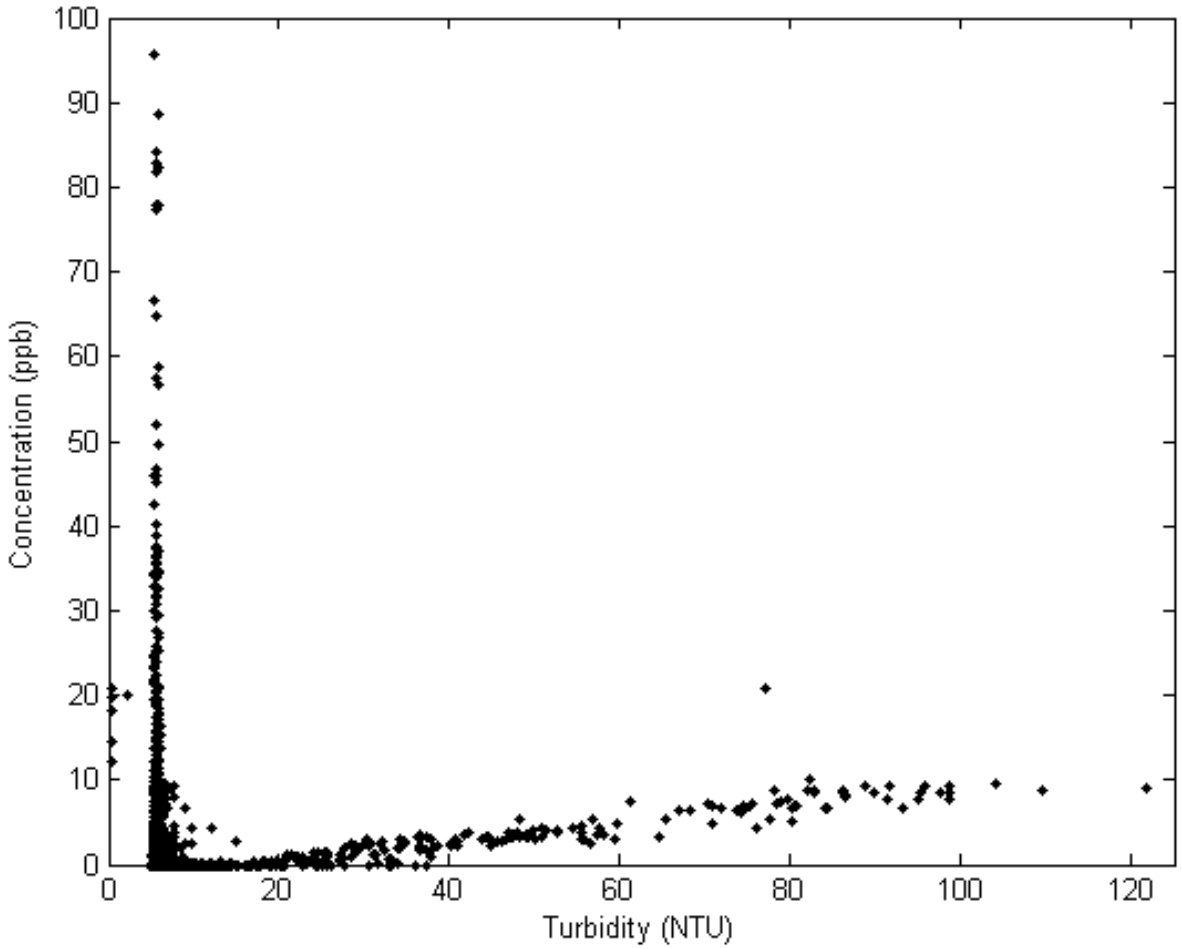

Figure 3.2. The relationship between dye concentration and turbidity. Data points with turbidity greater than 10 NTU were determined to be caused by the instruments striking the lake bed and resulted in elevated dye concentration, which were consequently adjusted to 0 ppb.

The horizontal diffusivity was determined from known dye concentrations gathered during dye surveys. For three dimensional spreading of dye injected instantaneously at a boundary the concentration can be computed with

$$C = \frac{2M}{(4\pi t)^{3/2}\left(K_x K_y K_z\right)^{3/2}} e^{\left(-\frac{x^2}{4K_x t}-\frac{y^2}{4K_y t}-\frac{z^2}{4K_z t}\right)}, \tag{3.6}$$

where M is the mass of dye injected, t is time after injection, x and y are coordinates along the east-west and north-south axes, respectively, z is the vertical coordinate, K_z is the vertical diffusivity, and K_x and K_y are the horizontal diffusivities. However, in addition to the southern boundary, the effects of the lake boundaries to the east and west must also be considered when estimating K_x. The method of images was subsequently used to address the effects of the east and west boundaries on spreading and the east-west location of the injection where the east-west basin width B is approximately 540 m and b_0 is the east-west distance from the injection point to the middle of the basin or 54 m. Assuming small vertical spreading and integrating over the vertical direction yields the column integral

$$\bar{C} = \frac{2M}{(4\pi t)\left(K_x K_y\right)^{1/2}} e^{-\frac{y^2}{4K_y t}}\left[e^{-\frac{(x-b_0)^2}{4K_x t}} + e^{-\frac{\left(x-(B-b_0)\right)^2}{4K_x t}} + e^{-\frac{\left(x+(B+b_0)\right)^2}{4K_x t}} + e^{-\frac{\left(x+(2B-b_0)\right)^2}{4K_x t}} + \right.$$

$$\left. e^{-\frac{\left(x-(2B+b_0)\right)^2}{4K_x t}} + e^{-\frac{\left(x-(3B-b_0)\right)^2}{4K_x t}} + e^{-\frac{\left(x+(3B+b_0)\right)^2}{4K_x t}} + e^{-\frac{\left(x-(4B-b_0)\right)^2}{4K_x t}} + \cdots\right]. \tag{3.7}$$

The mass of dye injected and time after injection is known. From the dye surveys, the column integral can be determined at points x and y. The contour at 1% of the maximum concentration denoted the extents of the dye cloud. Matching the 1% contour with the spreading equation allows the horizontal diffusivities to be estimated for the successful dye surveys.

CHAPTER 4. RESULTS

Introduction

The following section outlines the findings based on the measurements and processing techniques described in the previous chapter. The first section discusses the stratification, resulting buoyancy frequency, and wind present during the tracer study on July 20-22, 2009. The second section describes the internal wave field using a time series of isotherm displacement, spectra of the wind and isotherm displacement, and coherency and phase spectra between pairs of isotherm displacement. The next section proposes estimates of mixing via diffusivities from three methods. The final section quantifies transport of the tracer including geometry and velocity of the dye patch.

Stratification and Wind Forcing

Buoyancy Frequency

A temporal average of temperature and buoyancy frequency as a function of depth was computed from both the thermistor chain at the LDS in the south end of the lake and from thermistor chain #2 on the north side of the lake (Figure 4.1). The temporal mean of the water temperature profiles at both locations was almost exactly the same, with a slight temperature elevation in the metalimnion at thermistor chain #2 being the only deviation. The surface temperature at both locations was approximately 22°C, and the temperature at the bottom of the lake at the LDS was approximately 13°C. The temperature profile shows that a metalimnion was present from 12 m to 16 m depth and 16°C to 20°C with the maximum buoyancy frequency near 13 m.

Lake Number

The wind velocity before and during the dye injection was approximately 5-6 m s^{-1} from the south (Figure 4.2a-b). As a result, the Lake number for most of the day on July 20 remained between 1 and 10 (Figure 4.2c). However, on July 21, the wind speed dropped and

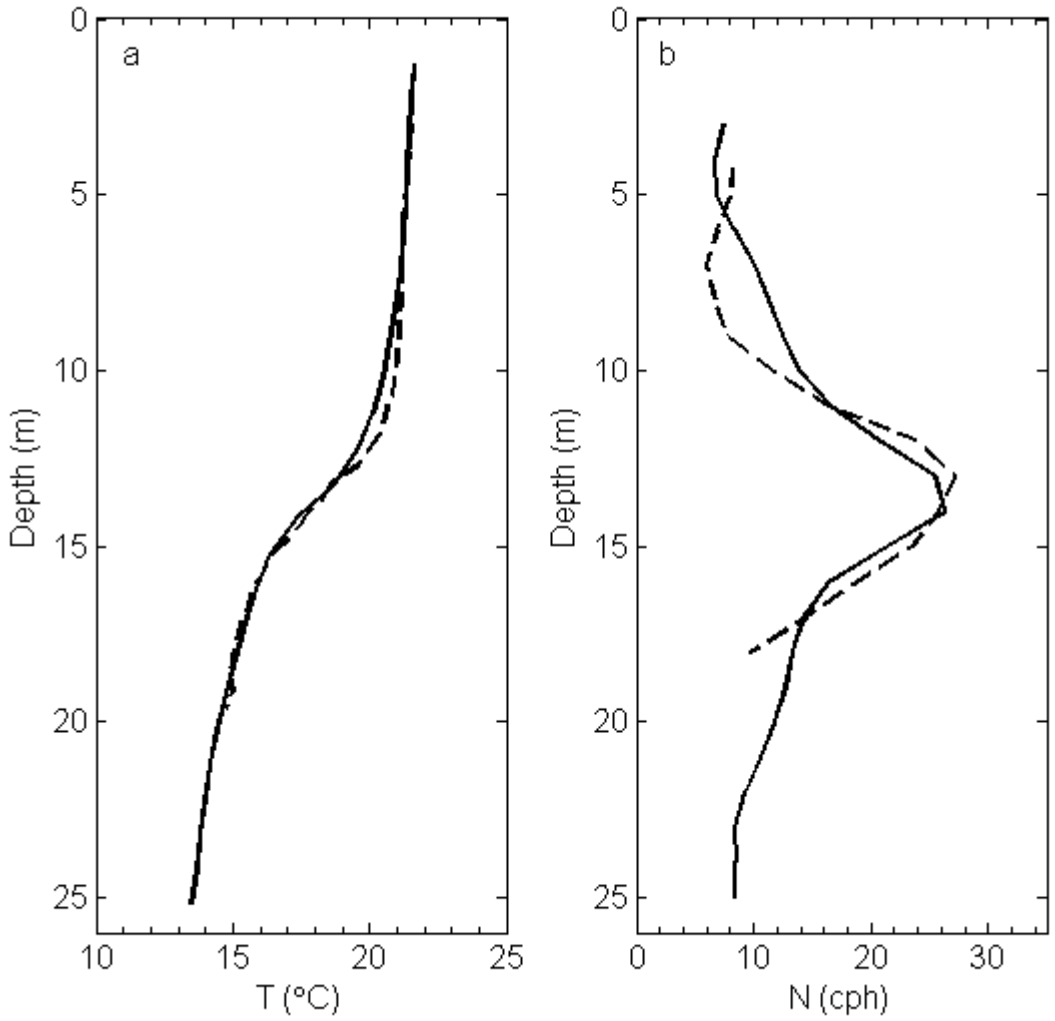

Figure 4.1. Stratification during the tracer experiment: (a) Time-averaged temperature profile and (b) time-averaged buoyancy frequency N as measured by the LDS thermistor chain (solid line) and the north thermistor chain (dashed line).

remained near 1-2 m s^{-1} while the wind direction was mainly from the west but was variable, causing the Lake number to increase above 10. The only exception was a brief storm in the afternoon which was associated with a temporary increase in wind speed and a spike in Lake number. On July 22, the wind speed was never greater than 1-2 m s^{-1} and the wind speed was highly variable; therefore, the Lake number remained greater than 10 for the rest of the time in the study.

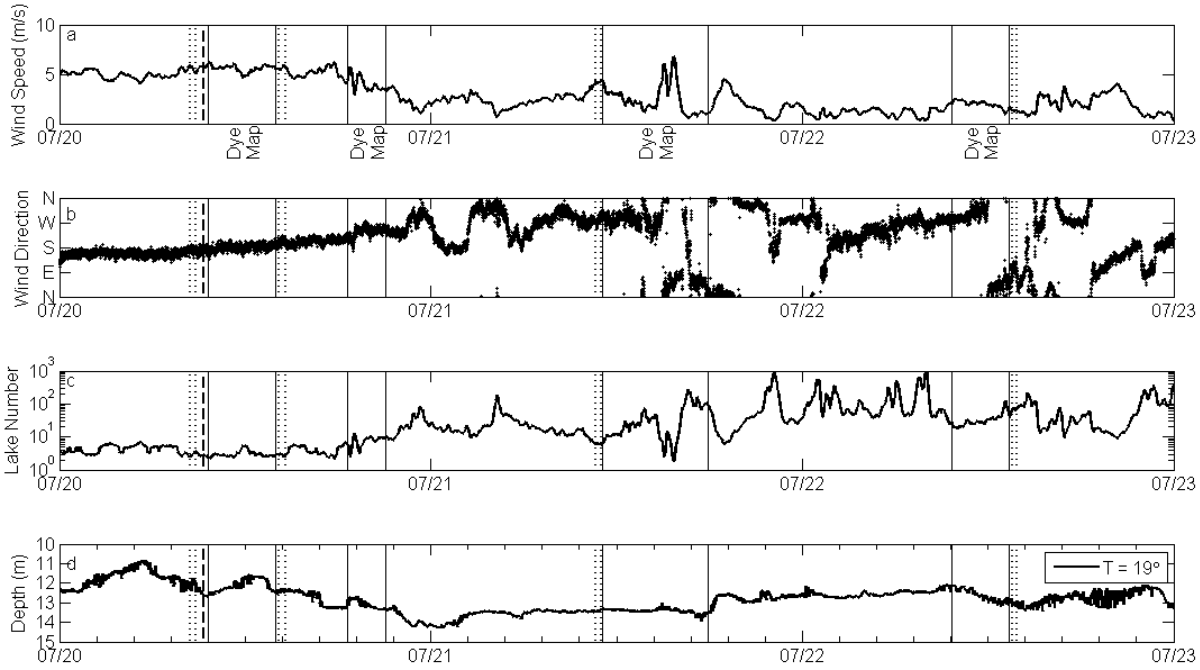

Figure 4.2. Conditions from July 20-22, 2009: (a) wind speed, (b) wind direction, (c) Lake number, and (d) displacement of the 19°C isotherm (the injection isotherm) at the LDS. The solid vertical line pairs identify periods when dye maps were surveyed, the dotted line pairs represent when microstructure measurements took place, and the heavy, dashed line denotes the injection time.

Internal Waves

Isotherm Displacement

In order to comprehend the isotherm displacement, the depth of the 19°C isotherm, the injection isotherm and location of the thermocline, was also examined during the same 72 h period using the temperature profiles collected by the LDS (Figure 4.2d). When the Lake number was less than 10, the isotherm responded as expected. As the southerly wind sustained a force on the lake, the epilimnion was pushed towards the north end of the lake; consequently, the thermocline responded by moving upward. In addition, during the first day of the tracer study, the 19°C isotherm experienced a displacement of roughly 3 m in 19 h. Assuming the maximum isotherm depth is the wave trough and the minimum isotherm depth the wave peak, a wave amplitude of approximately 1.5 m can be estimated. Any dissolved substance or particle that is naturally buoyant on the 19°C isotherm experienced a 3 m fluctuation in depth in less than a day due to the wind forcing experienced by the lake. However, for the entirety of July 21 and 22, the 19°C isotherm exhibited very little vertical displacement, dramatic change from the day of the dye tracer injection. Figure 4.3 and Figure 4.4 provide the depths of all the isotherms (20°C-14°C) present in the metalimnion during the three day period of the tracer study at the LDS and thermistor chain #2, respectively. Around mid-day on July 21, a large contraction of the metalimnion can be observed at both locations. Nonetheless, early in the day on July 20 and all day on July 22, the metalimnion thickness remains constant and all the isotherms seem to move coherently. Comparing the two isotherm plots at two different locations can reveal evidence used to predict the horizontal mode. For the first horizontal mode one to exist, corresponding isotherms must move out of phase between the two locations because the LDS and thermistor chain #2 are located at

opposite ends of the lake. For horizontal mode two to exist, corresponding isotherms must move in phase between the LDS and thermistor chain #2 because they are located at opposite ends of the lake. Later, the horizontal modes will be examined further using coherency and phase spectra of isotherm displacements. The observations from the isotherm-depth time series provide evidence for both V2H1 and V1H1 mode waves.

Vertical Mode Structure

The estimated temperature profile, resulting buoyancy frequency, and the profiles of vertical displacement and horizontal velocity for the first three vertical modes are found in Figure 4.5. The estimated natural periods of the VxH1 mode for x = 1, 2, and 3 are 13.4 h, 41.3 h, and 62.3 h, respectively. The periods of the VxH2-3 modes result in half and one-

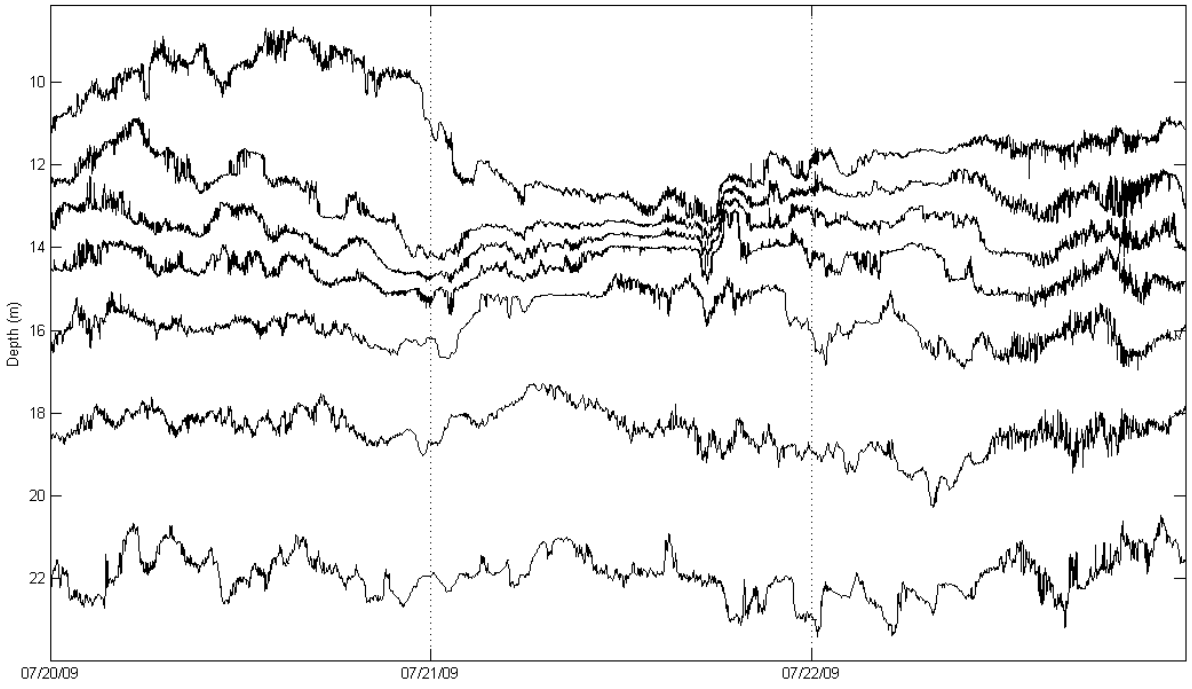

Figure 4.3. The depths at the LDS of the 20°C-14°C isotherms (spaced at 1°C) during the tracer study.

third the period of the VxH1 modes, respectively. The periods and frequencies of each mode can be found in Table 4.1. Assuming simple bathymetry, the velocity field was approximated for a standing wave for each mode. The effect of the Earth's rotation on seiche structure was examined by determining the Rossby radius L_R of West Okoboji Lake. Following Patterson et al. (1984), Vidal et al. (2005) defined the Rossby radius $L_R = 2L/fT_1$. In West Okoboji Lake, the basin length L at the thermocline was 7600 m, the Coriolis parameter f was 1×10^{-4} s^{-1}, and the period T_1 of the V1H1 seiche was 13.4 h. Vidal et al. (2005) determined the Rossby radius was only 25% larger than the maximum width of the Sau reservoir; therefore they determined that effects of Earth's rotation could not necessarily be neglected. However,

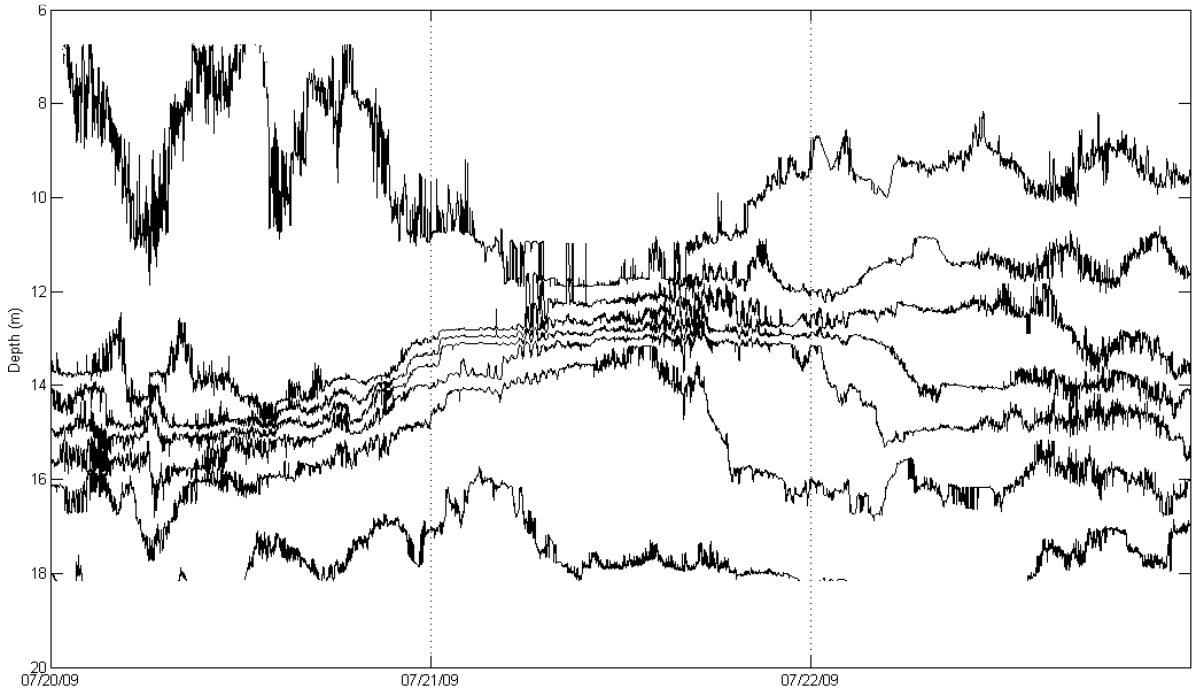

Figure 4.4. The depths at thermistor chain #2 of the 20°C-14°C isotherms (spaced at 1°C) during the tracer study.

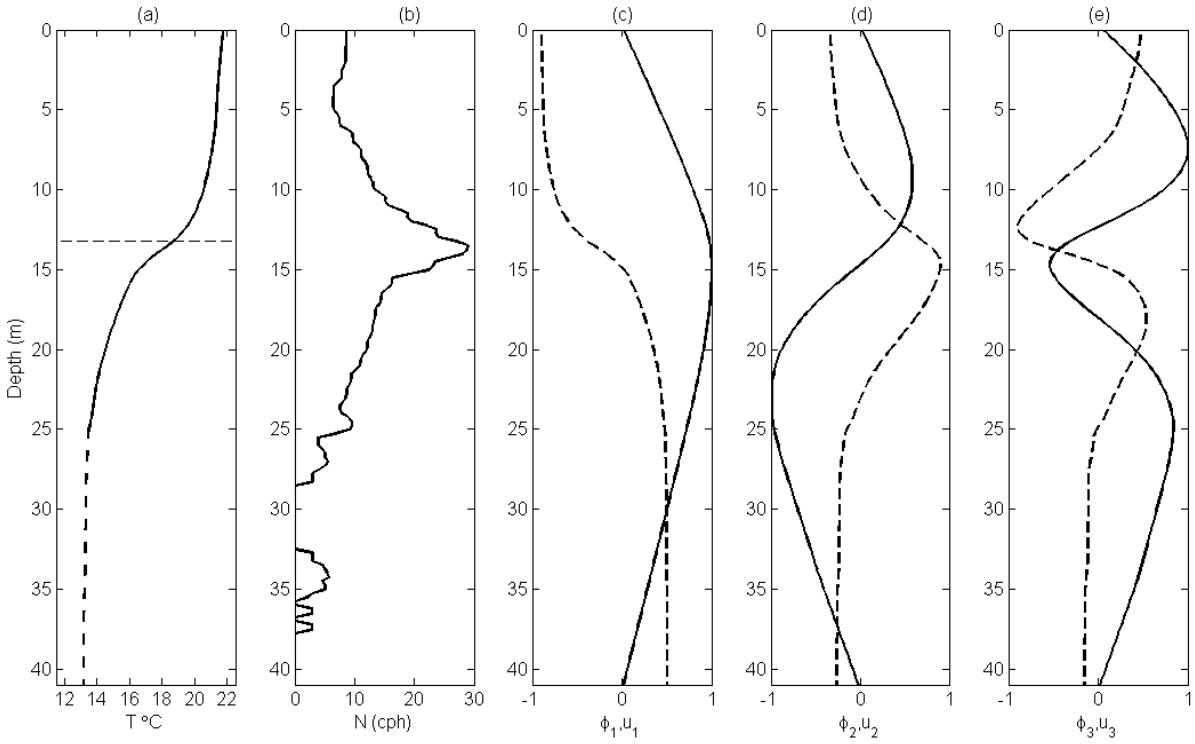

Figures 4.5. Mode structure in West Okoboji Lake during the dye tracer study: (a) the temperature profile to the maximum depth from the LDS thermistor chain (solid) and from ISULL temperature profile (dashed), (b) the resulting buoyancy frequency, and (c-d) the normalized vertical displacement (solid line) and horizontal velocity (dotted line) for the first, second, and third vertical modes, respectively. The horizontal dashed line in (a) represents the dye injection depth.

Table 4.1. Period and frequency of internal modes on July 20-22, 2009.

Mode	V1H1	V1H2	V1H3	V2H1	V2H2	V2H3	V3H1	V3H2	V3H3
Period (h)	13	6.7	4.5	41	21	14	62	31	21
Frequency (cpd)	1.8	3.6	5.4	0.58	1.2	1.7	0.39	0.77	1.2
Frequency (10^{-5} Hz)	2.1	4.1	6.2	0.7	1.3	2.0	0.5	0.9	1.3

in West Okoboji Lake, L_R = 3200 m, which is more than twice the width of the basin, making effects of Earth's rotation negligible.

Internal Wave Spectra

A second method used to identify the dominant mode seiche in a stratified lake is computing the power spectra of wind speed and isotherm displacement (e.g., Münnich et al. 1992, Lemckert et al. 2004, Vidal et al. 2005, MacIntyre et al. 2009). If there is a significant peak in the energy spectra of the isotherm displacements at the predicted mode frequencies, there is evidence for the existence of that particular mode. Münnich et al. (1992) and Lemckert et al. (2004) identified a peak when the energy spectra increased by more than an order of magnitude. In some of the plots a small crest is found at the V1H1 frequency, but no distinguishable peak in energy can be observed at the predicted frequencies of the first two vertical modes. In addition, all the power spectra of the isotherm displacement lack a large spike in spectral energy at any frequency, making it difficult to identify a particular mode (Figures 4.6-4.9).

As a final approach to examine the relationships between isotherms, the coherency and phase spectra were computed between all the isotherms. The locations of the horizontal uninode, binodes, and trinodes on July 20-22 in West Okoboji Lake are plotted in Figure 4.10. The locations of the horizontal nodes determine whether isotherms should be in or out of phase at different locations. Temperatures from the thermistor chain at the LDS were used because it was located nearest to the lake boundary; thus, it had a greater potential to record large isotherm displacements from internal seiching motions than thermistor chain #2. The coherency and phase of each isotherm was referenced from the 20.5°C isotherm, as it was the warmest isotherm present during the period of interest. If isotherms are not coherent, they

cannot be used in comparison of phase; therefore, following Münnich et al. (1992), only isotherms that had coherency of 0.5 or greater were considered.

The phase of each coherent isotherm with respect to the 20.5°C isotherm on July 20-22, 2009 at the theoretical frequencies of the first three vertical modes is presented in Figure 4.11a-c. Each peak is exactly 180° out of phase with the adjacent peaks. If the water column is in phase at the location of maximum displacement of the mode, that provides support for

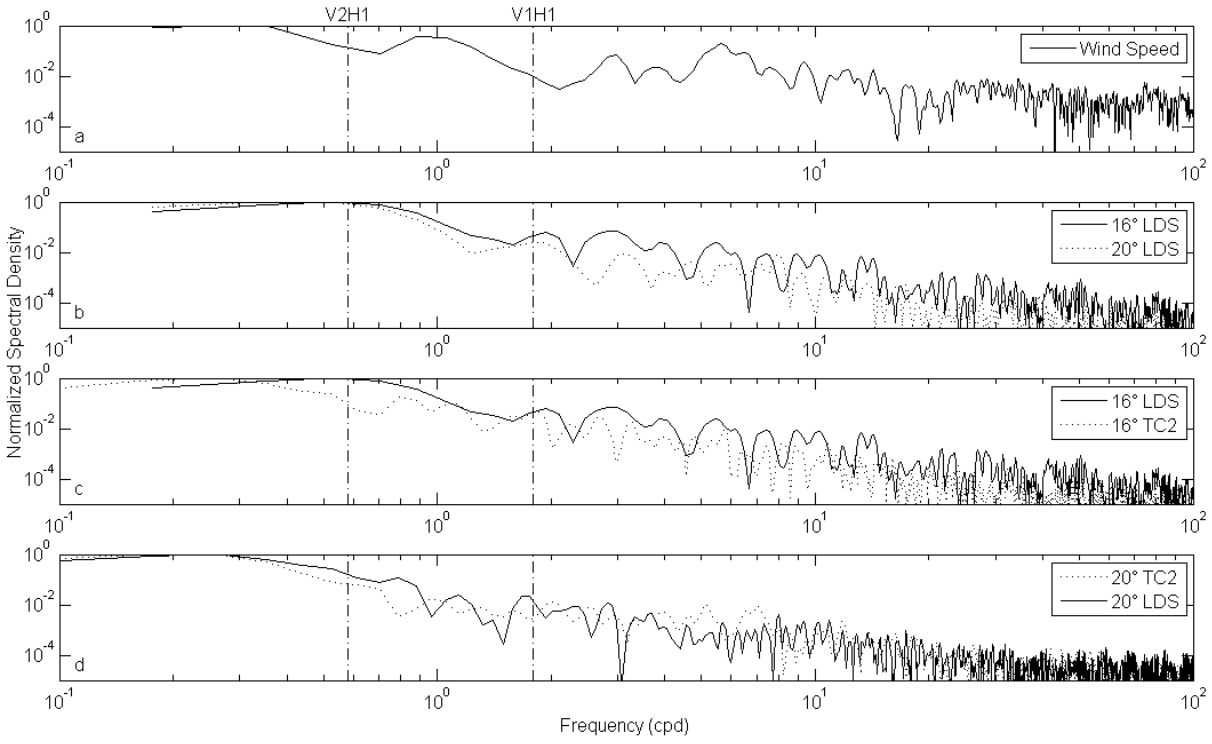

Figure 4.6. Normalized power spectra of (a) the wind speed at the LDS, (b) the displacement of the 16°C and 20°C isotherms at the LDS, (c) the 16°C isotherm displacement at the LDS and thermistor chain #2, and (d) the 20°C isotherm displacement at the LDS and thermistor chain #2. The frequencies of the V1H1 and V2H1 modes are indicated by the vertical dashed line. The power spectra are normalized by dividing by the maximum energy in the spectra.

the presence of that particular mode. At 15 m depth, the location of maximum vertical displacement of the V1H1 mode, the water column is approximately 90° out of phase (Figure 4.11a). At the V2H1 frequency (Figure 4.11b), the upper portion of the water column moves out of phase with the lower portion of the water column. The upper portion of the water column is approximately 180 degrees out of phase with the transition occurring half way between the peaks in theoretical maximum modal amplitude for the second mode. This

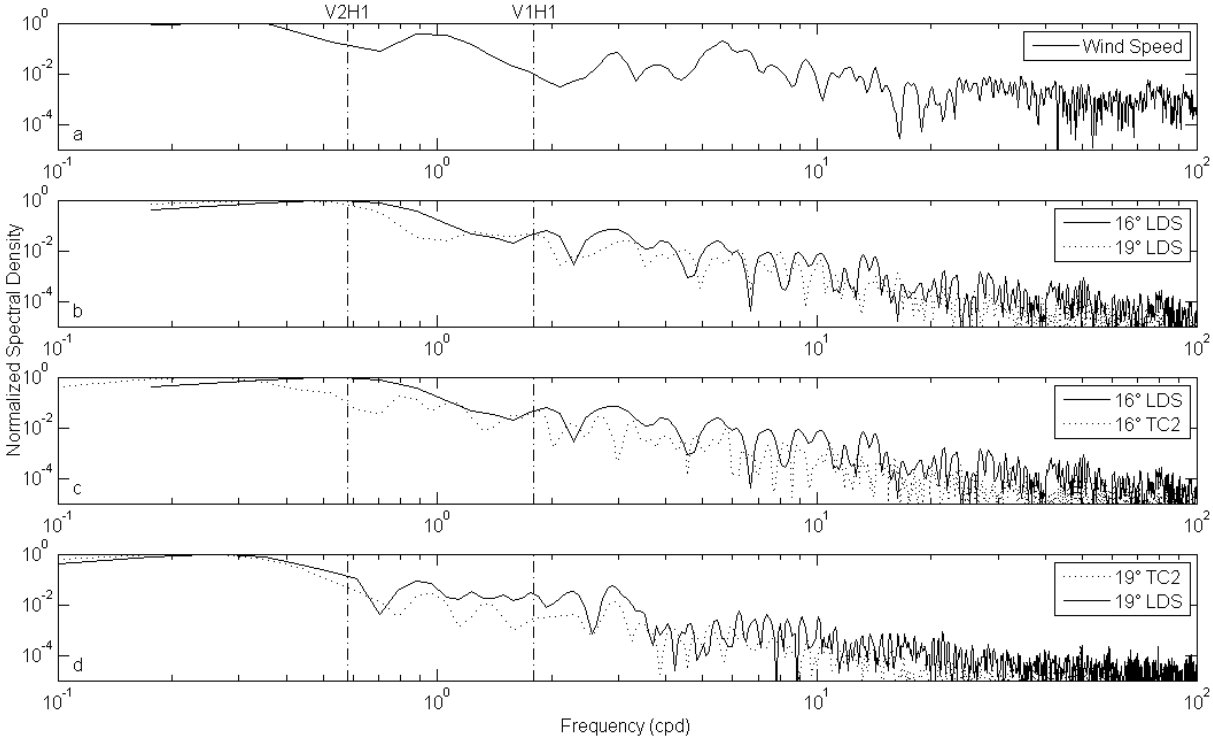

Figure 4.7. Normalized power spectra of (a) the wind speed at the LDS, (b) the displacement of the 16°C and 19°C isotherms at the LDS, (c) the 16°C isotherm displacement at the LDS and thermistor chain #2, and (d) the 19°C isotherm displacement at the LDS and thermistor chain #2. The frequencies of the V1H1 and V2H1 modes are indicated by the vertical dashed line. The power spectra are normalized by dividing by the maximum energy in the spectra.

behavior is in agreement with the presence of a second vertical mode. The phase profile of the V3H1 (Figure 4.11c) follows the theoretical phase profile with strong consistency overall. The phase profiles described above indicate that in the lake the potential exists for V2H1 and V3H1 seiches and does not necessarily rule out the presence of the V1H1 mode.

Several isotherm pairs (20°C and 16°C, 19°C and 16°C, 20°C and 15°C, and 19°C and 15°C) in the upper and lower metalimnion were used to test the vertical modes and to

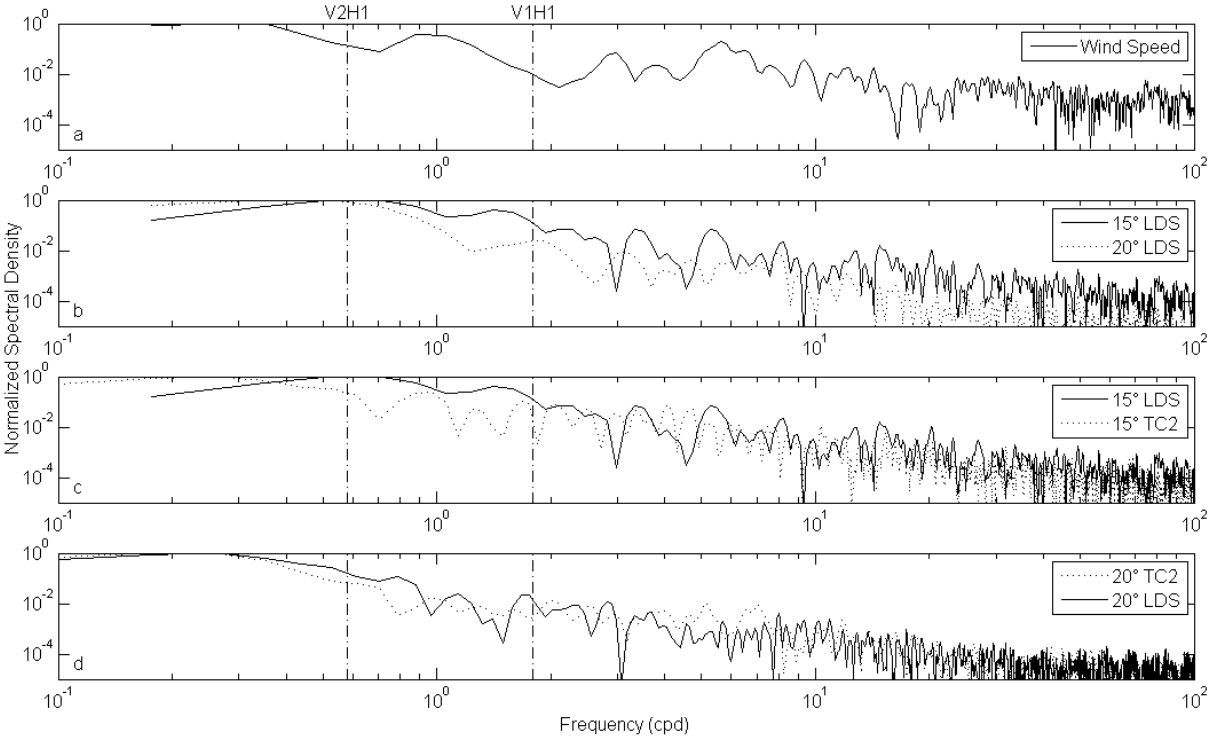

Figure 4.8. Normalized power spectra of (a) the wind speed at the LDS, (b) the displacement of the 15°C and 20°C isotherms at the LDS, (c) the 15°C isotherm displacement at the LDS and thermistor chain #2, and (d) the 20°C isotherm displacement at the LDS and thermistor chain #2. The frequencies of the V1H1 and V2H1 modes are indicated by the vertical dashed line. The power spectra are normalized by dividing by the maximum energy in the spectra.

determine the likelihood of the presence of higher horizontal modes. The coherency and phase spectra of the displacements of the 20°C and the 16°C isotherms at the LDS can be found in Figures 4.12a, 4.13a, and 4.14a for the VxH1-VxH3 modes, respectively. The coherency and phase spectra of the displacement of the 20°C isotherm at the LDS and thermistor chain #2 are displayed in Figure 4.12b, 4.13b, and 4.14b for the VxH1-VxH3 modes, respectively. The coherency and phase spectra of the displacement of the 16°C

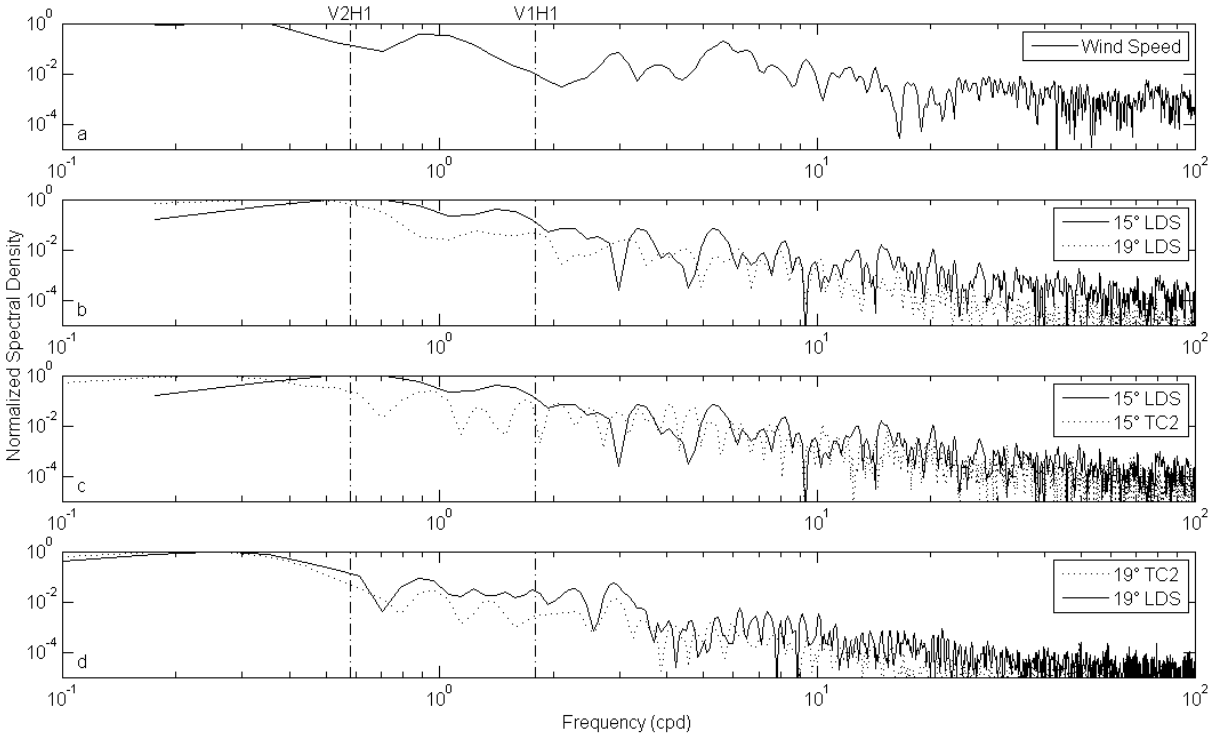

Figure 4.9. Normalized power spectra of (a) the wind speed at the LDS, (b) the displacement of the 15°C and 19°C isotherms at the LDS, (c) the 15°C isotherm displacement at the LDS and thermistor chain #2, and (d) the 19°C isotherm displacement at the LDS and thermistor chain #2. The frequencies of the V1H1 and V2H1 modes are indicated by the vertical dashed line. The power spectra are normalized by dividing by the maximum energy in the spectra.

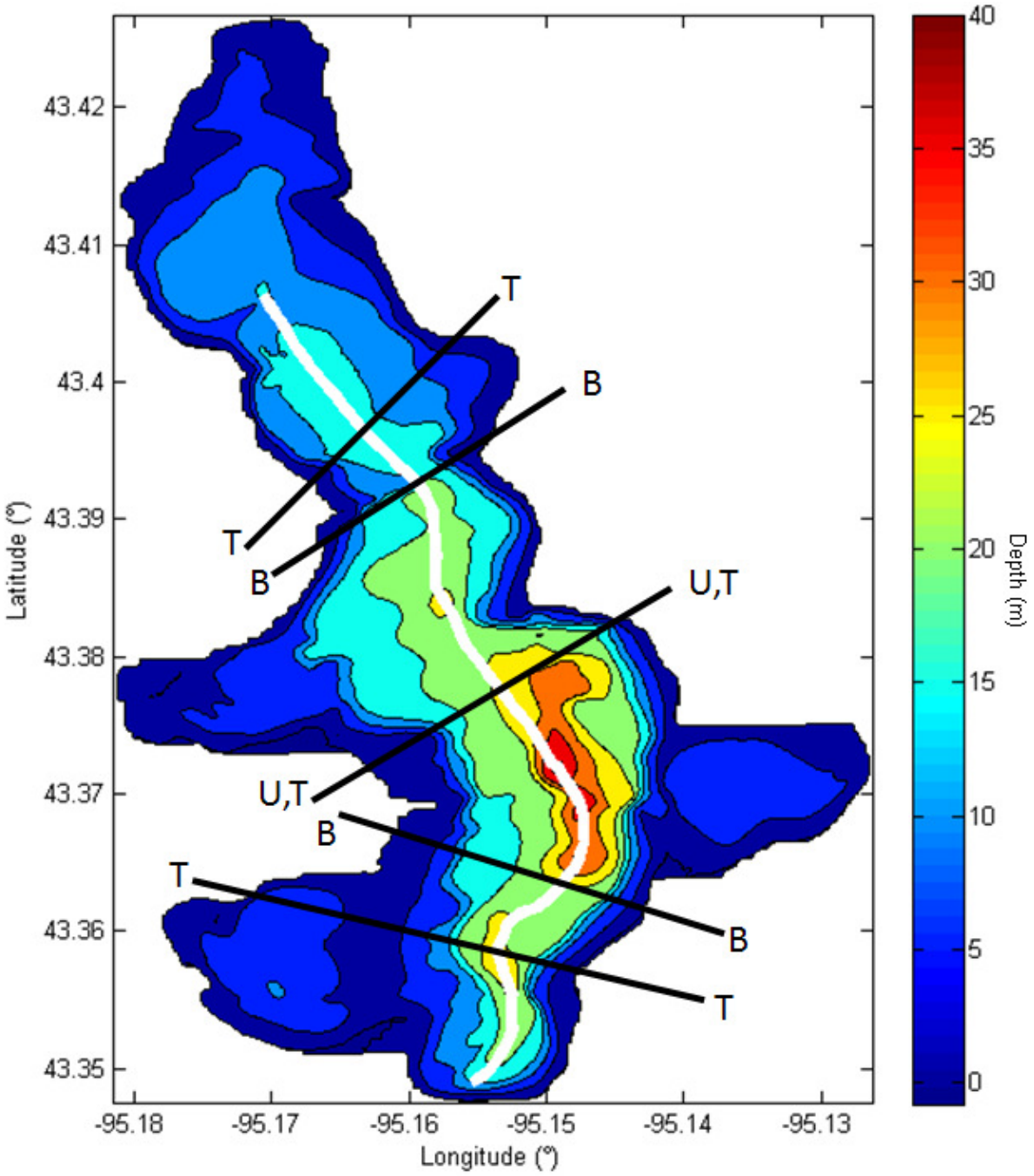

Figure 4.10. The location of the uninode (U), binodes (B), and trinodes (T) depicted by the solid black lines in West Okoboji Lake on July 20-22, 2009. The solid white line represents the thalweg at 13.25 m (the injection depth).

isotherm at the LDS and thermistor chain #2 are displayed in Figure 4.12c, 4.13c, and 4.14c for the VxH1-VxH3 modes, respectively. To determine the phase of an isotherm pair, the isotherms must be coherent; otherwise, the isotherm pair is not considered. The vertical mode can be determined from the phase at one location, and the horizontal mode present can be determined from the phase between the two locations at a given mode frequency. If the phase spectrum at a particular mode frequency is between -45° and 45°, the isotherm pair is considered to be in phase; otherwise, it is out of phase.

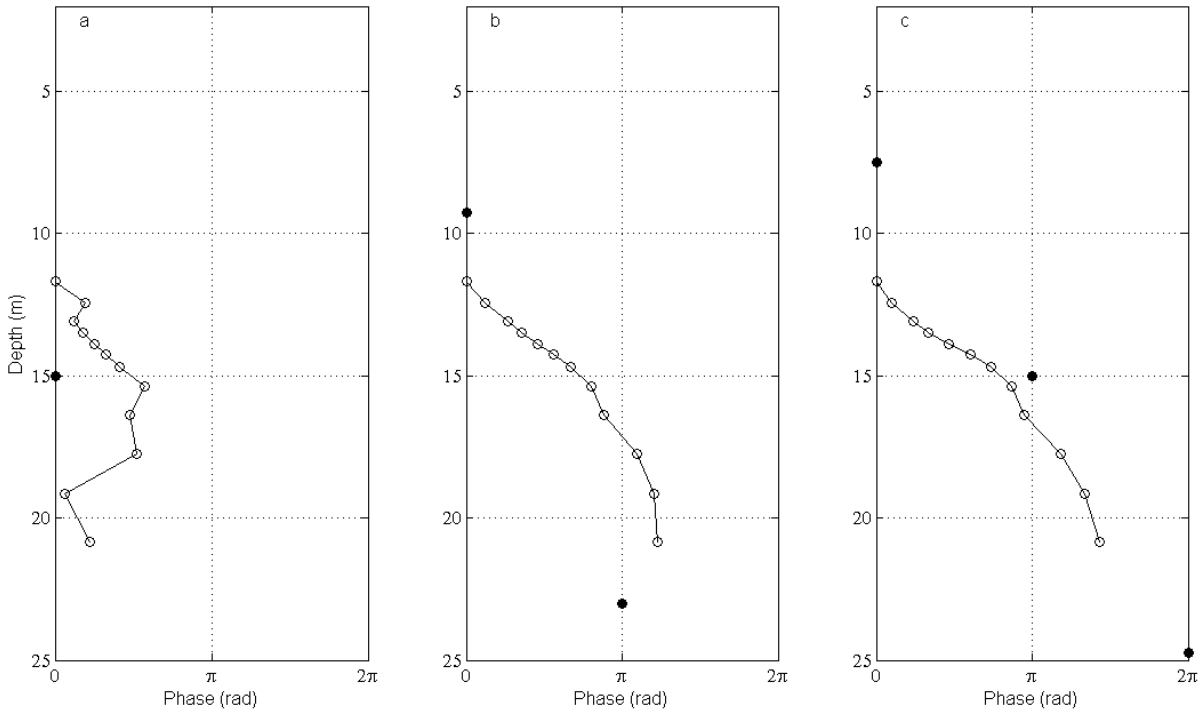

Figure 4.11. The phase of each isotherm (hollow circles) was referenced from the 20.5°C isotherm, the warmest isotherm during the dye study for the (a) first vertical mode, (b) second vertical mode, and (c) third vertical mode. The dark filled circles indicate the depths of the peaks in theoretical modal amplitude for each mode from Münnich et al. (1992).

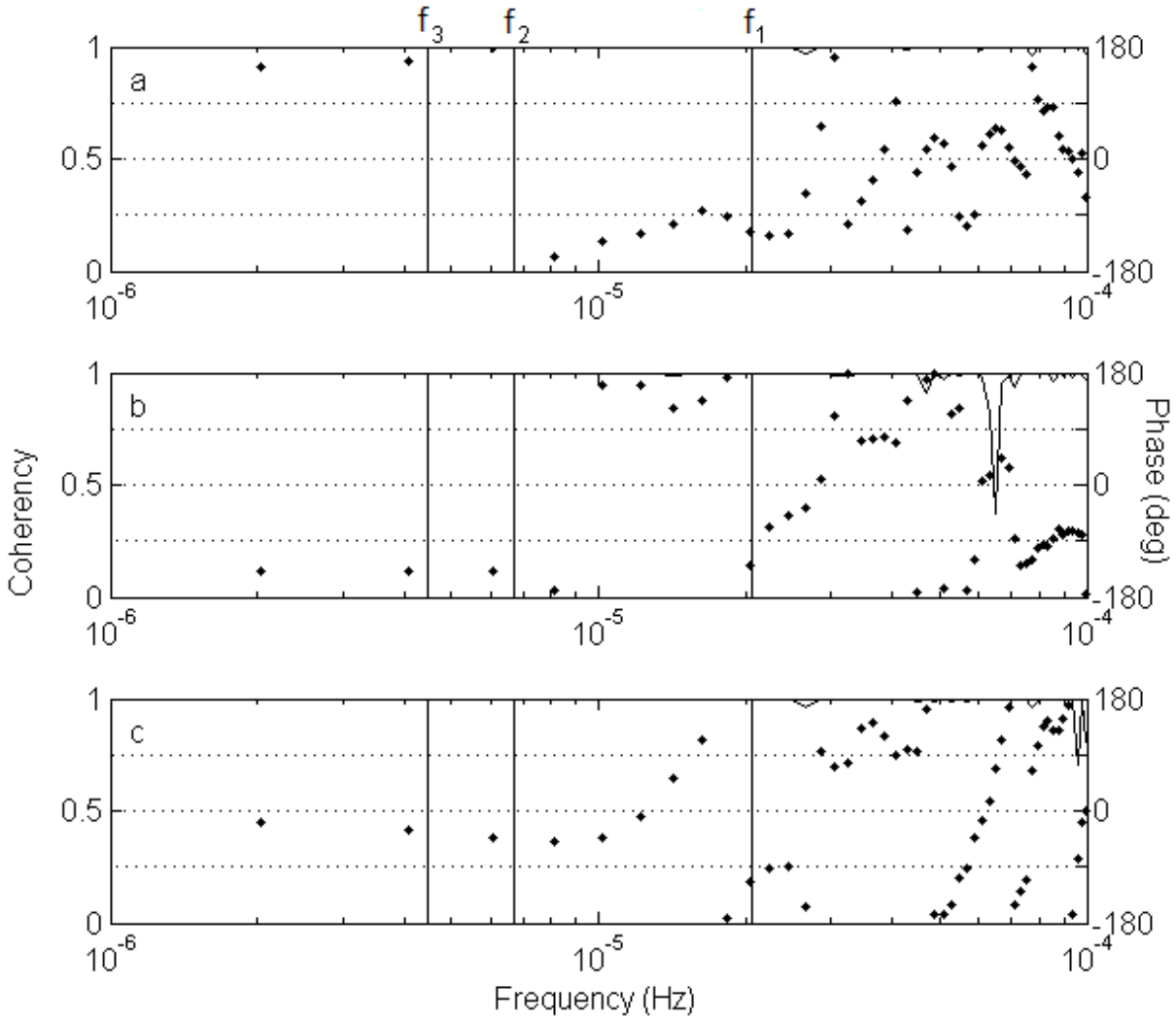

Figure 4.12. The coherency (solid line) and phase (diamonds) spectra at the estimated frequencies of the V1-3H1 frequencies (solid vertical lines): (a) between the 20°C and 16°C isotherm displacements as measured by the LDS thermistor chain, (b) between thermistor chain #2 and the LDS thermistor chain for the 20°C isotherm, and (c) between thermistor chain #2 and the LDS thermistor chain for the 16°C isotherm. The phase is only indicated when the coherency is greater than 0.5.

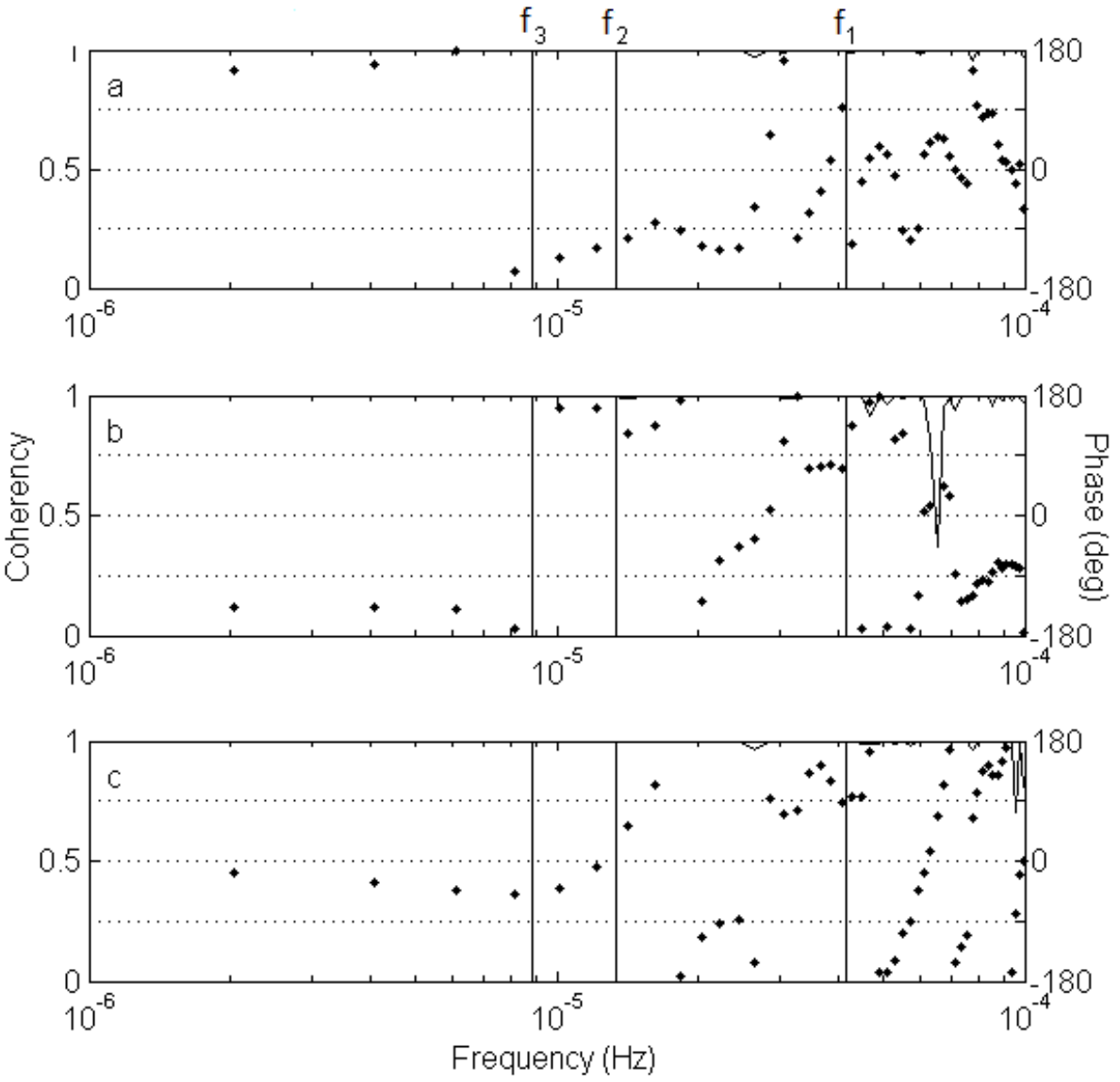

Figure 4.13. The coherency (solid line) and phase (diamonds) spectra at the estimated frequencies of the V1-3H2 frequencies (solid vertical lines): (a) between the 20°C and 16°C isotherm displacements as measured by the LDS thermistor chain, (b) between thermistor chain #2 and the LDS thermistor chain for the 20°C isotherm, and (c) between thermistor chain #2 and the LDS thermistor chain for the 16°C isotherm. The phase is only indicated when the coherency is greater than 0.5.

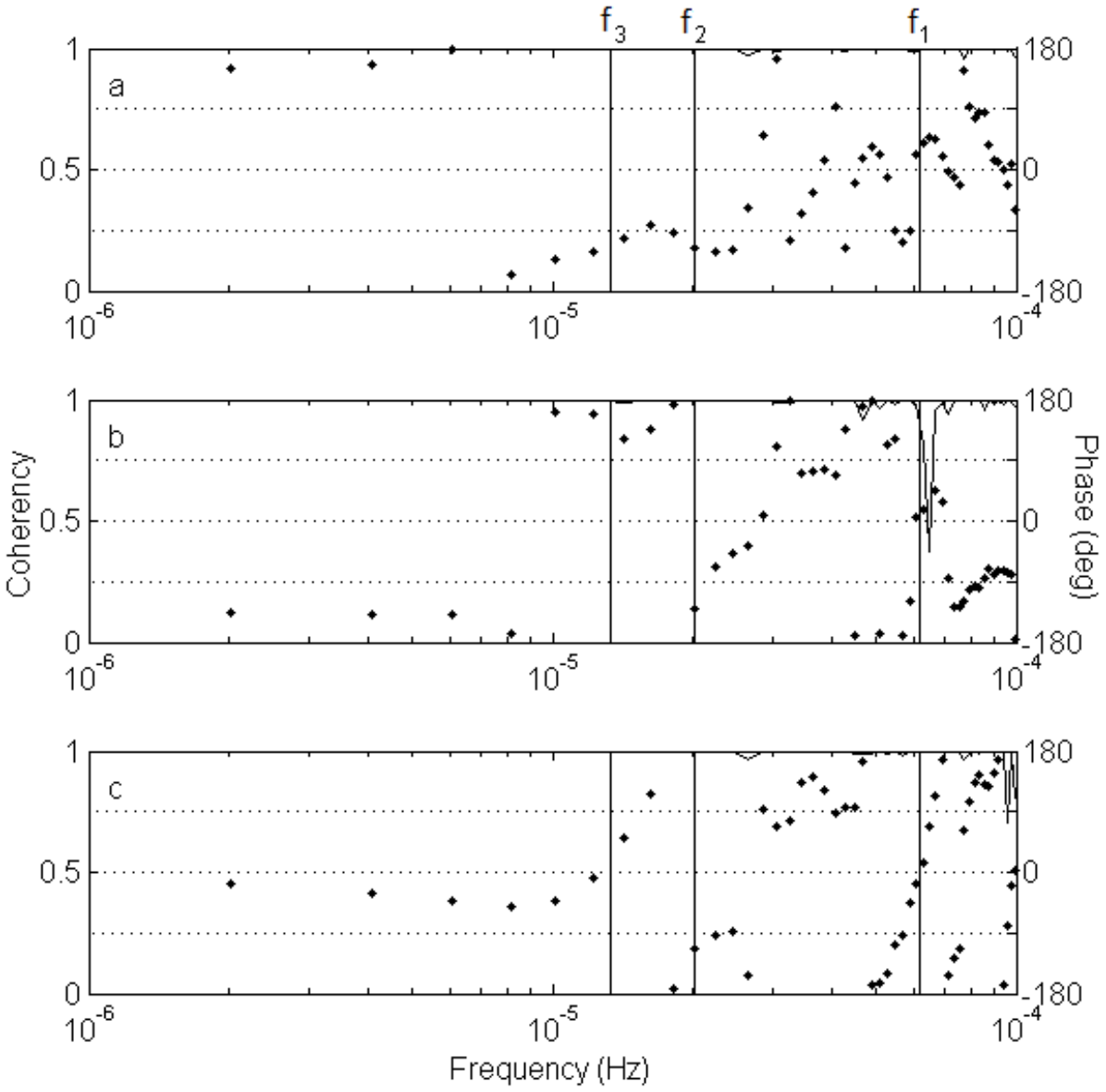

Figure 4.14. The coherency (solid line) and phase (diamonds) spectra at the estimated frequencies of the V1-3H3 frequencies (solid vertical lines): (a) between the 20°C and 16°C isotherm displacements as measured by the LDS thermistor chain, (b) between thermistor chain #2 and the LDS thermistor chain for the 20°C isotherm, and (c) between thermistor chain #2 and the LDS thermistor chain for the 16°C isotherm. The phase is only indicated when the coherency is greater than 0.5.

In order for the V1H1 seiche to be present, at the V1H1 seiche frequency, the isotherm in the upper metalimnion must be in phase with the isotherm in the lower metalimnion at the LDS, and the isotherms in the upper and lower metalimnion at the LDS must be out of phase with the upper and lower isotherm, respectively, at thermistor chain #2. For the V2H1 and the V3H1 seiche, all the isotherm pairs must be out of phase at the respective frequency. For the V1H2 and the V1H3, the opposite must be true: all the isotherms must be in phase at the respective frequency. The V2H2 and V2H3 modes require the upper and lower isotherms to be out of phase at the LDS, and the upper and lower isotherms at the LDS must be in phase with the upper and lower isotherms, respectively, at thermistor chain #2 at the mode frequencies. The V2H3 and V3H3 modes require the upper and lower isotherms to be out of phase at the LDS, and the upper and lower isotherms at the LDS must be out of phase with the upper and lower isotherms, respectively, at thermistor chain #2 at the mode frequencies.

Table 4.2 summarizes the results from the coherency and phase spectra shown in Figures 4.12-4.14. At nearly every frequency, the isotherm pairs have a coherency near one. While a single spectrum may show evidence for a particular mode, if the other spectra contradict it, there is no compelling reason to believe it is the dominant motion in the lake. From the four isotherm pairs, only a few times are all three spectra criteria satisfied providing evidence for a particular mode. However, since four different modes (V1H1, V2H1, V2H3, and V3H3) were identified, this suggests that no particular motion is dominant from July 20-22, 2009. Also, the larger the mode number identified, the larger the uncertainty of the method.

Table 4.2. Summary of the evidence from coherency and phase spectra for several different isotherm pairs at the dominant seiching modes. At the estimated seiching frequency, a seiche may be possible if the isotherm pair are coherent and of the proper phase shift at the same location for two isotherms and two different locations for the same isotherm. The white boxes are found when the requirements for the existence of the mode of interest have been satisfied and the shaded boxes occur when the requirement for existence are not satisfied because the isotherm pair is of the wrong phase or is not coherent. Only three times are all three requirements satisfied for the four isotherm pairs, suggesting the presence of that particular mode.

Isotherms	V1H1	V2H1	V3H1	V1H2	V2H2	V3H2	V1H3	V2H3	V3H3
20°C-16°C	in	out	out	in	out	out	in	**out**	out
20°C-20°C	out	out	out	in	in	in	out	**out**	out
16°C-16°C	out	out	out	in	in	in	out	**out**	out
19°C-16°C	in	**out**	out	in	out	out	in	**out**	out
19°C-19°C	out	**out**	out	in	in	in	out	**out**	out
16°C-16°C	out	**out**	out	in	in	in	out	**out**	out
20°C-15°C	in	out	out	in	out	out	in	**out**	**out**
20°C-20°C	out	out	out	in	in	in	out	**out**	**out**
15°C-15°C	out	out	out	in	in	in	out	**out**	**out**
19°C-15°C	**in**	out	out	in	out	out	in	out	out
19°C-19°C	**out**	out	out	in	in	in	out	out	out
15°C-15°C	**out**	out	out	in	in	in	out	out	out

Mixing

Vertical Eddy Diffusivity: *Microstructure*

Two profiles (onshore and offshore) of vertical eddy diffusivity from temperature microstructure taken on June 16, 2009 showed how topography affects mixing in West Okoboji Lake. At the approximate depth of the thermocline (14 m) on June 16, the vertical eddy diffusivity onshore was approximately two orders of magnitude greater than at the same depth offshore (Figure 4.15). This observation supports the idea that the majority of the mixing that occurs in lakes does so along the boundaries of the lake (Goudsmit et al. 1997; MacIntyre et al. 1999; Gloor et al. 2000; Wüest and Lorke 2003a; Lorke 2007). As identified in Figure 4.15a, there was a region about 2 m thick of heightened mixing along the sloping boundary onshore. Accordingly in Figure 4.15b, a layer near the lake bottom about 5 m thick associated with enhanced mixing was present offshore at the LDS. These observations suggest that a turbulent boundary layer was present along the bottom and side slopes of the lake at this time. The boundary layer thickness along the sloping boundary was not as great (2 m) as along the flat boundary (5 m), but the diffusivity was roughly an order of magnitude larger along the sloping boundaries.

Profiles of vertical eddy diffusivity from temperature microstructure recorded 0.5 h before the dye injection and 5.0, 25.5, and 52.5 h after injection are in Figure 4.16. The majority of the vertical diffusivities in the profile 0.5 h before the injection fell between 10^{-6} m^2 s^{-1} and 10^{-5} m^2 s^{-1}, with a slightly elevated region in the epilimnion (Figure 4.16a). The profile did not reach the injection depth and provided no clear evidence of enhanced mixing near the boundary because the vertical diffusivity showed minimal increase at the bottom; a phenomenon supported by the additional profiles. The vertical eddy diffusivity 5.0 h after

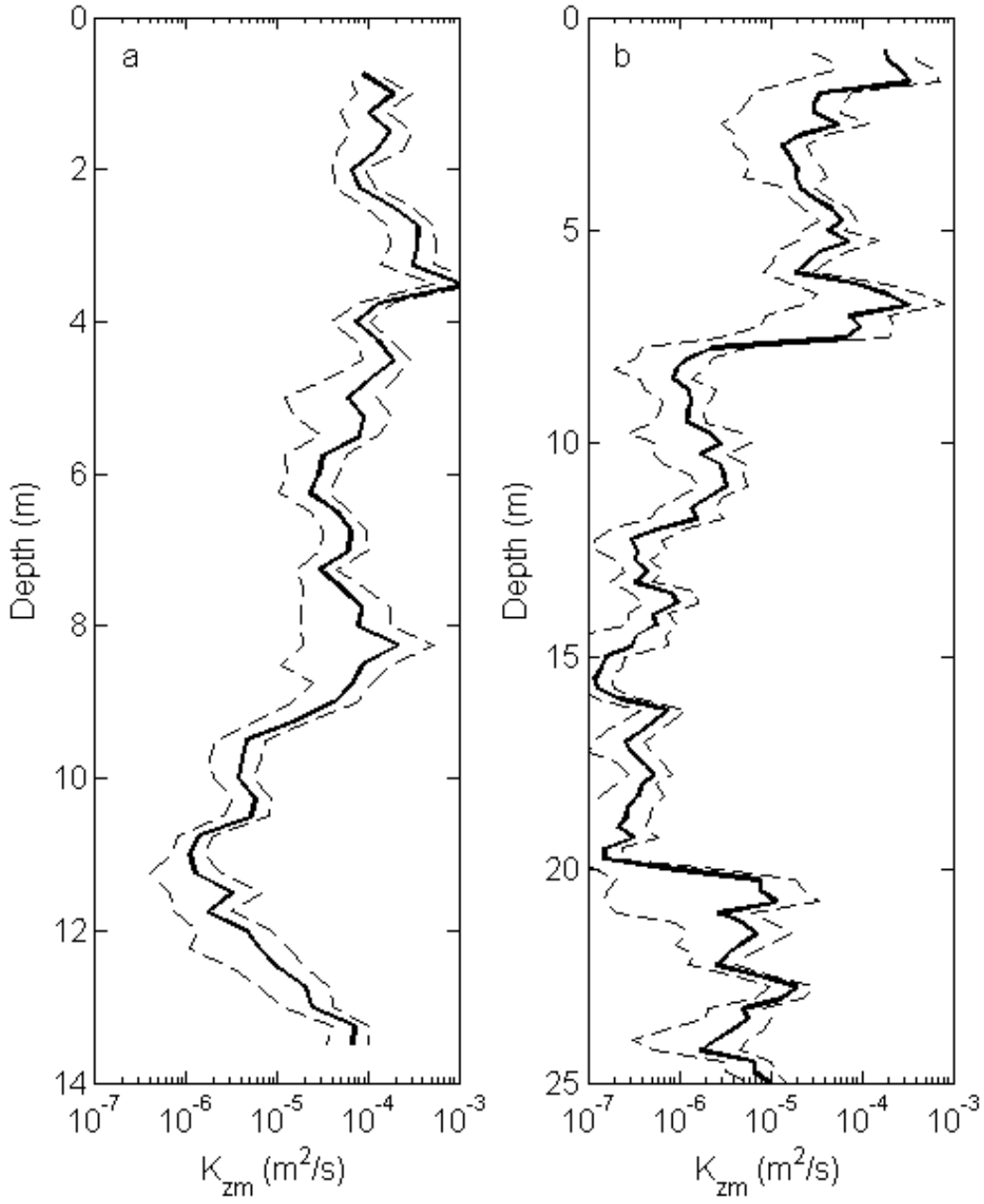

Figure 4.15. Profiles of vertical eddy diffusivity from microstructure measurements: (a) onshore, at the north end of the lake and (b) offshore, at the LDS on June 16, 2009. The dashed lines represent the 95% confidence limits of the entire profile.

injection was high in the epilimnion but decreased significantly to between 10^{-7} m^2 s^{-1} and 10^{-6} m^2 s^{-1} in the metalimnion near the lake boundary. In the profile 25.5 h after the injection the vertical diffusivity was higher in the epilimnion before decreasing to around 10^{-6} m^2 s^{-1} and 10^{-5} m^2 s^{-1} and increasing back to near 10^{-4} m^2 s^{-1}, then finally decreasing near 10^{-7} m^2 s^{-1} and 10^{-6} m^2 s^{-1} along the lake boundary. In the final profile collected at 52.5 h after the injection, the vertical eddy diffusivity was fairly uniform near 10^{-6} m^2 s^{-1} with a small

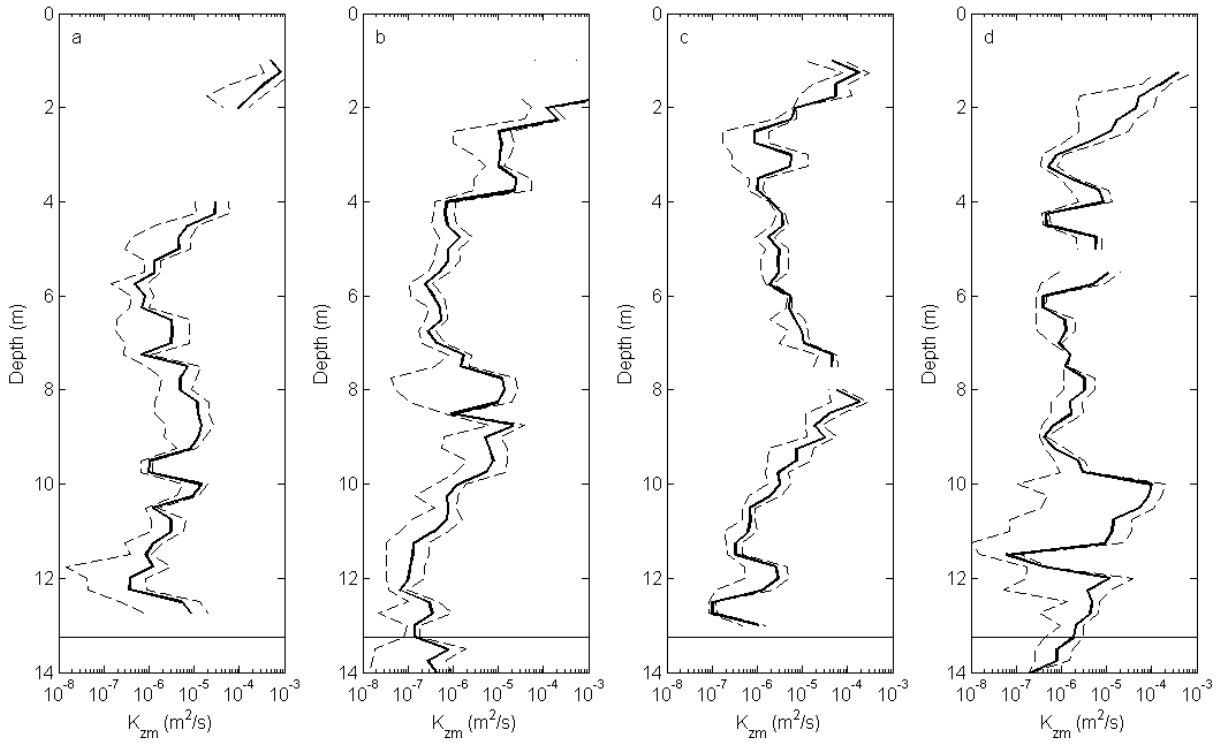

Figure 4.16. Profiles of vertical eddy diffusivity from microstructure measurements at the injection site (a) 0.5 h before, (b) 5.0 h, (c) 25.5 h, and 52.5 h after injection is represented by the heavy, solid black line. The dashed lines represent the 95% confidence limits of the entire profile. The solid horizontal line indicated the depth at which the dye was injected. The majority of the dye was detected between 12 m and 16 m depth.

increase at the top, and increase near 10 m to 10^{-4} m^2 s^{-1}, and a small decrease near the lake boundary. A noticeable reduction in the vertical eddy diffusivity is evident in the metalimnion near the lake boundary of the final three profiles which is not present in the first. At depths greater than 10 m, the values of vertical eddy diffusivity of the final three profiles were approximately one order of magnitude smaller than the profile collected just prior to the dye tracer injection. In the final two profiles, this result may be due to the lack of wind present at that time. The vertical eddy diffusivity during the dye study at the injection depth was estimated by determining the time averaged mean of the diffusivity from the first three profiles at or nearest to the injection depth. The time averaged vertical eddy diffusivity during the dye study from the microstructure profiles was approximately 10^{-6} m^2 s^{-1}, closely resembling results from previous studies, as discussed in chapter 5.

Vertical Eddy Diffusivity: *Heat Budget Method*

The vertical eddy diffusivity profiles computed with the heat budget method were similar at the LDS and thermistor chain #2. In the metalimnion, K_{zt} fell between 10^{-4} m^2 s^{-1} and 10^{-5} m^2 s^{-1}, and the vertical eddy diffusivity was larger than elsewhere in the profile (Figure 4.17). With K_{zt} falling to near 10^{-6} m^2 s^{-1} at the LDS, the smallest vertical diffusivities were found in the hypolimnion. From the profile of mean vertical eddy diffusivity, the single value of diffusivity was identified from the average value from thermistor chain #2 and the LDS thermistor chain at the injection depth in Figure 4.17. The vertical eddy diffusivity at the injection depth in West Okoboji Lake was approximately 2×10^{-5} m^2 s^{-1} at thermistor chain #2 and 10^{-5} m^2 s^{-1} at the LDS from the heat budget method (Jassby and Powell 1975), a little large compared to studies examining the hypolimnion of

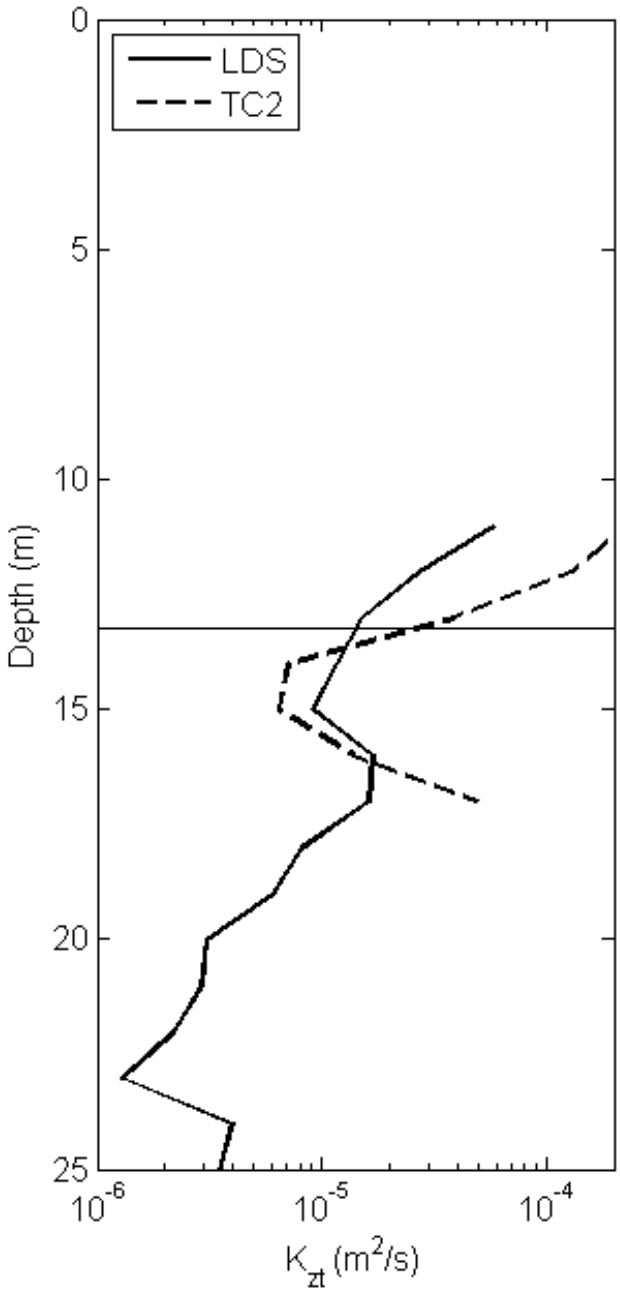

Figure 4.17. Profile of vertical eddy diffusivity from the thermistor chain at the LDS (solid) and thermistor chain #2 (dashed) on July 20-22, 2009. The solid horizontal line indicated the depth at which the dye was injected.

lakes. Since the LDS was closer to the location of the dye study the diffusivity observed at the LDS was used for the discussion.

Vertical Eddy Diffusivity: *Dye Tracking*

At the 10.5 h survey, the mean vertical profile over the entire horizontal area of the dye cloud extended approximately 2.1 m from 12.2 m to 14.3 m in depth with a maximum concentration of 2.1 ppb at 13 m depth (Figure 4.18). For the 29.2 h assessment, the mean dye cloud had an average vertical thickness of 3.5 m, at a depth between 12.3 m and 15.8 m,

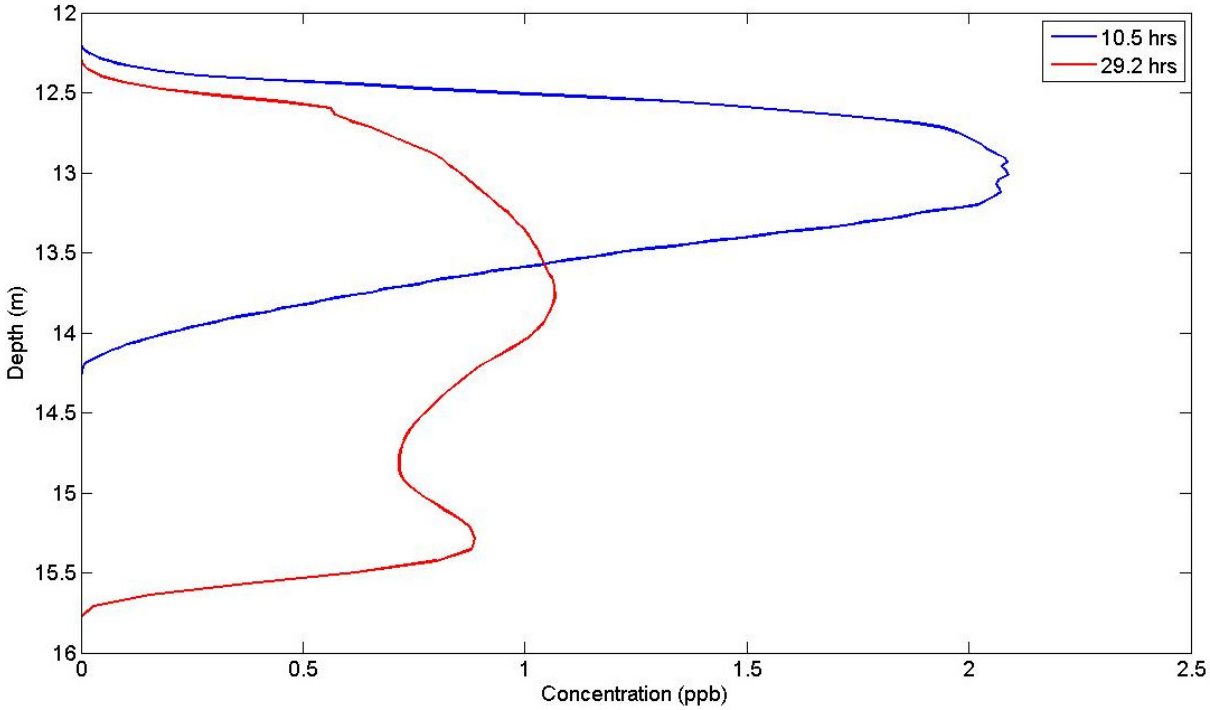

Figure 4.18. The depth-average dye concentration profile for the dye surveys centered at 10.5 h (blue) and 29.2 h (red) after dye tracer injection. The mean vertical profiles were computed using the entire horizontal area of the dye cloud. The concentrations were recorded as a function of temperature and converted to a function of depth using the average temperature profile at the LDS from July 20-22, 2009.

and a maximum concentration of 1.1 ppb at 13.8 m depth. The masses of tracer in the dye clouds measured at 10.5 and 29.2 h after injection differed by approximately 20%. The vertical eddy diffusivity calculated from the moment of concentration distribution from the mean dye profiles was approximately 4×10^{-6} m^2 s^{-1}, consistent with values from other studies.

Transport

Dye Tracer Maps

The dye cloud was mapped four times over a three day period from July 20-22, 2009 (Figures 4.19-4.24). The first dye map was gathered during the 4.5 h beginning immediately after injection, centered at approximately 2.5 h after injection. However, shortly after injection, the dye was still very concentrated at its center of mass. Because the SCUFA is accurate only at concentrations less than 200 ppb, the results from the dye map at 2.5 h after injection were not analyzed further. The second mapping of the dye cloud required 2.5 h (9.3-11.8 h after injection) and was centered 10.5 h after injection. At 10.5 h following dye injection, the dye front had propagated as far as 260 m from the injection point, resulting in a front velocity of 0.70 cm s^{-1}. The dye map was surveyed a third time for 6.8 h (25.8-32.6 h after injection), centered 29.2 h after the injection. The dye front had traveled 900 m into the lake's interior at its farthest point at a rate of 0.86 cm s^{-1} as determined from the dye map 29.2 h after injection. The final dye mapping required 3.7 h (48.4-52.1 h after injection) and was centered 50.2 h after injection. By this time much of the dye had diluted and was below the detectable limit of the SCUFA, and insufficient data were available for analysis of the 50.2 h dye map. From the plan-view dye maps at 10.5 h and 29.2 h, the total mass was only different by approximately 20% between the two dye surveys.

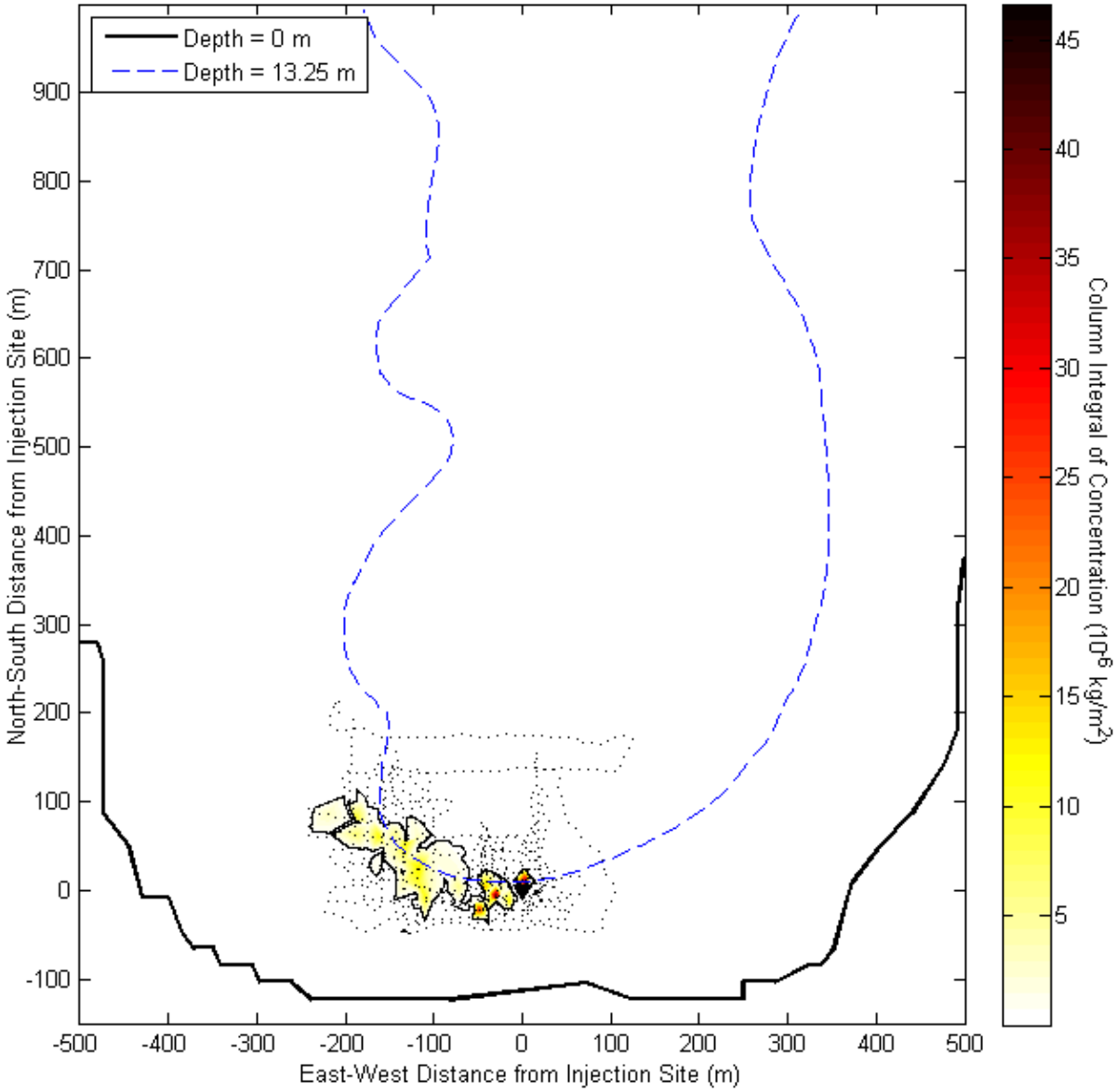

Figure 4.19. The results from the dye map survey centered at 2.5 h after injection (0-4.5 h). Using a data grid, the contour plot of the column integral displayed in the color bar was placed on a map of the lake's perimeter outlined with the heavy black line. The thin blue dashed line represents the injection isobath of 13.25 m. The thin black contour line was plotted where the column integral was one percent of the maximum column integral to outline the dye cloud. The boat track was also identified on the plot in the form of a dotted black line. Finally, the injection location was identified on the plot by the black triangle.

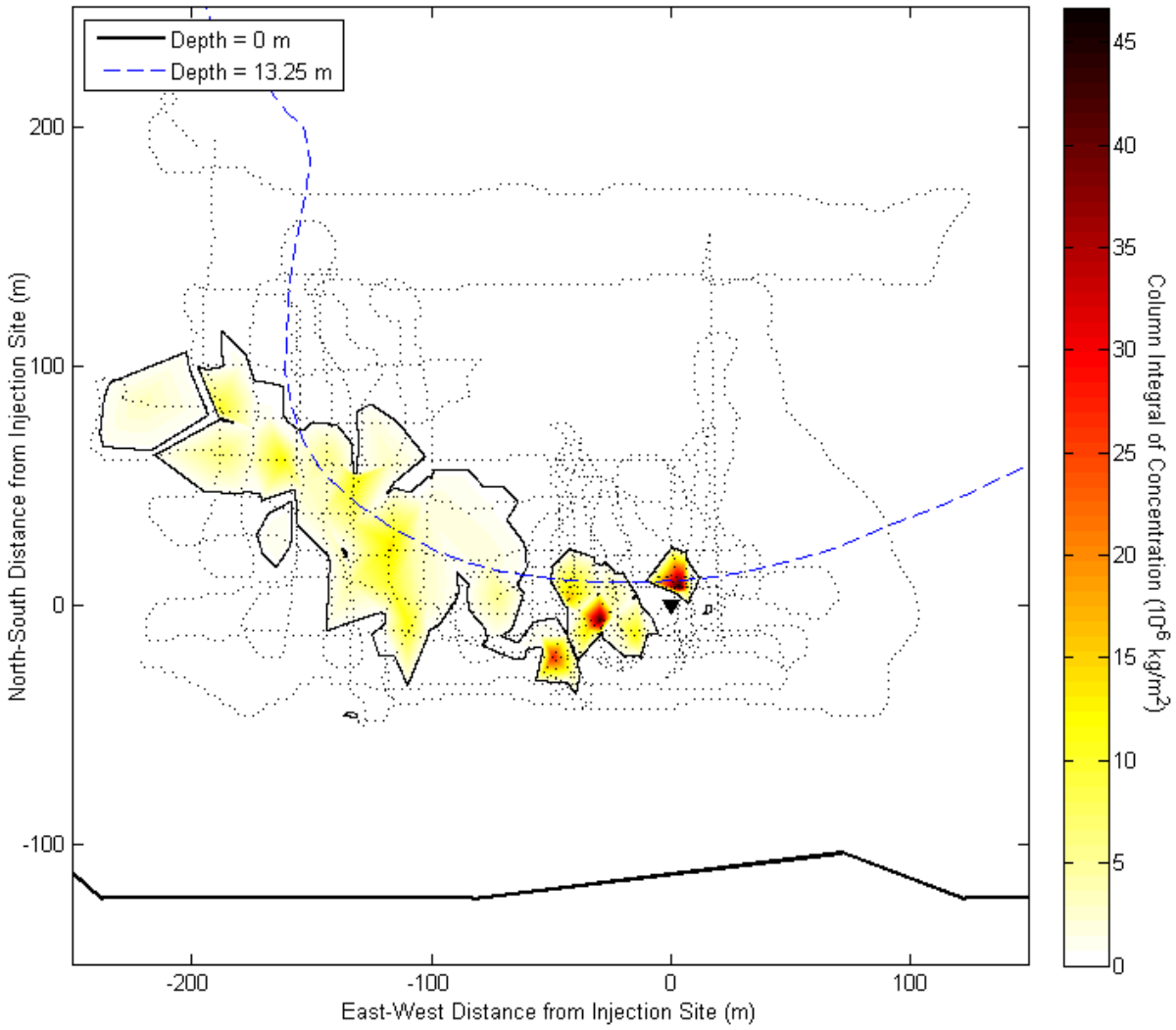

Figure 4.20. Same as Figure 4.19 but zoomed to the dye patch.

Horizontal Eddy Diffusivity

From the dye surveys collected at 10.5 h and 29.2 h, the horizontal diffusivity was estimated to be between 0.2×10^{-1} and 4×10^{-1} m^2 s^{-1} using Equation (3.7). In Equation (3.7), K_x and K_y were adjusted until the resulting extents of theoretical dye cloud matched the plan view of the outer edge of the dye maps collected at 10.5 h and 29.2 h in Figures 4.21 and

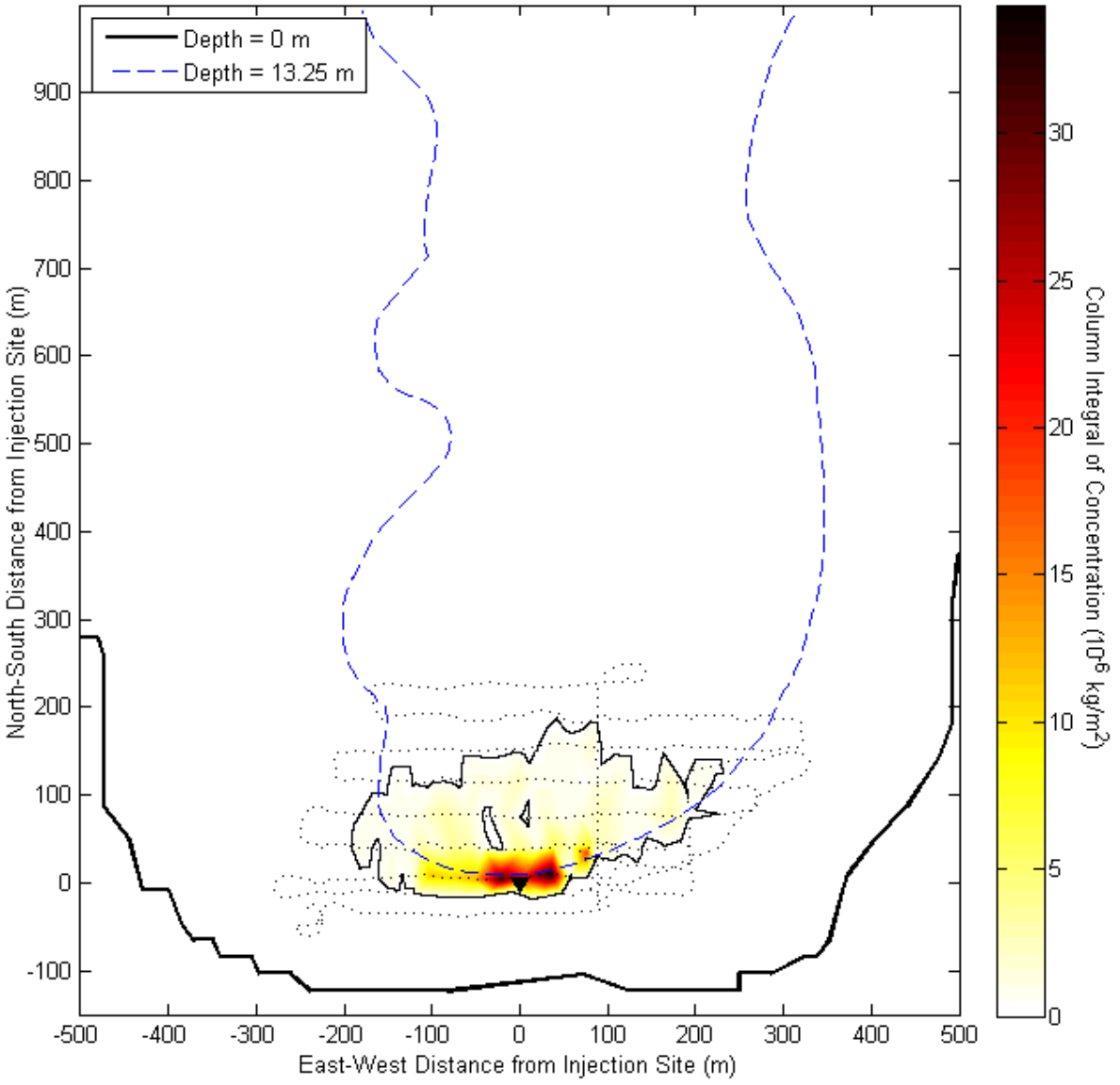

Figure 4.21. The results from the dye map survey centered at 10.5 h after injection (9.3-11.8 h). Using a data grid, the contour plot of the column integral displayed in the color bar was placed on a map of the lake's perimeter outlined with the heavy black line. The thin blue dashed line represents the injection isobath of 13.25 m. The thin black contour line was plotted where the column integral was one percent of the maximum column integral to outline the dye cloud. The boat track was also identified on the plot in the form of a dotted black line. Finally, the injection location was identified on the plot by the black triangle.

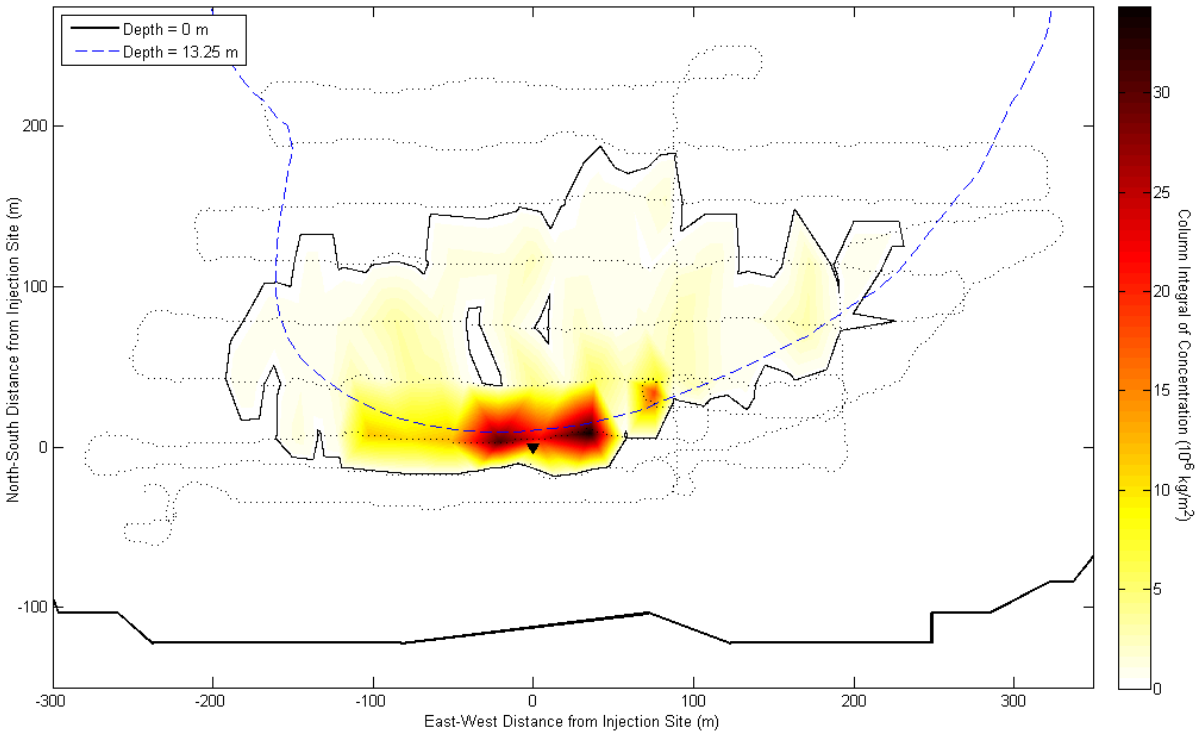

Figure 4.22. Same as Figure 4.20 but zoomed to the dye patch.

4.23. At 10.5 h, the western edge of the dye cloud estimated K_x at 0.9×10^{-1} m^2 s^{-1} and 0.4×10^{-1} m^2 s^{-1} for the eastern edge and at 29.2 h, both the western and eastern extents of the dye cloud resulted in K_x= 0.2×10^{-1} m^2 s^{-1}. At 10.5 h, K_y= 0.5×10^{-1} m^2 s^{-1} and at 29.2 h, K_y= 4×10^{-1} m^2 s^{-1}.

Summary

The external force of the wind was compared to the stabilizing force of the stratification to determine the Lake number over roughly a two month period in the late spring and early summer of 2009. The buoyancy frequency and wave structure was deduced

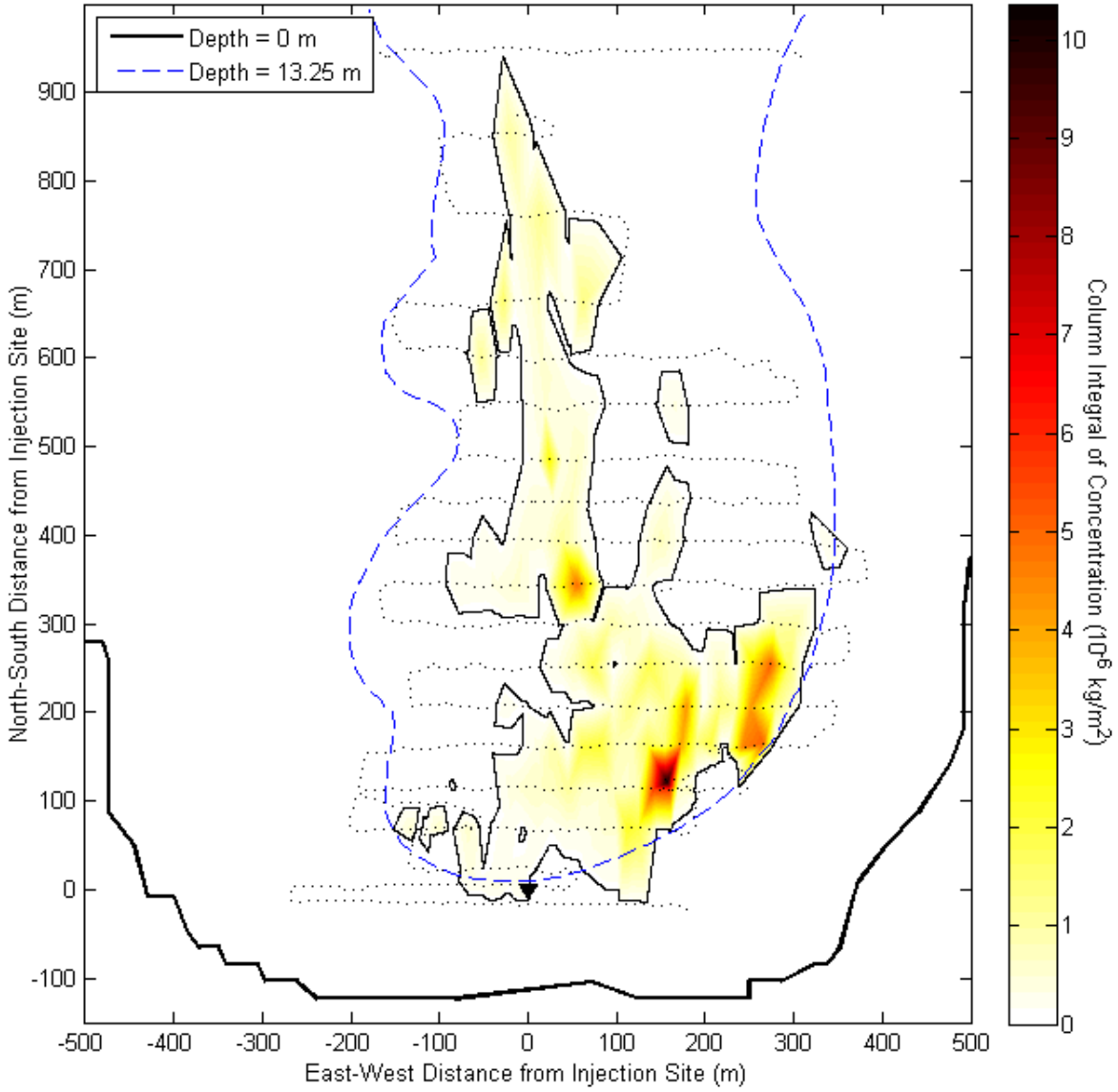

Figure 4.23. The results from the dye map survey centered at 29.2 h after injection (25.8-32.6 h). Using a data grid, the contour plot of the column integral displayed in the color bar was placed on a map of the lake's perimeter outlined with the heavy black line. The thin blue dashed line represents the injection isobath of 13.25 m. The thin black contour line was plotted where the column integral was one percent of the maximum column integral to outline the dye cloud. The boat track was also identified on the plot in the form of a dotted black line. Finally, the injection location was identified on the plot by the black triangle.

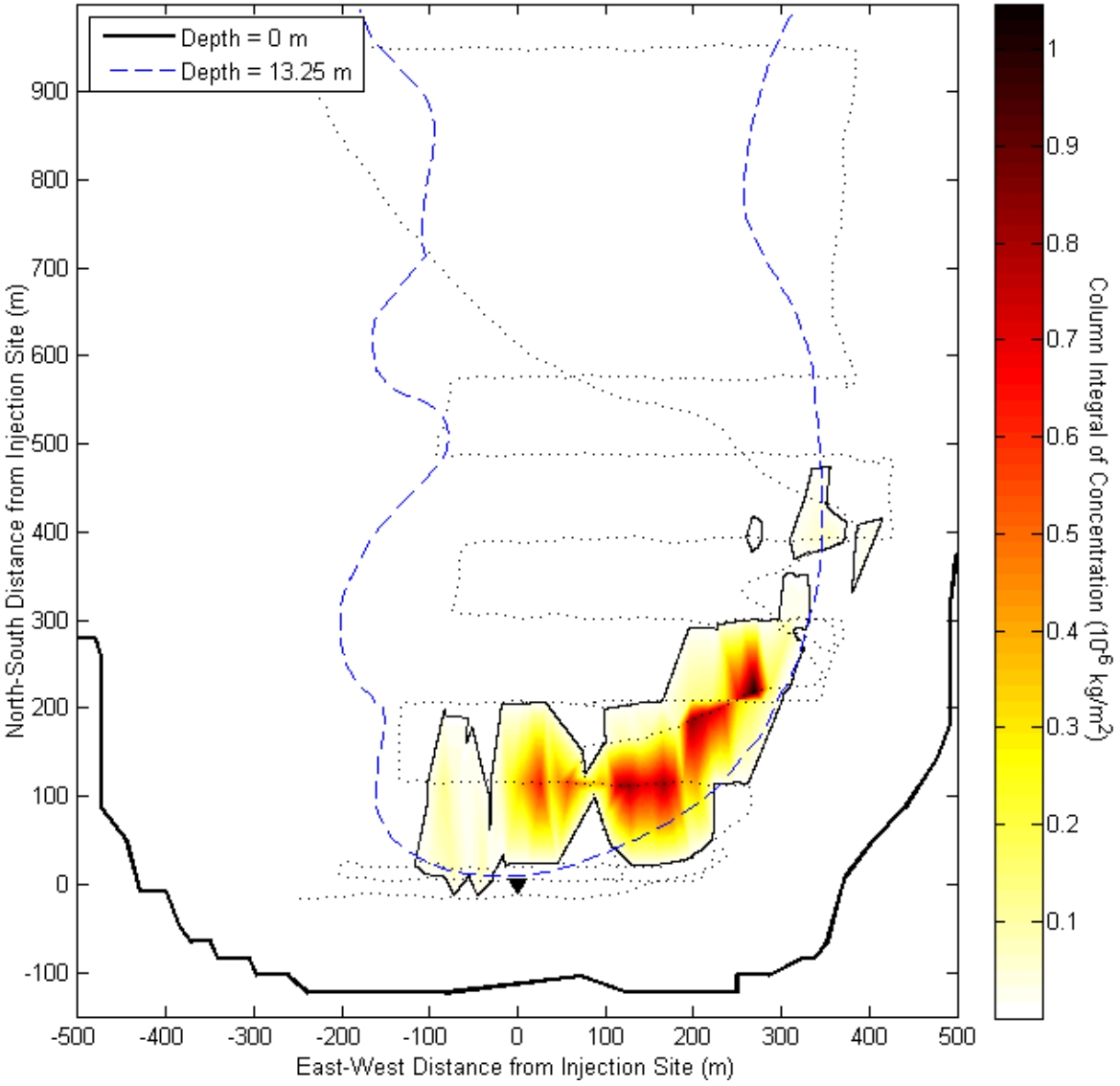

Figure 4.24. The results from the dye map survey centered at 50.2 h after injection (48.4-52.1 h). Using a data grid, the contour plot of the column integral displayed in the color bar was placed on a map of the lake's perimeter outlined with the heavy black line. The thin blue dashed line represents the injection isobath of 13.25 m. The thin black contour line was plotted where the column integral was one percent of the maximum column integral to outline the dye cloud. The boat track was also identified on the plot in the form of a dotted black line. Finally, the injection location was identified on the plot by the black triangle.

from the thermistor chains during a tracer study which took place from July 20-22, 2009. Estimates of mixing intensity, using vertical eddy diffusivity, were determined from three methods. The dye tracer provided the ability to track the fate of boundary fluid in the metalimnion over a period of approximately 52 h. From the dye tracer survey maps, an estimate of horizontal mixing was able to be obtained.

CHAPTER 5. DISCUSSION

Introduction

The results are evaluated in this chapter. This includes interpretation of the significance of the stratification and forcing, internal waves, mixing, and transport observed during the dye study. The first section summarizes the thermal structure of the lake and external forcing. The second section describes the internal wave field. The third section compares the vertical mixing observed from three different methods and previous work. The final section sheds light on the nature of the transport observed.

Stratification and Wind Forcing

During the dye study, the lake was much less stratified than previous tracer studies (e.g., Wüest et al. 1996, MacIntyre et al. 2009, Wain and Rehmann, in press). In West Okoboji Lake, the water temperature ranged from roughly 22°C at the surface to approximately 14°C at 25 m depth. However, the water temperature difference was approximately 14°C in Lake Alpnach over 34 m depth (Wüest et al. 1996) and 19°C in Ada Hayden Lake over 15 m depth (Wain and Rehmann, in press). The density difference between the surface layer and hypolimnion of West Okoboji was less than 2 kg m^{-3}, while the density difference of Mono Lake was approximately 16 kg m^{-3} (MacIntyre et al. 2009). The density differences, and other parameters, from other studies are compared to those in West Okoboji Lake in Table 5.1

Table 5.1. The lake conditions from previous studies compared to the values observed in West Okoboji Lake on July 20-22, 2009.

Paper	Wüest et al. (1996)	MacIntyre et al. (2009)	Wain and Rehmann (in press)	West Okoboji Lake
Density difference (kg m^{-3})	1.7	16	3.5	1.5
Max N (cph)	160	85	60	30
Peak wind (m s^{-1})	5.9	20	12.5	6.8
Mean wind (m s^{-1})	2.2	5	4	2.9
L_N range	4-10^4	3-300	2-600	1.8-940
Mean depth (m)	22	17	15	12
Maximum depth (m)	34	45	17	41
Surface area (km^2)	5	150	0.3	16
Dominant wave periods (h)	12, 24	15, 44	1.3	13, 41

Winds were weaker during the dye study than in other studies. The peak wind speed was 6.8 m s^{-1}, and the mean wind speed was 2.9 m s^{-1}. Wüest et al. (1996) observed an oscillatory wind that typically peaked daily near 4-5 m s^{-1} during the one month study. MacIntyre et al. (2009) observed wind speeds typically near 3-4 m s^{-1} with a few spikes around 10-15 m s^{-1} during the 18 day study. Wain and Rehmann (in press) observed a wind speed that predominantly was less than 3 m s^{-1} except for three brief spikes of 8 m s^{-1} and one of 12 m s^{-1} during the two-day study.

Although in West Okoboji Lake the wind observed was not as great, the weak stratification resulted in a Lake number equal to or less than in previous studies in lakes. The Lake number in Lake Alpnach was near 4 during the tracer study of Wüest et al. (1996). MacIntyre et al. (2009) found that the Lake number remained above 10 and usually $50 < L_N$

< 100 except for a couple times which corresponded to the peaks in wind velocity. Wain and Rehmann (in press) usually observed a Lake number of roughly 100 except for during the spikes in wind speed, where it is near 10. The smaller Lake number in West Okoboji Lake resulted in internal waves and transport similar or greater than previous studies, as discussed below.

The pink shaded rectangle in Figure 5.1 represents the conditions in West Okoboji Lake during the dye tracer study in July 20-22, 2009, when the depth ratio varied from 0.28 to 0.38 and W^{-1} varied from 0.001 to 0.14. The laboratory experiments of Horn et al. (2001) suggest that linear internal wave theory should be valid as the shaded region fall mainly in Regime 1.

Internal Waves

The actual periods of the internal seiches may be larger than those estimated with the n-layer method of Münnich et al. (1992). The model of Münnich et al. (1992) simplified the bathymetry as a rectangular prism with uniform length, width, and depth and estimated the first vertical mode period to be 13.4 h. Fee and Bachmann (1968) estimated the surface seiching periods of oscillation and the horizontal and vertical displacement in West Okoboji Lake by breaking the lake into a number of segments and applying the model of Defant (1918). By increasing the number of segments analyzed, greater consideration is provided to the complex bathymetry of West Okoboji Lake. The estimated period of the first mode seiche in West Okoboji Lake considering 160 individual segments was 25.8 min (Fee and Bachmann 1968). Although surface and internal seiches differ in a number of ways including wave period, the results of Fee and Bachmann (1968) should still provide

invaluable insight, especially since Lemmin and Mortimer (1986) successfully adapted the model for internal seiches. The period Fee and Bachmann (1968) calculated with only two sections was only approximately 70% of the period calculated with 160 sections. Therefore, one can deduce that the mode periods, estimated from Münnich et al. (1992) using only one section, may be underestimated.

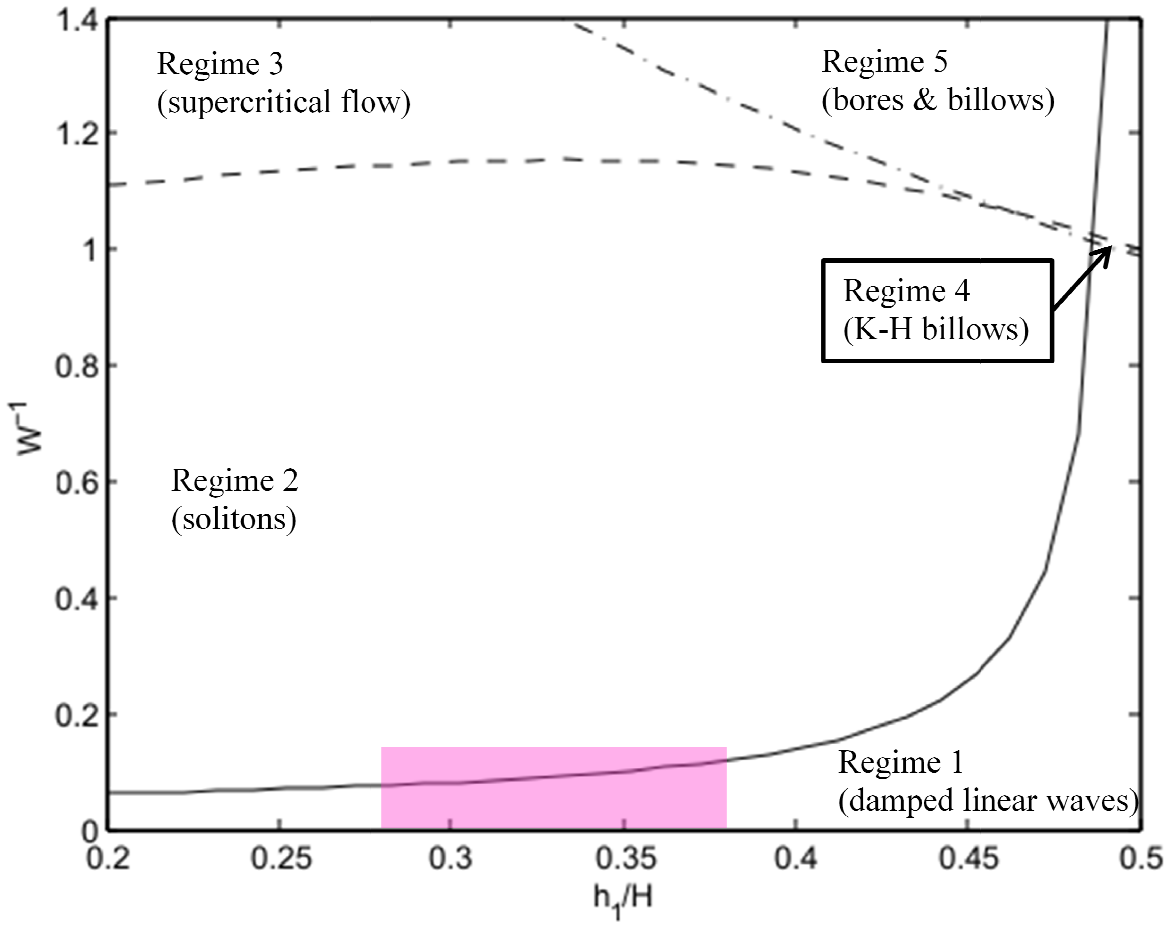

Figure 5.1. Five wave response regimes modified from Horn et al. (2001) that are determined from the Wedderburn number and the ratio of the thermocline to total lake depth. The pink shaded rectangle represents the predicted response of West Okoboji Lake based on the conditions during the dye tracer study.

As mentioned in Chapter 4, there are three common methods used to identify the internal wave field present in a stratified lake. The three most common approaches are isotherm displacement (e.g., Wiegand and Chamberlain 1987, Wüest et al. 1996, Marti and Imberger 2008), spectra of isotherm displacement (e.g., Münnich et al. 1992, Antenucci et al. 2000, MacIntyre et al. 2009), and coherency and phase spectra of isotherm displacement (e.g., Lemmin and Mortimer 1986, Gloor et al. 1994, Lemckert et al. 2004). The approaches used by previous studies to identify the seiching mode can be found in Table 5.2.

Table 5.2. The different approaches used to predict the dominant seiching mode from previous studies in stratified lakes.

Paper	Isotherm Displacement	Spectra	Coherency and Phase
Lemmin and Mortimer (1986)		×	×
Wiegand and Chamberlain (1987)	×	×	
Münnich et al. (1992)	×	×	×
Gloor et al. (1994)		×	×
Wüest et al. (1996)	×		
MacIntyre et al. (1999)		×	
Antenucci et al. (2000)	×	×	
Appt et al. (2004)		×	
Hondzo and Haider (2004)		×	
Lemckert et al. (2004)	×	×	×
Vidal et al. (2005)	×	×	
Marcé et al. (2007)	×	×	
Marti and Imberger (2008)	×	×	
MacIntyre et al. (2009)	×	×	
West Okoboji Lake	×	×	×

The isotherm displacement time series (Figures 4.3-4.4) at the LDS and thermistor chain #2 on July 20-22, 2009 provides evidence for both the V1H1 mode seiche and the V2H1 mode seiche. Near noon on July 21 at both locations, a contraction of the isotherms in the metalimnion is visible, which is a distinguishable feature of a second vertical mode. However, early in the day on July 20 and all day on July 22, the isotherms in the metalimnion seem to move coherently, indicative of first vertical mode. Also, when expanding the time series in Figures 4.3-4.4, there is no other evidence of metalimnic contraction or expansion, and the thickness of the metalimnion is static. Isotherm displacement-time series displaying similar trend at both locations provides evidence of the higher horizontal modes such as second or third because the isotherms are in phase at both locations.

As noted in the previous chapter, the spectra of the wind and a number of isotherm pairs at two different locations were plotted (Figure 4.6-4.9) to reveal the dominant modes by distinguishing any spikes in spectral energy at the predicted seiching modes. However, there were no distinguishable spikes in energy at any frequency in any of the spectra which hindered the ability to identify any particular mode. Coherency and phase spectra of displacement of isotherm pairs are helpful for internal wave analysis because they allow for examination of horizontal mode along with vertical modes. Analysis of a number of isotherm pairs revealed the V1H1, V2H1, V2H3, and V3H3 modes. Since four different waves were identified depending on which isotherm pairs were scrutinized, the dominant modes in the internal wave field may be difficult to identify. However, the V1H1 and V2H1 seem to be the most prevalent from the three different approaches, but there may not be a single dominant mode on July 20-22, 2009, rather a conglomeration of several modes could make up the wave field.

After analysis of the internal wave field via three different methods, the investigation reveals that no particular mode is dominant during the tracer study. One particular reason for a great deal of variability in the internal wave field is the period of the internal waves. It takes a constant wind for one-quarter of the wave period to initiate an internal seiche (Spigel and Imberger 1980). Thus, if the wind is constant but the direction is not constant as was the case during the tracer study, it may affect the internal wave field. If the wind direction changes regularly, it may not to have enough strength to tilt the surface layer initiating a seiche. With seiche periods of 13 h, 41 h, 62 h, a sustained wind for 3-15 h were not too common. During the roughly two month period of the LDS deployment, on only three occasions was wind of 4 m s^{-1} (the minimum to reduce the Lake number to 10 in West Okoboji Lake for summer stratification) sustained long enough to excite the first vertical mode, and the wind was never sustained long enough at 4 m s^{-1} to initiate the second or third mode. In a 25 day period, MacIntyre et al. (2009) also only observed a sustained wind on three occasions that reduced the Lake number to less than 10 to initiate seiching. However, since the period of the first mode was only approximately 1 h, Wain and Rehmann (in press) frequently observed suitable winds for seiching. In addition, since the wind direction is not considered when calculating the wave number, a low Lake number will result no matter how frequently the wind reverses direction.

The buoyancy frequency at the injection location, computed from microstructure profiles in Figure 4.16a was 0.028 rad s^{-1} and the slope at the injection site was approximately 10%. Therefore, the resulting critical frequency ω_c was 39 cpd. The wave frequencies ω computed from Table 4.1 was 1.8 cpd and 0.58 cpd for the first two vertical modes during the tracer study. Since $\omega/\omega_c << 1$ during the tracer study, the internal waves

reflecting along the injection slope were subcritical and little or no boundary mixing from reflecting internal waves occurred. The buoyancy frequency along the sloping boundary at the thermocline on June 16, computed from microstructure profiles in Figure 4.15a, was 0.025 rad s^{-1}, the slope at the boundary was approximately 1%, and the resulting critical frequency ω_c was 3.4 cpd. The wave frequencies ω computed from Münnich et al. (1992) was 1.1 cpd and 0.43 cpd for the first two vertical modes on June 16. Since $\omega/\omega_c << 1$ on June 16, the internal waves reflecting along the injection slope are subcritical and the observed boundary layer must have been generated by the damping of seiches.

The Iribarren number, the ratio of boundary slope to waveslope, is $\xi_n = S/(\zeta_0/\lambda)^{1/2}$. When the boundary slope S at the injection site is 10%, the wave amplitude ζ_0 is 1.5 m, and the wavelength λ is twice the fetch length, 15,200 m, the Iribarren number ξ_n is 10, therefore most of the wave energy is reflected away from the boundary. Based on the wave classification in Boegman et al. (2005a), the injection slope was classified as a collapsing breaker, which induces minimal boundary mixing. Figures 4.6-4.9 show no peaks in the energy spectra at the critical frequency of the injection slope. The absence of peaks in spectral energy at the critical frequency of the injection slope and the lack of dominant seiching motion were the reasons for the absence of boundary mixing during the tracer study which will be scrutinized in the follow section.

Mixing

Three methods were used to obtain vertical eddy diffusivity, an estimate of mixing intensity in the vertical direction. The three methods include microstructure profiles, the heat budget method, and the moments of concentration distribution from the mean dye profiles.

The vertical eddy diffusivity at the injection depth was estimated from microstructure profiles on three different occasions during the dye tracer study to be approximately 10^{-6} m^2 s^{-1}. The vertical eddy diffusivity in the metalimnion of West Okoboji Lake was estimated to be approximately 10^{-5} m^2 s^{-1} from the LDS temperature chain profiles using the heat budget method (Jassby and Powell 1975). The vertical eddy diffusivity calculated from the moment of concentration distribution from the mean dye profiles was approximately 4×10^{-6} m^2 s^{-1}. The vertical diffusivities observed during the dye study varied by less than an order of magnitude. The estimated diffusivity from the heat budget method and microstructure differed by a factor of two, and the diffusivity from the tracer dye distribution was slightly smaller.

Vertical diffusivities from onshore temperature microstructure measurements in the hypolimnion of a Swiss lake (Lake Alpnach) varied from 3×10^{-6} m^2 s^{-1} to 3×10^{-5} m^2 s^{-1} (Gloor et al. 2000), in the metalimnion of a lake in California (Mono Lake) had values ranging from 4×10^{-6} m^2 s^{-1} to 9×10^{-5} m^2 s^{-1} (MacIntyre et al. 1999), and in the metalimnion of a smaller lake in Iowa (Ada Hayden Lake) extended from 10^{-6} m^2 s^{-1} to 3×10^{-5} m^2 s^{-1} (Wain and Rehmann, in press). Vertical eddy diffusivities from temperature profiles using the heat budget method were determined to be between 4×10^{-6} m^2 s^{-1} in the upper hypolimnion of Lake Alpnach in Switzerland (Wüest et al. 1996). In an additional study in the hypolimnion of the same Swiss lake, vertical eddy diffusivities from temperature profiles using the heat budget method were determined to be between 10^{-6} m^2 s^{-1} to 9×10^{-6} m^2 s^{-1} (Goudsmit et al. 1997) and between 5×10^{-7} m^2 s^{-1} and 4×10^{-6} m^2 s^{-1} in the metalimnion of Mono Lake, California (MacIntyre et al. 1999). From a tracer study in a Swiss lake and the moment distribution equation, the vertical eddy diffusivity was found to be between 10^{-6} and 8×10^{-5}

m^2 s^{-1} (Goudsmit et al. 1997). In the upper hypolimnion of the same Swiss lake from a separate study, the vertical diffusivity was determined to be 3×10^{-6} m^2 s^{-1} from the basin scale application of the vertical spreading method and a dye tracer (Wüest et al. 1996). Using the same method, diapycnal diffusivities have been observed to range from 10^{-6} to 10^{-5} m^2 s^{-1} on the continental shelf south of New England (Ledwell et al. 2004).

In Table 5.3 and Figure 5.2, the vertical diffusivities from all of the previous studies as well as from West Okoboji Lake can be found sorted by the method. Some of the values

Table 5.3. The vertical diffusivities observed in lakes and the continental shelf estimated from microstructure profiles, the heat budget method, and vertical dye tracer distribution compared to the values observed in West Okoboji Lake on July 20-22, 2009.

Paper	Method	Location	Vertical Diffusivity (m^2 s^{-1})
MacIntyre et al. (1999)	microstructure	metalimnion	4×10^{-6} - 9×10^{-5}
Gloor et al. (2000)	microstructure	hypolimnion	3×10^{-6} - 3×10^{-5}
Wain and Rehmann (in press)	microstructure	metalimnion	10^{-6} - 3×10^{-5}
West Okoboji Lake	microstructure	metalimnion	10^{-6}
Wüest et al. (1996)	heat budget	hypolimnion	4×10^{-6}
Goudsmit et al. (1997)	heat budget	hypolimnion	10^{-6} - 9×10^{-6}
MacIntyre et al. (1999)	heat budget	metalimnion	5×10^{-7} - 4×10^{-6}
West Okoboji Lake	heat budget	metalimnion	10^{-5}
Wüest et al. (1996)	dye tracer	hypolimnion	3×10^{-6}
Goudsmit et al. (1997)	dye tracer	hypolimnion	10^{-6} - 8×10^{-5}
Ledwell et al. (2004)	dye tracer	continental shelf	10^{-6} - 10^{-5}
West Okoboji Lake	dye tracer	metalimnion	4×10^{-6}

observed from the heat budget method in West Okoboji Lake are slightly larger than some of the previous findings. This result can be attributed to the weak vertical density gradient present in West Okoboji Lake compared to Mono Lake, Lake Alpnach, Ada Hayden Lake, or the ocean. However, closer examination of the diffusivities from microstructure and the tracer in West Okoboji Lake reveal strong agreement with results from previous studies. A strong vertical density gradient would limit the vertical transport of matter, resulting in reduced vertical eddy diffusivity (Saggio and Imberger 2001).

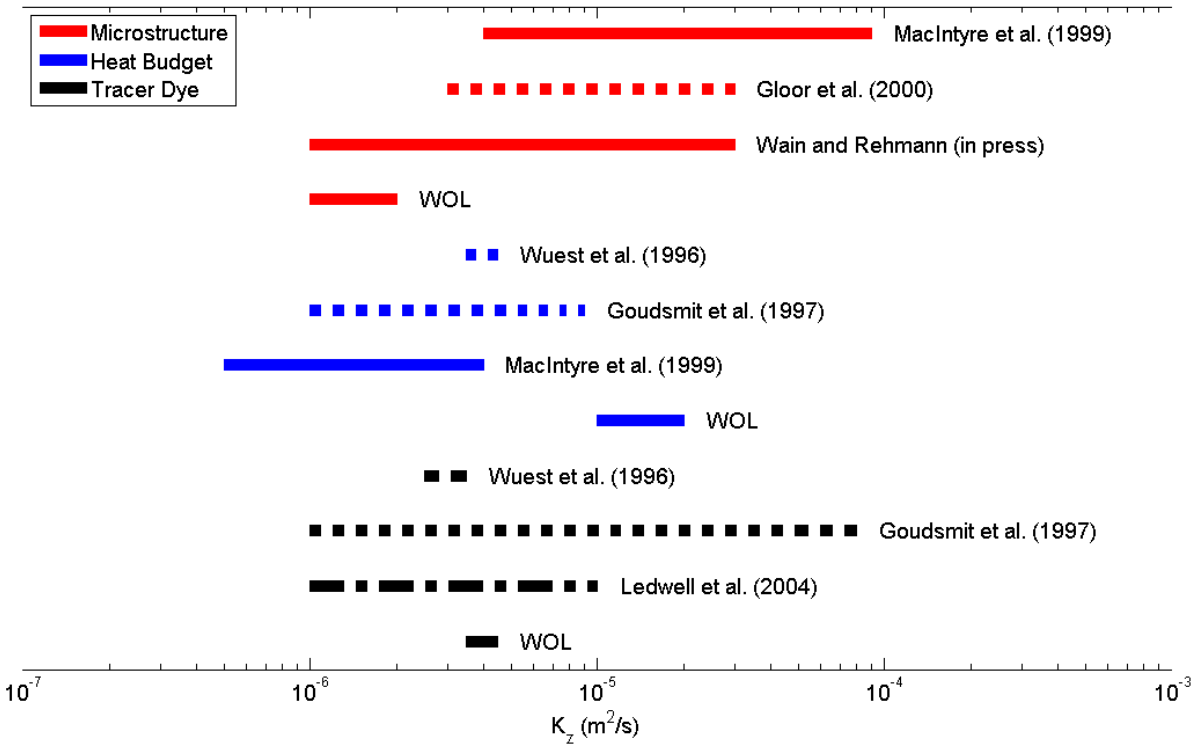

Figure 5.2. The vertical diffusivities observed in the metalimnion (solid) and hypolimnion (dotted) of lakes and the continental shelf (solid/dotted) estimated from microstructure profiles (red), the heat budget method (blue), and vertical dye tracer distribution (black) compared to the values observed in West Okoboji Lake on July 20-22, 2009.

To investigate the effects of both the stratification and the forcing on the mixing, the relationship between the normalized eddy diffusivity and the Lake number was examined. The daily logarithmic mean of the Lake number was computed from May 29 to July 22. Correspondingly, the daily logarithmic mean of the vertical eddy diffusivity in the metalimnion was calculated from the daily profiles of vertical diffusivity estimated at the LDS via the heat budget method over the same time frame. The metalimnion was estimated to be from 11 m to 16 m based on the evolving temperature profiles over the two-month span. A best fit line applied to the data (Figure 5.3) gives

$$K_{zt}/\nu = 10^2 L_N^{-0.9} \tag{5.1}$$

with $R^2 = 0.4$. The data are scattered, but the decrease in the vertical eddy diffusivity with increasing Lake number agrees with intuition and resembles the relationship $K_z/\nu \propto L_N^{-1.1}$ found for turbulence on the sloping boundary of Ada Hayden Lake (D. J. Wain, pers. comm.) By examining the vertical eddy diffusivity in the 1-2 m of the profiles in Figures 4.15 and 4.16, an interesting characteristic is observed. In Figure 4.15b, there is a noticeable elevation in diffusivity to near 10^{-5} m^2 s^{-1} in the bottom 5 m of the profile at the offshore site. However, in the last 2 m of the profile in Figure 4.15a, the vertical eddy diffusivity increases by nearly two orders of magnitude to 10^{-4} m^2 s-1 at the onshore site. The increase in diffusivity at the onshore site by nearly two orders of magnitude provides evidence for boundary mixing on June 16, 2009. The observations of boundary layer thickness were consistent with those of Gloor et al. (2000), who recognized that the thickness of turbulent layers is greater at the bottom of the lake than along its sloping sides. Gloor et al. (2000) observed boundary layers of mixed fluid with thicknesses around 2 m along a sloping boundary of 1.5%. A boundary layer of similar thickness formed on a slope of 0.5% where the onshore profiles were

recorded in West Okoboji Lake. Also, Gloor et al. (2000) observed a well-mixed boundary layer offshore with a thickness of approximately 4-5 m, and a boundary layer with a thickness of nearly 5 m formed offshore on June 16, 2009 in West Okoboji Lake. From Equation (2.11) established by Hondzo and Haider (2004), the sloping boundary layer thickness δ on June 16 when L_s=2780 m (the slope length above the thermocline), N=0.025 rad s^{-1} (from onshore microstructure profiles), $\varepsilon=3\times10^{-8}$ m^2 s^{-3} (from measurements performed onshore during the dye study from July 20-22, 2009 in Figure 4.16 show no increase in diffusivity along the lake boundary; therefore, boundary fluid mixed by turbulence is absent.

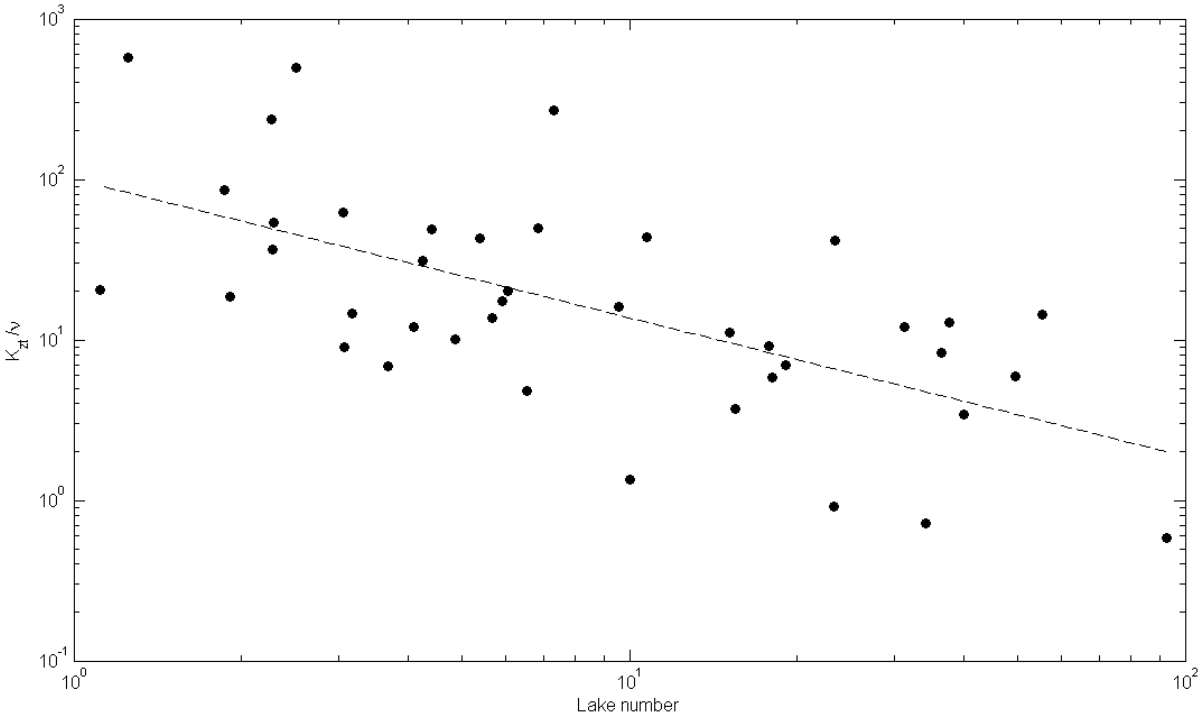

Figure 5.3. The dimensionless ratio of vertical eddy diffusivity from the heat budget method to kinematic viscosity in terms of the Lake number (circles). A best fit line (R^2 = 0.4) was used to determine an equation to estimate vertical diffusivity from the Lake number.

In addition, MacIntyre et al. (1999) established a Lake number of two as the threshold for boundary mixing. As seen in Figure 4.2c, a sustained Lake number of two was never obtained. However, on June 16, a sustained wind was observed and thus boundary mixing was observed. This provides further validation that no boundary mixing occurred from July 20-22, 2009.

Transport

Evidence supporting and refuting an intrusion formed by the gravitational collapse of mixed boundary fluid was examined. The effects of buoyancy, inertia, and viscosity can be compared quantitatively using the dimensionless parameters of turbulent Froude, Reynolds, and Grashof numbers as defined in Ivey and Imberger (1991). The centered displacement scale was 5.8 cm, and the dissipation and buoyancy frequency, computed from microstructure profiles in Figure 4.16a, were 9.3×10^{-9} m^2 s^{-3} and 0.028 rad s^{-1}, respectively and as a result, the $Fr_t = 0.62$, $Gr_t = 73$, $Re_t = 120$ at the injection depth. The turbulent Grashof number, which relates the effects of buoyancy and viscosity, exceeded 15; the effects of buoyancy dominated the effects of viscosity (Lemckert and Imberger 1995). Since the turbulent Reynolds number is much greater than 15, the viscosity has little effect on turbulence (Ivey and Imberger 1991). Given the values of these parameters, the boundary turbulence can best be described as an inertia-buoyancy force balance. According to Imberger and Ivey (1991), based on the turbulent Froude number and turbulent Reynolds number, decaying turbulence should be present in the lake at the time of the tracer study.

The Peclet number $Pe = uL_x/K_y$ relates advection to diffusion to see which was the dominant mechanism responsible for the transport of dye offshore between the surveys at

10.5 h and 29.2 h after injection. The velocity u = 0.3 cm s^{-1}, was defined as the quotient of the length scale L_x, the horizontal distance from the location of maximum concentration at 10.5 h to the location of maximum concentration of the 29.2 h survey (190 m), and the time elapsed between the two surveys (18.7 h). With the horizontal diffusivity in the north-south direction K_y=0.4 m^2 s^{-1}, from the spreading equation and the dye survey at 29.2 h, Pe=1.4. Therefore, the effects of advection and diffusion are approximately equal and neither mechanism can be individually responsible for the offshore transport witnessed in Figure 4.23.

The vertical profiles of eddy diffusivity show evidence of boundary mixing on June 16 due to the region of enhanced diffusivity near the lake boundary in both profiles and the diffusivity is about an order of magnitude at the boundary onshore. However, since all four microstructure measurements performed onshore during the dye study in Figure 4.16 show no increase in diffusivity near the boundary, boundary fluid mixed by turbulence is absent. In fact, the smallest vertical diffusivity is found along the boundary in all four measurements. Consequently, one can conclude that an intrusion of mixed fluid did not occur on July 20-22, 2009 simply due to the lack of mixed fluid near the lake boundary.

From the plan view dye survey maps at 10.5 h and 29.2 h after the injection in Figures 4.21 and Figure 4.23, the transport velocity of the dye cloud was calculated. The dye front propagated 260 m and 900 m which resulted in a front velocity of 0.70 cm s^{-1} and 0.86 cm s^{-1} for the dye surveys at 10.5 h and 29.2 h after the injection, respectively. These values are about two to three times greater than intrusion velocities observed in a lake (Wain and Rehmann, in press) and in a fjord (Inall 2009). The mean vertical thickness of the entire dye cloud varied from 2.0 m at 10.5 h after injection to 3.5 m 29.2 h after injection. Wain and

Rehmann (in press) estimated the Ozmidov scale $(\varepsilon/N^3)^{1/2}$ in Ada Hayden Lake to be 0.15 m. The observed intrusion had a thickness of approximately 1 m which was about six times the Ozmidov scale. With an Ozmidov scale of 0.04 m in West Okoboji Lake, it cannot accurately be used to scale the dye cloud thickness as in Wain and Rehmann (in press). The wave amplitude was estimated to be approximately 1.5 m on the first day of the tracer study, with the dye cloud thickness 1.3 and 2.3 times larger at 10.5 h and 29.2 h after the dye injection, respectively. Wain and Rehmann (in press) estimated the wave amplitude to be roughly on the order of 1 m, resulting in an intrusion thickness two times larger, which falls in the range observed in West Okoboji Lake.

Scaling was used to determine if the internal waves present during the study were capable of horizontal displacements large enough to transport the dye 900 m offshore by the dye survey at 29.2 h (Figure 4.23). First, the stratification was approximated as linear and bathymetry of the lake was simplified to a rectangular prism. Then the vertical isotherm displacement ζ is

$$\zeta = \zeta_0 \cos(kx)\sin(mz)\sin(\omega t), \tag{5.2}$$

where ζ_0 is the amplitude of the isotherm displacement, $k = n_x\pi/L_f$, $m = n_z\pi/\overline{H}$, $\omega = Nk/(k^2+m^2)^{1/2}$, L_f is the lake fetch, $\overline{H}$ is the mean lake depth, and n_x and n_z are horizontal and vertical wave numbers, respectively. The vertical velocity w is the time derivative of the isotherm displacement

$$w = \frac{d\zeta}{dt} = \zeta_0\omega\cos(kx)\sin(mz)\cos(\omega t), \tag{5.3}$$

and continuity gives the horizontal velocity u,

$$\frac{\partial u}{\partial x} + \frac{\partial w}{\partial z} = 0 \rightarrow u = -\int \frac{\partial w}{\partial z}dx = \frac{-\zeta_0\omega m}{k}\sin(kx)\cos(mz)\cos(\omega t). \tag{5.4}$$

Finally, the horizontal displacement ξ is found by integrating the velocity in time:

$$\xi = \int u\, dt = \frac{-\zeta_0 m}{k} \sin(kx_0)\cos(mz_0)\sin(\omega t), \tag{5.5}$$

where x_0 and z_0 are the location of the dye. The amplitude of the horizontal displacement is

$$\xi_0 = |\xi| = \frac{\zeta_0 m}{k} \sin(kx_0)\cos(mz_0), \tag{5.6}$$

where (x_0, z_0) is the location of the dye. For an injection near the boundary of a large lake kx_0<<1; therefore,

$$\xi_0 \sim \frac{\zeta_0 m}{k} kx_0 \cos(mz_0) = \zeta_0 m x_0 \cos(mz_0). \tag{5.7}$$

For an injection in the thermocline, the $\cos(mz_0)$ term will be near zero for odd vertical modes (n_z=1, 3, 5, etc.) as shown in Figure 4.5c-e. As a result, consider the V2H1 mode (from Table 4.1), such that n_x=1 and n_z=2, then $\cos(mz_0)$ =1 and

$$\xi_0 \approx \frac{\zeta_0 n_z \pi}{\bar{H}} x_0. \tag{5.8}$$

Thus, $\xi_0 \approx$ 90 m if the vertical wave amplitude ζ_0=1.5 m, the length from the boundary x_0=150 m (Figure 4.21), and $\bar{H}$=15 m near the dye cloud. A check of the Peclet number for wave advection can be estimated as $Pe_w = \frac{(\xi_0/T_2)\xi_0}{K_y}$. With K_y=0.4 m^2 s^{-1} and T_2=1.44×10^5 s, the period of the V2H1 mode, Pe_w=0.1. A small wave advection Peclet number coinciding with a small horizontal displacement provide strong evidence that advection by internal waves is not responsible for the offshore transport of dye observed in Figure 4.23.

The horizontal diffusivity was estimated between 0.2×10^{-1} and 4×10^{-1} m^2 s^{-1} using Equation (3.7). The results in West Okoboji Lake are similar to findings from other studies using a variety of models to estimate horizontal diffusivity from dye tracer injections and drifter studies. The horizontal eddy diffusivity observed from tracer surveys in the

epilimnion, metalimnion, and hypolimnion of Lake Ontario varied from 2×10^{0} m^2 s^{-1} to 2×10^{2} m^2 s^{-1}, 3×10^{-1} m^2 s^{-1} to 10^{2} m^2 s^{-1}, and 10^{-2} m^2 s^{-1} to 9×10^{-1} m^2 s^{-1}, respectively, using the Fickian diffusion model (Murthy 1976). The mean turbulent horizontal dispersion from the 19 surveys in a 3 month period fell between 0.7×10^{1} m^2 s^{-1} and 3×10^{1} m^2 s^{-1} at the mean hypolimnetic depth of 60 m, 40 m below the thermocline using a one-dimensional box diffusion model (Maiss et al. 1994). The observed dispersion rates from the diffusion model of Okubo (1971) in a Canadian lake fell between 10^{-3} m^2 s^{-1} and 3×10^{-2} m^2 s^{-1} using videotapes of dye tracer studies onshore and offshore in the epilimnion of a small lake (Lawrence et al. 1995). From a tracer study in the interior of a Swiss lake using the shear diffusion model of Carter and Okubo (1965), the horizontal diffusivity in the upper hypolimnion was found to be between 2×10^{-2} m^2 s^{-1} and 3×10^{-1} m^2 s^{-1} (Peeters et al. 1996). Stocker and Imberger (2003) performed six GPS drifter experiments in the surface layer of Lake Kinneret in Israel and observed an average dispersion coefficient of approximately 8×10^{0} m^2 s^{-1} to 9×10^{0} m^2 $s^{-1}$from the standard deviation cluster model, 10^{0} m^2 s^{-1} to 2×10^{0} m^2 s^{-1} from the Lagrangian statistics model, and 0.7×10^{1} m^2 s^{-1} to 3×10^{1} m^2 s^{-1} from the mean shear model. The disparity was attributed to the model as the same study was applied to all the models, but the dispersion coefficients were close enough that Stocker and Imberger (2003) confirmed that their estimate were accurate to the order of magnitude. From eight dye tracking experiments in a Canadian lake, Stevens et al. (2004) estimated the horizontal diffusivity in the epilimnion from 10^{-2} m^2 s^{-1} to 10^{1} m^2 s^{-1} from application of the Fickian diffusion model of Okubo (1971).

The horizontal diffusivities from all of the previous studies as well as from West Okoboji Lake can be found in Table 5.4 and Figure 5.4 increasing from smallest to largest.

Table 5.4. The horizontal diffusivities observed in the epilimnion, metalimnion, and hypolimnion of lakes from dye tracer or drifter studies in previous work compared to the values observed in West Okoboji Lake on July 20-22, 2009.

Paper	Study Type	Location	Horizontal Diffusivity ($m^2\ s^{-1}$)
Lawrence et al. (1995)	dye tracer	epilimnion	10^{-3} - 3×10^{-2}
Stevens et al. (2004)	dye tracer	epilimnion	10^{-2} - 1.3×10^{1}
Murthy (1976)	dye tracer	hypolimnion	10^{-2} - 9×10^{-1}
Peeters et al. (1996)	dye tracer	hypolimnion	2×10^{-2} - 3×10^{-1}
West Okoboji Lake	dye tracer	metalimnion	2×10^{-2} - 4×10^{-1}
Murthy (1976)	dye tracer	metalimnion	3×10^{-1} - 10^{2}
Stocker and Imberger (2003)	drifter	epilimnion	2×10^{0} - 3×10^{1}
Murthy (1976)	dye tracer	epilimnion	2×10^{0} - 2×10^{2}
Maiss et al. (1994)	dye tracer	hypolimnion	7×10^{0} - 3×10^{1}

The values observed in West Okoboji Lake fall right in the middle of the results. Many of the results with diffusivity greater than what was observed in West Okoboji Lake were observed in the epilimnion which is expected to be a region of greater diffusivity when compared to the metalimnion.

Summary

Compared to previous tracer studies in stratified lakes, the wind forcing was not as large in West Okoboji Lake but the weak stratification caused a Lake number that was smaller than observed in previous studies. A Lake number less than 10, as observed in West Okoboji Lake, should be sufficient to generate wind set-up throughout the water column initiating seiching (Imberger and Patterson 1990). After analysis of the internal wave

field via three different methods, the investigation reveals that no particular mode is dominant during the tracer study. Temporal variability in the wind may be the cause of this result. However, the V1H1 and V2H1 seem to be the most likely from the three different approaches, as evidence for both modes were found from two of the three methods. Close agreement was observed between all three methods used to estimate vertical eddy diffusivity. Overall, values of vertical and horizontal diffusivity estimated in West Okoboji Lake were consistent with previous studies in lakes and the ocean. All four measurements performed onshore during the dye study from July 20-22, 2009 in Figure 4.16 show no increase in

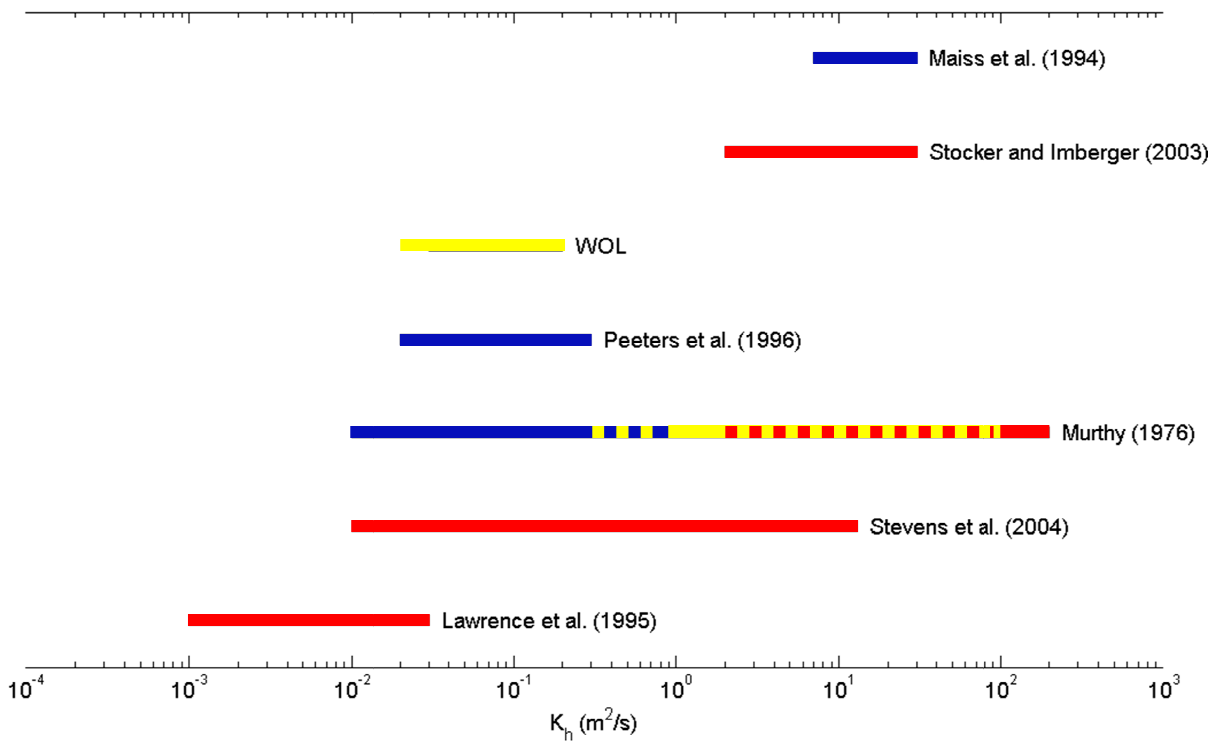

Figure 5.4. The horizontal diffusivities observed in the epilimnion (red), metalimnion (yellow), and hypolimnion (blue) of lakes from dye tracer or drifter studies in previous work compared to the values observed in West Okoboji Lake on July 20-22, 2009.

diffusivity along the lake boundary; therefore, boundary mixing is absent. An intrusion and horizontal displacement from internal waves were ruled out as transport mechanisms due to the absence of mixed boundary fluid and the large disparity between estimated and observed horizontal displacement, caused by internal waves.

CHAPTER 6. CONCLUSION

Summary

Mixing in a temperate lake during summer stratification affects a number of biological and chemical processes that have large ecological impacts. Wind forced mixing is the main mechanism that can completely stir a stratified water body. The mixed fluid caused by the wind can transport fluid and solutes that were once near lake boundaries to other parts of the lake where they can be used to increase or possibly decrease bioproductivity. Boundary transport of nutrients and dissolved gasses plays a vital role in determining the trophic status of a water body. The overall impact of wind driven mixing and transport is an important component in the global heat budget and the quality of the world's water bodies.

Temperature recording chains were used to identify profiles of temperature and buoyancy frequency in West Okoboji Lake. Meteorological data were recorded in order to determine the Lake number. The vertical mode structure and period were estimated using an n-layer model. Isotherm displacement, energy spectra of isotherm displacement, and coherency and phase spectra of displacement of isotherm pairs were used to assess the internal wave field. The vertical eddy diffusivity was estimated using microstructure profiles, the heat budget method, and dye distribution and compared with values observed in previous studies. The geometry and shape of the dye cloud was identified from four separate surveys. The horizontal eddy diffusivity was identified from the horizontal spreading of the dye plume and compared to findings from other tracer studies in lakes. Several different mechanisms were scrutinized as the possible mechanism for the transport of the dye.

Significant Findings

The investigation performed at West Okoboji Lake near Arnolds Park, Iowa during the summer of 2009 led to a number of conclusions:

1. The Lake number on July 20, 2009 during the dye injection ranged between 1 and 10, and on July 21-22, the Lake number increased to near 100.
2. The theoretical periods of the first three vertical modes were 13.4 h, 41.3 h, and 62.3 h, respectively from the n-layer model developed by Münnich et al. (1992).
3. From the isotherm displacement time series, energy spectra of isotherm displacement, and coherency and phase spectra of displacement of isotherm pairs the V1H1 and V2H1 with some ambiguity seem to be the most likely modes present during July 20-22, with two of the three approaches providing supporting evidence.
4. The vertical eddy diffusivity during the tracer study in the metalimnion from microstructure profiles, the heat budget method, and dye tracer distribution was 10^{-6} m^2 s^{-1}, 10^{-5} m^2 s^{-1}, and 4×10^{-6} m^2 s^{-1}, respectively.
5. At 10.5 h and 29.2 h following dye injection, the dye front had propagated as far as 260 m and 900 m from the injection point, resulting in a front velocity of 0.70 cm s^{-1} and 0.86 cm s^{-1}, respectively.
6. From the dye surveys collected at 10.5 h and 29.2 h after injection, the horizontal diffusivity compensating for the lake boundaries to east, south, and west was estimated to be between 0.2×10^{-1} m^2 s^{-1} and 4×10^{-1} m^2 s^{-1}.
7. An intrusion and horizontal displacement from internal waves were ruled out as transport mechanisms because of the absence of mixed boundary fluid and the

large disparity between estimated and observed horizontal displacement, respectively.

Therefore any dissolved gas, nutrient, or pollutant located near the boundary on July 20, 2009 would be transported offshore up to 900 meters to the stratified lake interior in little more than one day. This redistribution of gasses, nutrients, and nutrients in the lakes interior could drastically affect the lake's ecosystem. The hypothesis that a mode one seiche will be excited from wind forcing was confirmed. However, evidence supporting the existence of other modes was also obtained. The hypothesis stating that boundary mixing will result from internal waves was disproven because no boundary mixing was observed. The hypothesis that an intrusion would form was not supported by the observations, including the lack of boundary mixing.

Future Work

Further research includes applying the methods used in this study to different lakes to determine to what extent the results are affected from variability in bathymetry or size. Application to larger or smaller lakes would provide a better understanding of what role the scale of the lakes plays in terms of mixing and transport. A further understanding of why the absence of a boundary layer occurred even when the Lake number is sufficiently small would also be useful. Also, a more accurate way to estimate the mode periods and types needs to be examined as well as a more efficient process to identify transport mechanisms. Over the two-month period of the field study, a number of profiles using the CTD profiler were collected, which also could be used to estimate vertical eddy diffusivity. It would be interesting to see how those compared with the other methods used in this study and in addition how the

diffusivity changed over time. The Aquadopp profiler, an instrument which measured acoustic velocity profiles near the lake boundary, was deployed for a portion of the study period. The velocity profiles could be used to estimate continuous profiles of turbulent kinetic energy dissipation. It would be interesting to see if a correlation exists between the Lake number and the dissipation of turbulent kinetic energy. Finally, an acoustic Doppler current profiler (ADCP) was also deployed during part of the field study. The ADCP might be able to reveal seiching direction, currents, and periods as well as the mean background currents in the lake. It would be intriguing to see if the mean current of the lake could be related to the Lake number.

REFERENCES

Antenucci, J. P., J. Imberger, and A. Saggio. 2000. Seasonal evolution of the basin-scale internal wave field in a large stratified lake. Limnol. Oceanogr. **45:** 1621-1638.

Appt, J., J. Imberger, and H. Kobus. 2004. Basin-scale motion in stratified upper Lake Constance. Limnol. Oceanogr. **49:** 919-933.

Armi, L. 1978. Some evidence for boundary mixing in deep ocean. J. Geophys. Res. **83:** 1971-1979.

Barry, M. E., G. N. Ivey, K. B. Winters, and J. Imberger. 2001. Measurements of diapycnal diffusivities in stratified fluids. J. Fluid Mech. **442:** 267-291.

Boegman, L., G. N. Ivey, and J. Imberger. 2005a. The degeneration of internal waves in lakes with sloping topography. Limnol. Oceanogr. **50:** 1620-1637.

---. 2005b. The energetics of large-scale internal wave degeneration in lakes. J. Fluid Mech. **531:** 159-180.

Browand, F. K., D. Guyomar, and S. C. Yoon. 1987. The behavior of a turbulent front in a stratified fluid: experiments with an oscillating grid. J. Geophys. Res. **92:** 5329-5341.

Cacchione, D., and C. Wunsch. 1974. Experimental study of internal waves over a slope. J. Fluid Mech. **66:** 223-&.

Caldwell, D. R., J. M. Brubaker, and V. T. Neal. 1978. Thermal microstructure on a lake slope. Limnol. Oceanogr. **23:** 372-374.

Carter, H. H., and A. Okubo. 1965. A study of the physical processes of movement and dispersion in the Cape Kennedy area.

Chen, C. T., and F. J. Millero. 1977. Use and misuse of pure water PVT properties for lake waters. Nature **266:** 707-708.

Dauxois, T., Young, W.R., 1999. Near-critical reflection of internal waves. J. Fluid Mech. 390, 271 – 295.

Defant, A. 1918. Neue Methode zur Ermittlung der Eigenschwingungen (Seiches) von abgeschlossenen Wassermassen (Seen, Buchten, usw.). Ann. Hydrograph. Berlin, **46:** 78-85.

De Silva, I. P. D., J. Imberger, and G. N. Ivey. 1997. Localized mixing due to a breaking internal wave ray at a sloping bed. J. Fluid Mech. **350:** 1-27.

Dickson, R. R., and I. N. McCave. 1986. Nepheloid layers on the continental slope west of Porcupine Bank. Deep-Sea Res. **33:** 791-818.

Eckert, W., J. Didenko, E. Uri, and D. Eldar. 2003. Spatial and temporal variability of particulate phosphorus fractions in seston and sediments of Lake Kinneret under changing loading scenario. Hydrobiologia **494:** 223-229.

Eriksen, C. C. 1985. Implications of ocean bottom reflection for internal wave spectra and mixing. J. Phys. Oceanogr. **15:** 1145-1156.

---. 1998. Internal wave reflection and mixing at Fieberling Guyot. J. Geophys. Res. **103:** 2977-2994.

Fee, E. J., and R. W. Bachmann. 1968. An empirical study of the defant method of seiche analysis. Limnol. Oceanogr. **13:** 665-669.

Fischer, H. B., E. J. List, R. C. Y. Koh, J. Imberger, and N. H. Brooks. 1979. Mixing in Inland and Coastal Waters. Academic Press.

Fricker, P. D., and H. M. Nepf. 2000. Bathymetry, stratification, and internal seiche structure. J. Geophys. Res **105:** 14,237-14,251.

Garrett, C. 1979. Comment on 'Some evidence for boundary mixing in the deep ocean' by Laurence Armi. J. Geophys. Res **84:** 5095-5095.

---. 1990. The role of secondary circulation in boundary mixing. J. Geophys. Res. **95:** 3181-3188.

Garrett, C., and W. Munk. 1979. Internal waves in the ocean. Ann. Rev. Fluid Mech. **11:** 339-369.

Garrett, C., P. MacCready, and P. Rhines. 1993. Boundary mixing and arrested Ekman layers: Rotating stratified flow near a sloping boundary. Annu. Rev. Fluid Mech. **25:** 291-323.

Gilbert, D., and C. Garrett. 1989. Implications for ocean mixing of internal wave scattering off irregular topography. J. Phys. Oceanogr. **19:** 1716-1729.

Gloor, M., A. Wüest, and M. Münnich. 1994. Benthic boundary mixing and resuspension induced by internal seiches. Hydrobiologia **284:** 59-68.

Gloor, M., A. Wüest, and D. M. Imboden. 2000. Dynamics of mixed bottom boundary layers and its implications for diapycnal transport in a stratified, natural water basin. J. Geophys. Res. **105:** 8629-8646.

Goudsmit, G. H., F. Peeters, M. Gloor, and A. Wüest. 1997. Boundary versus internal diapycnal mixing in stratified natural waters. J. Geophys. Res. **102:** 27,903-27,914.

Gregg, M. C. 1998. Estimation and geography of diapycnal mixing in the stratified ocean, p. 305-338. *In* J. Imberger [ed.], Physical Processes in Lakes and Oceans. Coastal and Estuarine Studies. American Geophysical Union, Washington, D.C.

---. 1999. Uncertainties and limitations in measuring ε and χ_T. Journal of Atmospheric and Oceanic Technology **16:** 1483-1490.

Hondzo, M., and Z. Haider. 2004. Boundary mixing in a small stratified lake. Water Resources Research **40:** W03101, doi:10.1029/2002WR001851.

Hopfinger, E. J. 1987. Turbulence in stratified fluids: a review. J. Geophys. Res. **92:** 5287-5303.

Horn, D. A., J. Imberger, and G. N. Ivey. 2001. The degeneration of large-scale interfacial gravity waves in lakes. J. Fluid Mech. **434:** 181-207.

Imberger, J., and J. C. Patterson. 1990. Physical limnology. Advances in Applied Mechanics **27:** 303-475.

Inall, M. E. 2009. Internal wave induced dispersion and mixing on a sloping boundary. Geophysical Research Letters **36**: L05604, doi:10.1029/2008GL036849.

Ivey, G. N., and G. M. Corcos. 1982. Boundary mixing in a stratified fluid. J. Fluid Mech. **121:** 1-26.

Ivey, G. N., and R. I. Nokes. 1989. Vertical mixing due to the breaking of critical internal waves on sloping boundaries. J. Fluid Mech. **204:** 479-500.

Ivey, G. N., and J. Imberger. 1991. On the nature of turbulence in a stratified fluid. Part I: The energetics of mixing. J. Phys. Oceanogr. **21:** 650-658.

Ivey, G. N., K. B. Winters, and J. R. Koseff. 2008. Density stratification, turbulence, but how much mixing? Annu. Rev. Fluid Mech. **40:** 169-184.

Jassby, A., and T. Powell. 1975. Vertical patterns of eddy diffusion during stratification in Castle Lake, California. Limnol. Oceanogr. **20:** 530-543.

Kalff, J. 2002. Limnology. Prentice-Hall.

Koop, C. G. 1976. Instability and turbulence in a stratified shear layer. NSF and ONR Report. Dept. of Aerospace Engineering, University of Southern California. 134 pp.

Lawrence, G. A., K. I. Ashley, N. Yonemitsu, and J. R. Ellis. 1995. Natural dispersion in a small lake. Limnol. Oceanogr. **40:** 1519-1526.

Ledwell, J. R., and A. Bratkovich. 1995. A tracer study of mixing in the Santa Cruz Basin. J. Geophys. Res. **100:** 20,681-20,704.

Ledwell, J. R., and B. M. Hickey. 1995. Evidence for enhanced boundary mixing in the Santa Monica Basin. J. Geophys. Res. **100:** 20,665-2,0679.

Ledwell, J. R., E. T. Montgomery, K. L. Polzin, L. C. St. Laurent, R. W. Schmitt, and J. M. Toole. 2000. Evidence for enhanced mixing over rough topography in the abyssal ocean. Nature **403:** 179-182.

Ledwell, J. R., T. F. Duda, M. A. Sundermeyer, and H. E. Seim. 2004. Mixing in a coastal environment: 1. A view from dye dispersion. J. Geophys. Res. **109**: C10013, doi:10.1029/2003JC002194.

Lemckert, C. J., and J. Imberger. 1993. Axisymmetrical intrusive gravity currents in linearly stratified fluids. J. Hydraul. Eng. **119:** 662-679.

Lemckert, C. J., and J. Imberger. 1995. Turbulence within inertia-buoyancy balanced axisymmetric intrusions. J. Geophys. Res. **100:** 22,649-22,666.

Lemckert, C., J. Antenucci, A. Saggio, and J. Imberger. 2004. Physical properties of turbulent benthic boundary layers generated by internal waves. J. Hydraul. Eng. **130:** 58-69.

Lemmin, U., and C. H. Mortimer. 1986. Tests of an extension to internal seiches of defants procedure for determination of surface seiche characteristics in real lakes. Limnol. Oceanogr. **31:** 1207-1231.

Lindenschmidt, K. E., and I. Chorus. 1998. The effect of water column mixing on phytoplankton succession, diversity and similarity. Journal of Plankton Research **20:** 1927-1951.

Lorke, A. 2007. Boundary mixing in the thermocline of a large lake. J. Geophys. Res **112:** C09019, doi:10.1029/2006JC004008.

Lorke, A., and A. Wüest. 2005. Application of coherent ADCP for turbulence measurements in the bottom boundary layer. J. Atmos. Oceanic Technol. **22:** 1821-1828.

Lorke, A., F. Peeters, and A. Wüest. 2005. Shear-induced convective mixing in bottom boundary layers on slopes. Limnol. Oceanogr. **50:** 1612-1619.

Lorke, A., L. Umlauf, and V. Mohrholz. 2008. Stratification and mixing on sloping boundaries. Geophys. Res. Lett. **35:** L14610, doi:10.1029/2008GL034607.

Lowe, R. J., P. F. Linden, and J. W. Rottman. 2002. A laboratory study of the velocity structure in an intrusive gravity current. J. Fluid Mech. **456:** 33-48.

MacIntyre, S., K. M. Flynn, R. Jellison, and J. R. Romero. 1999. Boundary mixing and nutrient fluxes in Mono Lake, California. Limnol. Oceanogr. **44:** 512-529.

MacIntyre, S., J. F. Clark, R. Jellison, and J. P. Fram. 2009. Turbulent mixing induced by nonlinear internal waves in Mono Lake. Limnol. Oceanogr. **54:** 2255-2272.

Maiss, M., J. Ilmberger, A. Zenger, and K. O. Münnich. 1994. A SF_6 tracer study of horizontal mixing in Lake Constance. Aquatic Sciences **56:** 307-328.

Marcé, R., C. Feijoó, E. Navarro, J. Ordoñez, J. Gomà, and J. Armengol. 2007. Interaction between wind-induced seiches and convective cooling governs algal distribution in a canyon-shaped reservoir. Freshw. Biol. **52:** 1336-1352.

Marti, C. L., and J. Imberger. 2008. Exchange between littoral and pelagic waters in a stratified lake due to wind-induced motions: Lake Kinneret, Israel. Hydrobiologia **603:** 25-51.

McPhee-Shaw, E. E., and E. Kunze. 2002. Boundary layer intrusions from a sloping bottom: A mechanism for generating intermediate nepheloid layers. J. Geophys. Res **107**: 3050, doi:10.1029/2001JC000801.

Morillo, S., J. Imberger, J. P. Antenucci, and P. F. Woods. 2008. Influence of wind and lake morphometry on the interaction between two rivers entering a stratified lake. J. Hydraul. Eng. **134:** 1579-1589.

Munk, W. H. 1966. Abyssal recipes. Deep-Sea Res. **13:** 707-730.

Münnich, M., A. Wüest, and D. M. Imboden. 1992. Observations of the second vertical mode of the internal seiche in an alpine lake. Limnol. Oceanogr. **37:** 1705-1719.

Murase, J., Y. Sakai, A. Kametani, and A. Sugimoto. 2005. Dynamics of methane in mesotrophic Lake Biwa, Japan. Ecol. Res. **20:** 377-385.

Murthy, C. R. 1976. Horizontal diffusion characteristics in Lake Ontario. J. Phys. Oceanogr. **6:** 76-84.

Nash, J. D., E. Kunze, J. M. Toole, and R. W. Schmitt. 2004. Internal tide reflection and turbulent mixing on the continental slope. J. Phys. Oceanogr. **34:** 1117-1134.

Okubo, A. 1971. Oceanic diffusion diagrams. Deep-Sea Res. **18:** 789-802.

Osborn, T. R. 1980. Estimates of the local rate of vertical diffusion from dissipation measurements. J. Phys. Oceanogr. **10:** 83-89.

Osborn, T. R., and C. S. Cox. 1972. Oceanic fine structure. Geophys. Fluid Dyn. **3:** 321–345.

Ostrovsky, I., Y. Z. Yacobi, P. Walline, and I. Kalikhman. 1996. Seiche-induced mixing: Its impact on lake productivity. Limnol. Oceanogr. **41:** 323-332.

Patterson, J. C., P. F. Hamblin, and J. Imberger. 1984. Classification and dynamic simulation of the vertical density structure of lakes. Limnol. Oceanogr. **29:** 845-861.

Peeters, F., A. Wüest, G. Piepke, and D. M. Imboden. 1996. Horizontal mixing in lakes. J. Geophys. Res. **101:** 18,361-18,375.

Phillips, O. M. 1970. On flows induced by diffusion in a stably stratified fluid. Deep-Sea Res. **17:** 435-443.

Phillips, O. M., J. H. Shyu, and H. Salmun. 1986. An experiment on boundary mixing - mean circulation and transport rates. J. Fluid Mech. **173:** 473-499.

Polzin, K. L., J. M. Toole, J. R. Ledwell, and R. W. Schmitt. 1997. Spatial variability of turbulent mixing in the abyssal ocean. Science **276:** 93-96.

Rao, Y. R., N. Hawley, M. N. Charlton, and W. M. Schertzer. 2008. Physical processes and hypoxia in the central basin of Lake Erie. Limnol. Oceanogr. **53:** 2007-2020.

Rehmann, C. R., and T. F. Duda. 2000. Diapycnal diffusivity inferred from scalar microstructure measurements near the New England shelf/slope front. J. Phys. Oceanogr. **30:** 1354-1371.

Rehmann, C. R., and J. R. Koseff. 2004. Mean potential energy change in stratified grid turbulence. Dyn. Atmos. Oceans **37:** 271-294.

Romero, J. R., R. Jellison, and J. M. Melack. 1998. Stratification, vertical mixing, and upward ammonium flux in hypersaline Mono Lake, California. Archiv für Hydrobiologie **142:** 283-315.

Ruddick, B., D. Walsh, and N. Oakey. 1997. Variations in apparent mixing efficiency in the North Atlantic Central Waters. J. Phys. Oceanogr. **27:** 2589–2605.

Rudnick, D. L. and others 2003. From tides to mixing along the Hawaiian ridge. Science **301:** 355-357.

Saggio, A., and J. Imberger. 2001. Mixing and turbulent fluxes in the metalimnion of a stratified lake. Limnol. Oceanogr. **46:** 392-409.

Shih, L. H., J. R. Koseff, G. N. Ivey, and J. H. Ferziger. 2005. Parameterization of turbulent fluxes and scales using homogeneous sheared stably stratified turbulence simulations. J. Fluid Mech. **525:** 193-214.

Slinn, D. N., and J. J. Riley. 1996. Turbulent mixing in the oceanic boundary layer caused by internal wave reflection from sloping terrain. Dyn. Atmos. Oceans **24:** 51-62.

Smith, R. 1982. Dispersion of tracers in the deep ocean. J. Fluid Mech. **123:** 131-142.

Soga, C. L. M., and C. R. Rehmann. 2004. Dissipation of turbulent kinetic energy near a bubble plume. J. Hydraul. Eng. **130:** 441-449.

Spigel, R. H., and J. Imberger. 1980. The classification of mixed-layer dynamics in lakes of small to medium size. J. Phys. Oceanogr. **10:** 1104–1121.

Stevens, C., and J. Imberger. 1996. The initial response of a stratified lake to a surface shear stress. J. Fluid Mech. **312:** 39-66.

Stevens, C. L., and G. A. Lawrence. 1997. Estimation of wind-forced internal seiche amplitudes in lakes and reservoirs, with data from British Columbia, Canada. Aquat. Sci. **59:** 115-134.

Stevens, C., G. Lawrence, P. Hamblin, and E. Carmack. 1996. Wind forcing of internal waves in a long narrow stratified lake. Dyn. Atmos. Oceans **24:** 41-50.

Stevens, C. L., G. A. Lawrence, and P. F. Hamblin. 2004. Horizontal dispersion in the surface layer of a long narrow lake. J. Environ. Eng. Sci. **3:** 413-417.

Stocker, R., and J. Imberger. 2003. Horizontal transport and dispersion in the surface layer of a medium-sized lake. Limnol. Oceanogr. **48:** 971-982.

Sundermeyer, M. A., and J. R. Ledwell. 2001. Lateral dispersion over the continental shelf: Analysis of dye release experiments. J. Geophys. Res. **106:** 9603-9621.

Sutherland, B. R., P. J. Kyba, and M. R. Flynn. 2004. Intrusive gravity currents in two-layer fluids. J. Fluid Mech. **514:** 327-353.

Thompson, R. O. R. Y., and J. Imberger. 1980. Response of a numerical model of a stratified lake to a wind stress. Proc. 2nd Intl Symp. Stratified Flows, Trondheim. **1:** 562-570.

Thorpe, S. A. 1982. On the layers produced by rapidly oscillating a vertical grid in a uniformly stratified fluid. J. Fluid Mech. **124:** 391-409.

---. 1998. Some dynamical effects of internal waves and the sloping sides of lakes, p. 441-460. *In* J. Imberger [ed.], Physical Processes in Lakes in Oceans. Coastal and Estuarine Studies., American Geophysical Union, Washington, D.C.

Thorpe, S. A., and M. White. 1988. A deep intermediate nepheloid layer. Deep-Sea Res. A **35:** 1665-1671.

Turner, J. S. 1973. Buoyancy Effects in Fluids. Cambridge University Press.

Vidal, J., X. Casamitjana, J. Colomer, and T. Serra. 2005. The internal wave field in Sau reservoir: Observation and modeling of a third vertical mode. Limnol. Oceanogr. **50:** 1326-1333.

Wain, D. J., and C. R. Rehmann. 2005. Eddy diffusivity near bubble plumes. Water Resources Research **41**: W09409, doi:10.1029/2004WR003896.

---. 2010. Transport by an intrusion generated by boundary mixing in a lake. Water Resources Research**:** in press.

Wells, J. R., and K. R. Helfrich. 2004. A laboratory study of localized boundary mixing in a rotating stratified fluid. J. Fluid Mech. **516:** 83-113.

Weyhenmeyer, G. A. 1996. The influence of stratification on the amount and distribution of different settling particles in Lake Erken. Can. J. Fisheries Aquat. Sci. **53:** 1254-1262.

Wiegand, R. C., and V. Chamberlain. 1987. Internal waves of the second vertical mode in a stratified lake. Limnol. Oceanogr. **32:** 29-42.

Wilson, J. F., E. D. Cobb, and F. A. Kilpatrick. 1986. Fluorometric procedures for dye tracing. United States Geological Survey Techniques for Water Resources Investigation. Book 3, Chapter A12.

Wüest, A., and A. Lorke. 2003a. The effect of the bottom boundary on diapycnal mixing in enclosed basins, p. 9-15. *In* P. Müller and D. Henderson [eds.], Near-Boundary Processes and Their Parameterization, Proc. Aha Hulikoa Hawaiian Winter Workshop.

---. 2003b. Small-scale hydrodynamics in lakes. Annu. Rev. Fluid Mech. **35:** 373-412.

Wüest, A., D. C. Van Senden, J. Imberger, G. Piepke, and M. Gloor. 1996. Comparison of diapycnal diffusivity measured by tracer and microstructure techniques. Dyn. Atmos. Oceans **24:** 27-39.

Wunsch, C. 1970. On oceanic boundary mixing. Deep-Sea Research **17:** 293-&.

Wunsch, C., and R. Ferrari. 2004. Vertical mixing, energy and thegeneral circulation of the oceans. Annu. Rev. Fluid Mech. **36:** 281-314.

Young, W. R., P. B. Rhines, and C. J. R. Garrett. 1982. Shear flow dispersion, internal waves and horizontal mixing in the ocean. J. Phys. Oceanogr. **12:** 515-527.